Faculdade de Engenharia da Universidade do Porto

Development of lightweight and cost-efficient exterior body panels for electric vehicles

André Magalhães Sá Camboa

Thesis submitted under the framework of the MIT Portugal Program
Engineering Design and Advanced Manufacturing for the degree of
Doctor of Philosophy in Leaders for Technical Industries

Supervisor: Prof. Dr. João Pedro Lourenço Gil Nunes
Co-supervisor: Prof. Dr. Fernando Jorge Lino Alves

2016

"Perfection is achieved, not when there is nothing more to add, but when there is nothing left to take away".

Antoine de Saint-Exupery

Abstract

As consequence of low batteries autonomy, the majority of electric vehicles still present a reduced public demand which is translated in a slow market growth and consequently in low production volumes.

In order to overcome the autonomy limitations, and so to contribute to increase its demand, different solutions might be adopted, among them, to reduce vehicles weight by adopting more lightweight materials. In parallel, low production volumes narrow the lightweight materials choice, once these are associated to highly cost demanding manufacturing processes. This issue has especial significance in what respects to the exterior body panels where the conventional infrastructure is still mainly metal dependent with high inherent tooling costs.

Exploring and testing a possible solution for the problem stated above is the main objective of this research and this is accomplished by demonstrating what can be achieved with a polymer-metal hybrid structure of polydicyclopentadiene. For this, the bonnet of MobiCar was used as object of study and its design, prototyping, mechanical simulation and validation, cost and environmental impact are herein documented.

The design phase count on the creation of several bonnet frames through computer aided design and engineering software that enabled achieving the minimum required targets in terms of stiffness and weight. The bonnet was then fabricated using two manufacturing processes: reaction injection moulding for the exterior panel and metal stamping for the metallic frame. The assembly was performed using adhesive bonding. Its structural validation was done in the end, where several mechanical simulations, previously performed during the design phase, were replicated in a real environment.

In order to understand the cost efficiency, as well as the environmental impacts of this solution, in a mass production scenario, a process-based cost model and a life cycle assessment model were created too.

Resumo

Grande parte dos automóveis elétricos apresenta ainda uma procura reduzida por parte do público como consequência da baixa autonomia das baterias, o que se traduz num crescimento lento do seu mercado e em baixos volumes de produção.

Como forma de superar as limitações de autonomia e contribuir para um aumento da procura, várias melhorias terão de ser adoptadas, entre elas, diminuir o peso dos veículos usando materiais mais leves. No entanto, os baixos volumes de produção reduzem a escolha de materiais leves uma vez que estes estão normalmente associados a tecnologias de produção com custos elevados. Este facto ganha ainda mais relevo quando nos referimos aos paneis exteriores de automóveis onde a infraestrutura convencional é ainda hoje maioritariamente baseada em metal estampado.

Explorar e testar uma possível solução para o problema apresentado é o objetivo principal deste projeto de investigação e isso é conseguido demonstrado o que pode ser alcançado com uma estrutura hibrida polímero-metal de polidiciclopentadieno. Para explorar esta solução foi utilizado como objeto de estudo o capô do MobiCar, estando a sua concepção, prototipagem, simulação e validação mecânica, custo e impacto ambiental aqui documentados.

A fase de concepção teve como base a criação de várias estruturas para o capô através de ferramentas de desenho e engenharia assistida por computador que permitiram alcançar os objetivos mínimos exigidos de rigidez e peso. Depois do desenvolvimento, foi feito um protótipo do capô usando dois processos de produção: injeção de moldes de reação para a produção do painel exterior e estampagem para a produção do reforço metálico. A sua montagem foi depois realizada por colagem. A validação estrutural foi efetuada no fim, onde várias das simulações previamente feitas foram replicadas em ambiente real.

Para perceber a eficiência de custo e impacto ambiental da solução desenvolvida, num ambiente de produção em massa, foram também criados um modelo de engenharia de custos e um modelo de análise do ciclo de vida do produto.

Acknowledgements

I am grateful to my supervisors for their support in all challenges I found during this research work. I am also grateful for the technical support provided by CEIIA and INAPAL-Metal engineering teams, as well as to the individuals from FEUP, ISEP and PIEP who contributed for the technical support, among them, Dr. Bernardo Ribeiro, Paulo Machado, Miguel Vaz, Ricardo Malta, Carla Monteiro, Prof. Dr. João Silva, Prof. Dr. Arnaldo Pinto, Carla Silva and Nuno Vieira.

I would like to acknowledge to the MIT Portugal Program team who has created an extraordinary program by providing new knowledge and opportunities for everyone who participates and who has contributed for me to achieve some of my life goals including to collaborate with a great automotive manufacturer like Jaguar Land Rover.

I would like to say thank you to my parents and girlfriend for their tireless support and encouragement. Thank you also to my friends for the remarkable moments on both spare and working times.

Index

List of figures

List of tables

Abbreviations

AHSS	Advanced high strength steel
HSS	High strength steel
Al	Aluminium
ATF	Authorized treatment facilities
CAAM	China association of automobile manufacturers
CAD	Computer aided design
CEIIA	Centre for excellency and innovation for automobile industry
CFRP	Carbon fibre reinforced composites
DCPD	Dicyclopentadiene
DOF	Degrees of freedom
EDTA	Electric drive transportation association
ELV	End of life vehicles
EP	Epoxy
ETE	Effective transfer efficiency
EU	European
EV	Electric vehicle
FEA	Finite element analysis
FLC	Forming limit curve
FLD	Forming limit diagram
GFRP	Glass fibre reinforced composites
ICE	Internal combustion engine
JP	Japan
LPA	Low profile additives
Mg	Magnesium
MMA	Methacrylate
OEM	Original equipment manufacturer
PBCM	Process-based cost model
PDCPD	Polydicyclopentadiene
PEEK	Polyester-ether-ketone

PEI	Polyether-imid
PET	Polyesters
PF	Phenol-formaldehyde
PMH	Polymer-metal hybrid
PMMA	Polymethyl-methacrylate
PP	Polypropylene
PPE	Polyphenylene-ether
PPO	Polyphenylene-oxide
PPS	Polyphenylene-sulfide
PS	Polystyrene
PU	Polyurethane
PUR	Reinforced polyurethane
PVA	Polyvinyl-acetate
RIM	Reaction injection moulding
ROMP	Ring opening metathesis polymerization
RRIM	Reinforced reaction injection moulding
RTM	Resin transfer moulding
SMC	Sheet moulding compound
SRIM	Structural reaction injection moulding
TIM	Thermoplastic injection moulding
ULSAB	Ultra-light steel auto body
UP	Unsaturated polyesters
USA	United States of America
WM	Whole metal

1. Introduction

The transportation paradigm is suffering changes driven by the increasing price of crude and the need to decrease CO_2 emissions. Automotive manufacturers are pushed to develop vehicles capable of using alternative energy sources with relatively competitive energy efficiency and reduced environmental impact. A change that is even sustained by some economy forecast and scientific studies where it is possible to see that the most promising solution for the next few decades is the adoption of the electric mobility (EM), by requiring lower operational costs due to more efficient powertrains. The studies add that EM should also offer zero CO_2 tailpipe emissions depending on the energy source [1, 2].

Although electric energy has already been used as propulsion in some vehicles, its massive introduction in automotive market is still an enormous challenge. Current electric vehicles (EVs) still offer low batteries energy storage capacity. A problem that has been contributing for a low demand, slow market growth and, consequently, for low annual production volumes. In parallel, a more frequent demand for new vehicle models and designs creates additional pressure on original equipment manufacturers (OEMs) by requiring more recurrent investment in tooling. Driven by these market circumstances, automotive manufacturers seek mainly for vehicle weight reduction, by implementing lightweight materials that can be shaped through technologies with acceptable time to market, production cadences and cost.

Contrary to high production volume industries where cars are manufactured by processes that require large initial tooling investment, it is estimated that EVs will need to use other solutions to achieve the market by a competitive price. This scenario is specially narrowing in what respects to the exterior body panels where the use of metals, such as steel, aluminium (Al) or magnesium (Mg) is especially intensive. Here, metals shall be reduced, replaced or combined with other materials, once they entail large investment in tooling, which currently accounts for about 40% of the total vehicles production investment [3].

Reinforced composites like glass fibre (GFRC), or carbon fibre (CFRC) can also be implemented as alternative material even entailing some engineering challenges. Composites have been showing enhanced strength, corrosion resistance and cost efficiency for a wide range of production volumes (large, medium and low) depending on the manufacturing technology.

GFRC, for instance, allows external body panels manufacturing through several process types, among them Sheet moulding compounds (SMC), Resin Transfer Moulding (RTM) and hand lay-up. SMC may only be used for large production series of vehicles, presenting some recycling and repairing limitations with higher costs than those in steel. RTM, on the other hand, is a recurrent option to reduce hand labour, costs (relatively to manual moulding when high cadence is required) and to achieve repeatability, even presenting long cycle times for medium/large parts. For low production volumes, hand lay-up is more commonly used. It is a labour intensive process which requires superior manpower skills, respective costs and larger cycle times than RTM.

CFRC, on the other hand, tend to be applied when high stiffness/weight ratios are required, just like in the competition vehicles or exotic ones with elevated price ranges. CFRC is produced in small rates with a great number of requirements and costs, and depending on the components, these might even exceed the material technologies previously mentioned.

Polymers, per se, start to be implemented more frequently on the exterior body panels, since they typically offer lightweight results independently on their type (thermoplastics or thermosets). Such attributes allow obtaining more energy savings during the vehicle life than the energy required to produce the polymeric parts itself.

For low production volumes thermosets are preferred over thermoplastics since this type of polymers do not require elevated injection pressures and therefore expensive tools. Among the variety of the available thermosets, polydicyclopentadiene (PDCPD) is, apparently, one appropriated as well as one of the less explored solutions by electric automotive industry. While PDCPD was originally used on the exterior body of trucks and agricultural vehicles, its total application on the automotive industry is still little explored, specially knowing this material allows cost efficient results in production volumes between 500 and 30.000 units [4-6].

Considering this, the use of PDCPD, as an automotive exterior body material, was explored in this research work and special focus was given to its application on the EVs where low production volumes are still estimated and lightweight components are required. For this, an EV named MobiCar, from the research & development division of the Centre of

Excellency and Innovation for Mobility Industries (CEIIA) was used as object of study and its bonnet was chosen to be manufactured due to its small dimensions, low geometry complexity, consortium R&D budget and time available. The MobiCar is a two seater car concept developed to explore several automotive technologies in several areas, among them interiors, seat, powertrain, chassis and exteriors. It was thought to have an autonomy target of 100km and a maximum speed and weight of 80km/h and 400kg, respectively.

All this work is shown herein through four main parts. The first part contextualizes the work, the objectives and the expected contribution to the automotive industry. The second part presents a brief history of the EVs and its current market scenario. It summarizes also some material and assembly technologies used in automotive exterior body panels, as well as the state of art of the PDCPD. The third part covers all bonnet development, including an introduction to the materials used and a detailed report of the design, mechanical simulations, prototyping and testing. Tooling development is also covered within this section. The fourth part demonstrates the cost efficiency and the environmental impact of the bonnet, in a mass production scenario.

1.1. Motivation

Two key factors have triggered this research work. One is the actual investment and materials selection uncertainty for EVs exterior body panels which are subject to low production volumes. The other is the interest of CEIIA in the explored technology and the lack of research done so far about the use of PDCPD as exterior material in EVs.

1.2. Consortium

CEIIA provided all the engineering support ensuring experience in design, development and testing of new mobility solutions and systems. CEIIA participation included the necessary technical and technological support performing all phases of product development, from the concept design, validation, virtual development, structural design and prototyping.

For the development phase, this project counted also on the collaboration of INAPAL-Metal which is a company focused in manufacturing steel parts. It provides sheet metal forming, welding, riveting and gluing technologies for automotive industry. The group

INAPAL-Metal has also a unit assembly for outdoor parts (Class A) using welding technology and clinching, being Autoeuropa the main customer.

1.3. Work contribution

This research work was positioned in the context of the MIT Portugal Program in Engineering Design and Advanced Manufacturing with the supervision of João Pedro Lourenço Gil Nunes from University of Minho, Fernando Jorge Lino Alves from Faculty of Engineering of University of Porto and the participation of professor Randolph E. Kirchain from Massachusetts Institute of Technology. It aims to contribute for a new position of the Portuguese industry, exploring innovative solutions to vehicle´s exteriors. The technical solutions resulting from this research work will represent a growth for the various businesses of the partnership. This PhD project has also a considerable upside potential considering the various global initiatives that are being generated for the promotion of EM.

2. State of art

This section presents a brief electric vehicle (EV) history including its current market condition. Existing materials and manufacturing processes used in the exterior automotive body panels are also addressed herein and why EVs might require alternative ones. An introduction to polydicyclopentadiene (PDCPD) and its state of art is also demonstrated.

2.1. Brief electric vehicles history

Automotive history has more than one century of achievements and challenges. The first internal combustion engine (ICE) was demonstrated in 1885 by the German Carl Benz, but the first low-priced mass production vehicle arisen in Detroit, where Ransome E. Olds started their company called Oldsmobile. They began to produce lightweight vehicles with little complex mechanics and design. Their sells rise from 600 till 6.500 between 1901 and 1905. Such success was overtaken 3 years later by Henry Ford who created the Ford Model T. Model T was produced between 1908 till 1927 and it had its upraise in 1914 when Henry Ford created the modern mass production assembly line, which contributed for the productivity growth and to unit cost decrease. In 1910 were produced almost 20.000 at a unit cost of 850$, while, in 1916 were produced 600.000 at a unit cost of 360$. Ford T was definitely a mass production vehicle counting on nearly 15.000.000 units produced [7, 8].

Since then, ICE vehicles have been always achieving the greatest market slice till today. However, with current 96% of the world´s transportation systems depending on petroleum-based fuels (about 40% of the world oil consumption) associated to a constant price uncertainty and the need to decrease tail pipe emissions (which contributes for the greenhouse effect by releasing gases such as CO_2 CH_4 and N_2O) the paradigm begins to change [8-12].

Automotive manufacturers besides being forced to develop more efficient vehicles by reducing roller resistance, vehicles weight, improve aerodynamics and drive train designs, they have also to develop new engine technologies capable of using alternative energy

sources with relatively competitive energy efficiency and reduced environmental impact [9, 13, 14]. Changes that supported by some economy forecasts and scientific studies led them to develop EVs which, besides having lower operational costs due to more efficient powertrains, can also offer zero CO_2 tailpipe emissions depending on the energy source [1, 2, 15, 16].

Electric propulsion vehicles don't represent a new technology, they have, in fact, failed their market introduction for nearly a century. It was in the middle of 19^{th} century that the first EV appeared, but it was only in 1890s that the first original equipment manufacturers (OEMs) selling EVs arisen by growing to more than 20 in 1910s and then decreasing to a marginal value after 1920. In 1913, while Model T presented a production volume of 180.000 units, the EVs only presented 60.000 units, never profiting from an economy of scale.

Several years have passed, and, it would be in 70s decade that EV has witnessed a great period in its history when several attempts to re-introduce them took place. The main automotive manufacturers from United States of America (USA), Europe (EU) and Japan (JP) strove on the development of better electric cars with improved batteries and drive systems. Great improvements were achieved but none have reached the market and these motivations remained so far with more or less enthusiasm in both USA and EU. During 90s decade, PSA and Renault introduced some electric models but, again, with no success, remaining on low volume sells (approx. 10.000 units) [8, 11, 17]. Figure 2.1 presents the EVs attempts to reach the market between 70s decade to 2010 in USA [17].

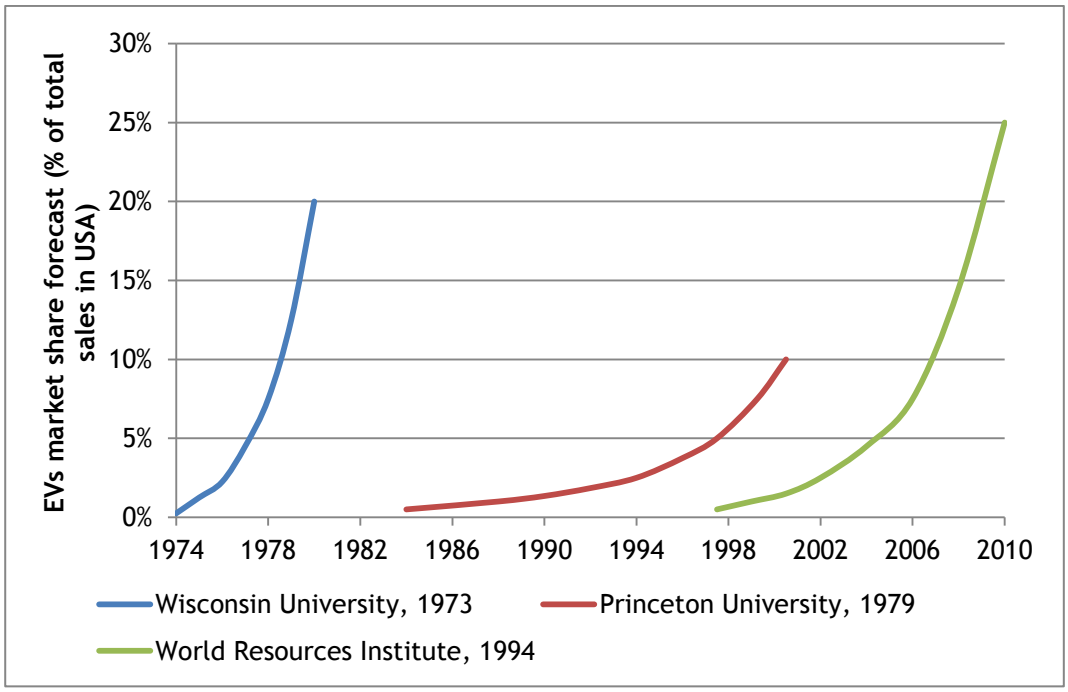

Figure 2.1 – EVs introduction attempts between 1973 and 2010.

At the moment, EVs are still in the race for the market against ICE vehicles. The majority of automotive manufacturers such as Nissan, BMW, Chevrolet, Citroen, among others, have one fully functional electric model or a concept [18, 19], but their massive market introduction is still/again an enormous challenge due to their low batteries energy storage capacity. A problem that EVs face since the beginning of their history, when traditional batteries available were lead acid based, and besides their lower cost, they did not offer much more than 50km range. Today, batteries offer much more than that but they are still under of what an ICE vehicle can do. In addition, EVs remained always more expensive than other vehicle technology which also contributes for their low demand in almost all world countries [17, 20-22].

Low sales always followed EVs history and during the current market attempt (according to the Figure 2.1) the same is happening. In 2008, for instance, when EVs reached Irish market, only 5 cars were sold and even after four years this value has increased to only 44 units. In 2013, 58 units were sold which still represents a marginal growth since its reintroduction in that same country. Germany observed a higher sales figure, however only from 162 to 8804 units between 2009 and 2014 [23-25]. 2014 was, in fact, the year that all EU countries presented their highest EVs sales volume, but counting only on 66439 units all together, as may be seen in Figure 2.2 [26].

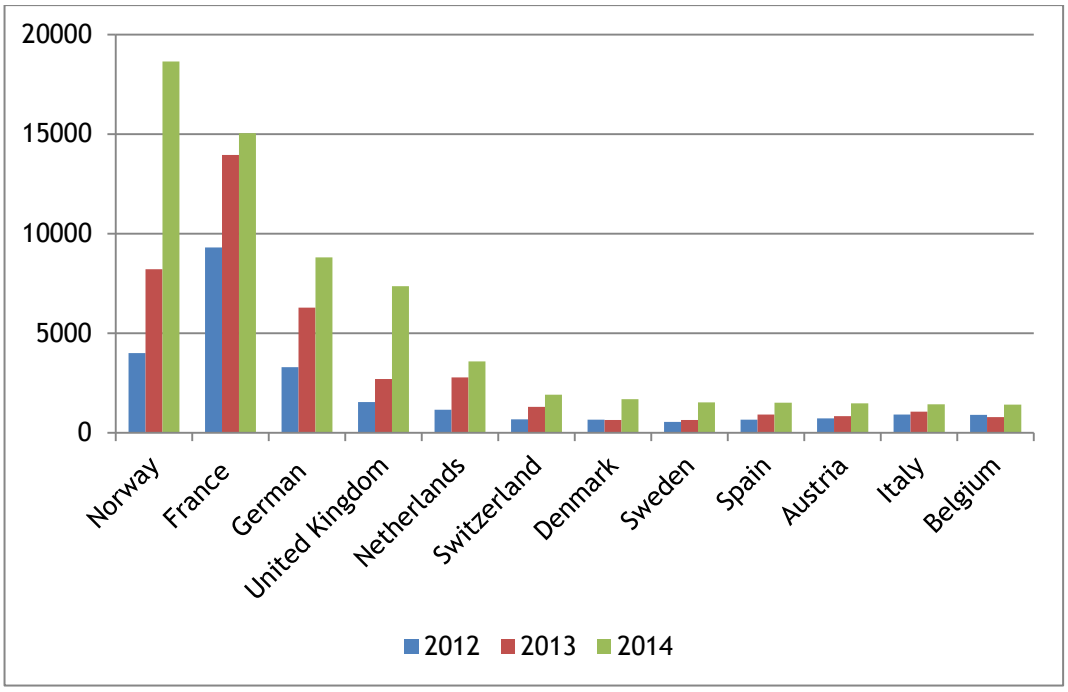

Figure 2.2 – EVs sales by EU country from 2012 to 2014.

Among the sales number, Renault ZOE and Nissan Leaf can be highlighted as the bestselling models (Figure 2.3 and Figure 2.4, respectively). Renault Zoe is a five-seater car based on the same platform of the Renault Clio and is equipped with an electric powertrain with 85hp, 220Nm, and about 160km of mixed driving. This car was firstly introduced in 2012 and so far more than 20.000 units were sold. Nissan Leaf, like ZOE, is a five-seater car with a pure electric powertrain but this one offers 110hp, 280Nm and 200km of autonomy. Nissan Leaf was firstly introduced in 2010 and presents about 170.000 units sold worldwide till today.

Figure 2.3 – Renault ZOE [27].

Figure 2.4 – Nissan Leaf [28].

USA and China presented also their highest EV sales value in 2014 (66.000 and 45.000 units respectively), according to China Association of Automobile Manufacturers (CAAM) and Electric Drive Transportation Association (EDTA) [29, 30]. In spite of such growth, a low volume sales concern remains, since the number of units sold is distributed among all current available EVs, i.e. even more marginal figures are expected by brand and vehicle model. Under this situation, the selection of materials, manufacturing processes and components configuration becomes challenging for automotive manufacturers, especially regarding the exterior body panels (see Figure 2.5).

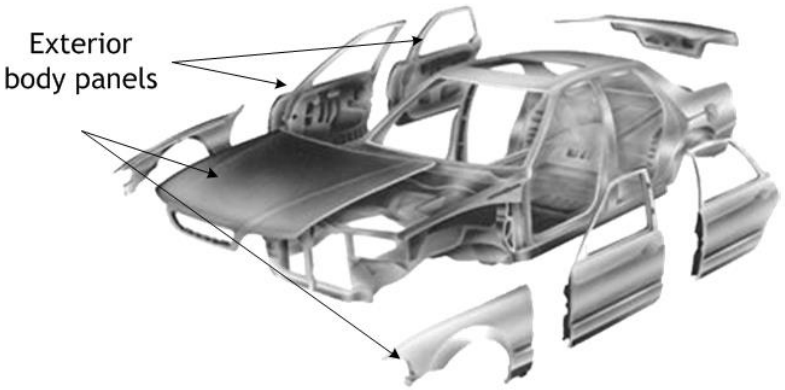

Figure 2.5 – Body panels example [31].

2.2. Materials and manufacturing processes for body panels

Current automotive design and manufacturing is metal-intensive, based on an infrastructure originated in the beginning of the 1900s. Actually, the traditional way of manufacturing exterior panels for automobiles is through metal stamping technologies and steel is the most common material since 1920s decade, because it can offer good strength and stiffness properties, even with very small thicknesses. This is something that nowadays is even more feasible by recurring to high strength steel (HSS). This material can offer high deep drawing formability, adequate plasticity and high impact absorbing capacity [3, 32, 33]. Projects like the Ultra-Light Steel Auto Body (ULSAB) [34] were even created, especially for design optimization methods for automotive body steel structures by studying concepts as hollow resistance and reliability. Last ULSAB studies states that it is possible to achieve 20% savings in body weight without any cost penalty recurring to advance steel alloys, as well as innovative fabrication and assembly processes [35]. It states also that about 25% weight saving, at an incremental cost of only 0.50€/kg may be achieved with advanced high-strength steels (AHSS) [36, 37].

In spite of its good mechanical properties, steel has an elevated density comparing to other materials, having the triple of aluminium (Al) and the quintuple of magnesium (Mg), and presents some corrosion problems too. Besides that, this solution entails a significant tooling investment which is not suitable for low production volumes. It also demands exterior surface (A class) quality control which, occasionally, is made through tactile verification at 100% of the car and other methods on random samples [38].

Al has considerably increased its market penetration in what respects to the body structure, mainly due to weight savings and the possibility of using the manufacturing infrastructure already conceived for steel [39]. Al body panels combine low density, high strength and excellent corrosion resistance, becoming a good choice for the automotive industry, even presenting some welding limitations [40]. About 50% of weight reduction can be achieved over conventional steel bodies and 20 to 25% over advanced steel concepts [35]. Al is produced in several alloys[1], but 5XXX and 6XXX series are the most common ones in the automotive industry. 6XXX series alloys, in spite of their elevated cost, are commonly used on outer panels where dent resistance and surface features are most important, while 5XXX

[1] Aluminum alloys 1XXX – Pure aluminum; 2XXX – Aluminum and Copper; 3XXX – Aluminum and Manganese; 4XXX- Aluminum and Silicon; 5XXX - Aluminum and Magnesium; 6XXX – Aluminum, Magnesium and Silicon; 7XXX – Aluminum, Magnesium and Zinc.

series alloys are used in inner panels and reinforcements, where these last mentioned issues are less critical [35, 41]. Besides all adequate attributes, the cost of Al per weight is higher than steel and requires more expensive tools to overcome forming issues, like increased springback effects. It requires also slower production volumes to prevent rupture and damage and the development of a stamping tool itself is also slow. These issues lead Al to be more used in high-end or high cadence vehicles [3, 42-44].

Mg, not so common as steel and Al, presents low density alloys but with some disadvantages such as poor creep resistance at temperatures above 100ºC and worst corrosion resistance than steel. Besides that, Mg presents even more expensive manufacturing costs than the other metallic materials [43, 45].

It is clear that the use of materials reliant on stamping processes, to give shape to the automotive body panels, only becomes profitable when the series to be produced have a considerable size, typically dozens or hundreds of thousands of units per year, something that nowadays is still inappropriate for EVs. While conventional automobiles keep using metal in their exteriors, it is estimated that EVs have to adopt non-metallic materials such as polymers or composites which are associated to more cost efficient manufacturing processes in narrowing production volumes. Its use is even supported by studies that estimates that by 2030 automotive manufactures will recognize polymers and composites as preferred material solution once they meet, in most of the cases, performance and sustainability requirements [33, 35, 36, 46-50]. In fact, the use of composite materials has been constantly increasing, once these material types are very sought by their high stiffness, strength, corrosion and impact resistance, as well as low density. Composites are a combination of a reinforcing material within a matrix material that together can provide specific properties, hardly obtained with one single material. While the reinforcement material provides enhanced strength and stiffness, the matrix material may provide enhanced stability and protection from corrosion. The matrix can be either thermoplastic or thermosetting, being thermoplastic such as polypropylene (PP), polyether-ether-ketone (PEEK), polyphenylene sulphide (PPS) and polyether-imide (PEI), mostly preferred over thermosettings due to its recyclability properties [51-53].

Carbon based composites are the first choice for first class applications, where the cost is justified by the high stiffness/weight ratios required, for instance, structural parts for sport car chassis or monocoque bodies. The production rate of such parts is usually small and the requirements high, as well as the cycle times, once the inherent processing technologies are typically based in compression moulding and autoclave. And since this material tends to be adopted by expensive brands, the manufacturers tend also to suggest a high retailing

price, high enough to recover the elevated costs. However, when tens of thousands of cars are annually produced, autoclave cure becomes too slow and expensive to be used [50, 54, 55].

In spite of manufacturing costs, the use of composites with carbon fibres can be already seen nowadays in the electric automotive industry. BMW I3, for instance, presents an exterior body (Figure 2.6) composed by PP with enclosed carbon fibres which is attached to a metallic tubular structure.

Figure 2.6 – BMW I3 with polypropylene body panels [56].

Glass fibre reinforced composites (GFRC) are employed to manufacture external body panels as rear body panels in many commercial vehicles through the use of sheet moulding compound (SMC), processed by heat compression moulding. In spite of the benefits of SMC, it may only be used for large production series of vehicles, presenting some recycling and repairing limitations and higher costs than steel. For small/medium production volumes, hand lay-up labour intensive techniques are usually employed to manufacture GFRC. However, these manufacturing processes have also some constraints like high manpower skills and respective cost.

Resin Transfer Moulding (RTM) process is a recurrent option which allows consistent quality and repeatability, reduced hand labour costs, good quality of the final product and economical results due to its non-expensive process equipment. RTM is highly adequate for production volumes of about 30.000 units per year. This process allows also the manufacturing of large and complex parts as well as the incorporation of metal inserts [46, 57-59]. However, surface class A through RTM is still challenging because it is highly dependent on material and process issues. Defects such as ripples, waviness, pinholes and sink marks, associated to a dimensional inaccuracy caused by resin cure shrinkage makes it

inappropriate for car body panels, once a considerable amount of rework is required [33]. Low profile additives (LPA) may be required to achieve such surface quality and this has generated motivation for research [59-61]. Later findings on this topic, refer that the addition between 10 to 20% of LPAs like Polymethyl-methacrylate (PMMA); Polyvinyl-acetate (PVA); Polystyrene (PS); Polyurethane (PUR) and Polyesters (PET) help to achieve surface roughness lower than 0.56μm (Class A reference for a painted steel sheet). However long cycle times are required even balancing gel times and resin injection pressures [3, 59]. In spite of GFRC attributes and the possibility of achieving enough surface quality, apparently none of the commercially available EVs present an exterior with this material.

More reduce cycle times can be achieved with polymers. However, apparently, its use without any reinforcement is not extensively applied within the automotive exterior body, apart from components where structural integrity is less required such as front fenders. This solution can even be seen in the Renault Zoe front fenders, where a modified polyphenylene ether (PPE), consisting in an amorphous blend with the polyphenylene oxide (PPO) and polystyrene (PS), called of Noryl™ has been applied. This material ensures high thermal and chemical resistance, good dielectric properties, excellent hydrolysis resistance, and dimensional stability with good inherent processability, as well as low density. The resin may be designed to replace many kinds of metal parts such as stamped steel, cast metal, and brass, even in functional assemblies. Besides the good properties of thermoplastics, their manufacturing costs are comparable to metal stamping, being again only adequate for high production volumes.

On other hand, thermosets have also been widely used in many external and inner parts of automotive and transportation vehicles due to their cost efficient potential resulting from their low processing pressure and tooling investment. While it may be considered necessary to develop new opportunities and methodologies to recycle thermosets and to accomplish future rules, the industry tends to implement them to obtain high enough environmental sustainable results. In spite of unsaturated polyesters (UP), epoxy (EP), phenol-formaldehyde (PF) and polyurethane (PU) being the mostly used resins, thermosets have other opportunities yet to be studied, such as PDCPD that is commonly processed by reaction injection moulding (RIM) and, accordingly to the objectives of this work, it was herein exploited as being a good solution for application in the exterior body panels of EVs.

2.3. Dicyclopentadiene RIM

RIM was developed by Bayer in 1969 and is a manufacturing process that, instead conventional shaping processes, involves chemical reactions to form physical objects. This is quite different from thermoplastic injection moulding (TIM) where mould cooling is used to form a solid polymer. In RIM process, fast reactions are required to form three dimensional polymeric networks. It is a process based in a combination of two or more liquid components inside a mixing head which are then injected into a mould where the polymerization takes place. The volumetric flow rates of the two reactants (A and B) are accurately controlled to provide the correct stoichiometric ratio and the complete cure.

RIM requires low temperature processing and due to the low viscosity monomers or oligomers used, it requires also low injection pressures [62-66]. With this, a higher range of materials may be used in the mould depending on the requirements. On the other hand it allows large and intricate parts to be moulded with lower clamping forces [67]. Figure 2.7 depicts the main architecture of a RIM system, while Tables 2.1 and 2.2 present the main differences between RIM and TIM and the main RIM process requirements.

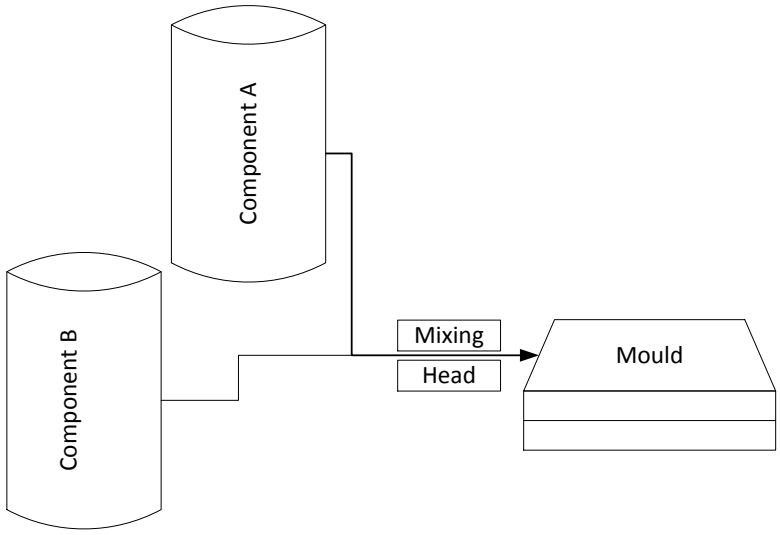

Figure 2.7 – Reaction injection moulding process diagram.

Table 2.1 – Main differences between the processing parameters of RIM and thermoplastic injection moulding (TIM) [68].

PROCESS PARAMETERS	RIM	TIM
Mould temperature [ºC]	70	25
Typical Injection Temperatures [ºC]	40	180-350
Material viscosity [Pa.s]	0.1 – 1	100 -100.000
Injection pressure [MPa]	0.1	1.5-40
Clamping force [1m^2 surface part] [ton]	50	150-4.000

Table 2.2 – Main RIM material requirements. (To) is the initial temperature, (η) is the monomer viscosity, (tg) is the glass transition temperature (ad) is the adiabatic temperature (Tdegrad) is the degradation temperature (tf) is the filling time (Tw) is the wall temperature [68].

PARAMETER	REQUIREMENT
Supply	Stable ≥ 1 week
	Pumpable
Condition	T_o <60ºC <150 (high temperature machine)
	Gas dispersion
Meter	Two components
	±0.5% stoichiometry
Mix	η < 1Pa.s
	Compatibility
	$t_{g.ad}$ > 0.1s
Fill	$t_{g.ad}$ > t_f > 1s
	η < 10 – 100 m Pa.s to prevent bubbles
Cure	T_w <100ºC <200ºC (high temperature mould)
	T_w < T_{degrad} < ΔT_{ad}
	Control by products
	Compensate for shrinkage
Demould	T_w < melting or phase mix temperature
	T_w > glass transition, precipitation
	3min (sufficient green strength), 45s (high production)
	Easy mould release
Finish	Minimum flash
	Minimize post cure
	Paintable

Besides the development and growth of RIM technology have always been associated to PU, other non-urethane chemical materials such as polyurea, nylon, PDCPD, EP and unsaturated polyester, have also been tried on this technology. For instance, nylon rim presented a slow but steady progress during the last decade. It consists in a copolymerization of nylon with an elastomer with different ratio values depending on the final use of the parts. Such combination allows reducing the viscosity of the material during the injection and the processing cost. This technology presents good ratio between stiffness and toughness. The resistance to fatigue and abrasion are also good, as well as the resistance to chemical compounds except to concentrated acids. In early 90s DSM tried this application in the automotive exterior body panels but without success, once this technology presents higher costs than other RIM technology [69]. Nylon, nowadays is mostly used in technical components and accounts for a presence of only 15 to 25kg per car [70].

Arising in 1980, dicyclopentadiene (DCPD) is a liquid engineered resin developed especially for reaction injection moulding (RIM), structural RIM (SRIM), RTM, near shape casting and rotational moulding. DCPD is a di-olefin monomer found in the off streams of petrochemical refineries used as a chemical intermediate for both flame retardants, EPDM elastomers and added to unsaturated polyester resin systems to enhance thermal stability. Dicyclopentadiene can be cracked into the monomer cyclopentadiene (C_5H_6) via thermal cracking and exists in two stereoisomers forms, the exo and endo isomers, being this last, the most common product sold as $C_{10}H_{12}$ (4,7·methano-3a,4,7,7a-tetrahydroindene) [68, 71].

The DCPD polymerization is based in metathesis chemistry and occurs via Ring Opening Metathesis Polymerization (ROMP). A more detailed description can be found elsewhere [62] and its molecular transformation process illustration can be seen in Figure 2.8. The polymerization results in a crosslinking process (three dimensional network structure) due to its highly exothermic reaction which starts from 40/60ºC till 150ºC. This reaction is promoted by various complexes of Tungsten and Molybdenum in conjunction with organo-metallic compounds of Al, Tin or Zinc. Other catalysts, such as *Grubbs* catalysts (based on transition metals) made the PDCPD polymerization more robust and reduces also its odour [64, 72-76]. The combination of those components could be set in order to control viscosity (which may vary from 170 to 330Cp), impact properties (which may vary from 4 to 4.6 J/cm) and its cycle time (which may vary from 4 to 10min). The material is self-demoulding, not requiring any releasing agents and its post-cure is also unnecessary [67].

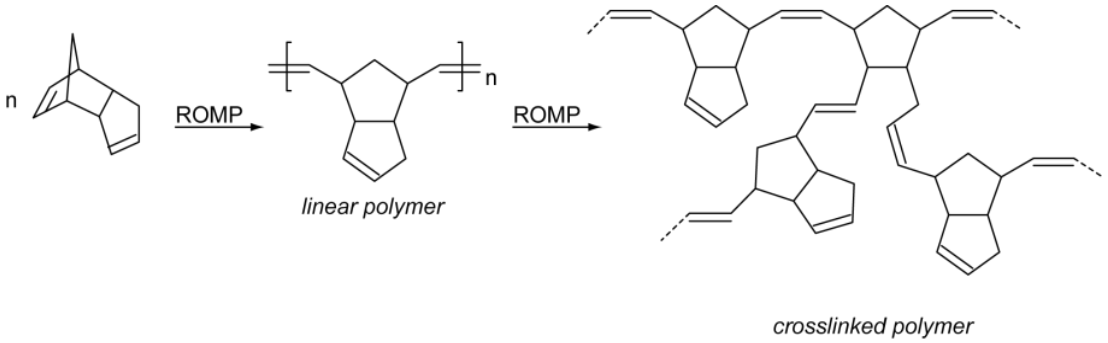

Figure 2.8 - Ring Opening Metathesis Polymerization of DCPD [73].

PDCPD varies from no colour to light yellow or orange depending on catalysts used and curing temperature. During the polymerization, an approximately 6% reduction in the volume of the liquid material happens as it solidifies into the mould. The average shrinkage is around 1%, on both parallel and perpendicular to the flow path. Part shrinkage depends on part thickness and can be controlled by process parameters, wall thicknesses variation and part design. A minimum amount of material needs to be injected in order to promote a proper reaction and a minimum thickness of 3mm is advised [64, 68, 77, 78]. This material ensures low density (1030 kg/m^3) and a great economic potential for low production volumes. Besides that, PDCPD presents good mechanical properties even at cryogenic temperatures, among them good impact resistance, good corrosion and chemical resistance even at extreme temperatures (from -40°C to +160°C), as well as fracture toughness, Class A quality surface and good paint adhesion. Additional studies even state that PDCPD is suitable for high voltage and frequency applications due to its low dielectric constant and high thermal stability [71-73, 77, 79].

PDCPD was firstly used on the manufacturing of exterior components for trucks and agricultural vehicles. It has also been used in the fabrication of snowmobiles, boat housings, chlorine cell covers, wastewater treatment equipment and even cryogenic tanks [6, 67, 74, 80, 81]. Currently, one of the most relevant applications for PDCPD is the bonnet on the new W900L model from Kenworth Truck Co, as can be seen in Figure 2.9. Here PDCPD replaced a spray-up GFRC at no additional cost and 38kg weight saving [5].

Figure 2.9 – Kenworth truck bonnet [82].

PDCPD was also applied on the restyled model of Buddy from Elbil Norge in Norway as may be seen in Figure 2.10. All exterior panels and some interior components were made of PDCPD, allowing 50kg weight savings compared to the previous model made in GFRC and ABS. With this material, the 400kg of total weight target, imposed by EC directives since 2005 for vehicles type L7, was accomplished.

Figure 2.10 – Elbil Norge buddy with PDCPD body panels [83].

For specific components, such as exterior body panels, PDCPD presents lower mechanical properties by its own, requiring the application of sub-structures or metallic stiffening reinforcements to avoid undesired deformations that can result from applied loads and/or thermal expansion generated by the exposure to high environmental temperatures.

The combination of PDCPD with other stiffer materials, such as metals, besides being challenging due to the inert molecular structure of PDCPD, that does not promote attachments to other molecules without recurring to conventional joint methodologies, can even have a positive outcome. This allows to form polymer-metal hybrid (PMH) components which allow a significant reduction of weight, while the structural integrity might be kept [39, 74].

2.4. Assembly

The emerging need for non-conventional materials, on exterior body panels, can have a positive influence on vehicles weight and cost. But the use of polymers, composites or even a materials mix, requires the analysis of adequate assembly processes, once combining dissimilar materials raise questions over service conditions, structural efficiency and joining performance [84, 85]. The joining methodologies available today for mixed material parts, like PMH ones, can be divided in three different categories: mechanical, welding and adhesive.

In mechanical joints, parts are fixed together through macroscopic, microscopic or any other physical interference. The most used type of mechanical fastenings are the self-tapping screws, clinching, riveting and overmoulding [86, 87]. Extensive literature about this topic is available elsewhere [51, 88-92].

Clinching is a well-known joining process used to create permanent joints without any material addition. This process has been growing replacing spot welding, especially in new alternative material applications [85, 93]. Clinching is a joining method based in the surface deformation through a punch and die tool. The deformation is created in both surfaces generating an interlocking geometry between them and no material is added. This has several advantages, among them, requiring simple equipment, low running costs and low cycle times (approx. 1.8sec per point). Besides such qualities, several authors are still working on the development of innovative clinching tools based in one single stroke in order to decrease, even more, the cycle time and material stresses [94]. Clinching requires also little surface inspection or preparation and ensures easy disassembling. The structural integrity of the joint is also well predictable through mechanical analysis. However, this process is highly dependent on the surface thicknesses and presents high concentrated stresses on the joints originating cracking most of the times by the polymeric element. Conventionally, thicker wall sections are required, in order to avoid stress concentrations, occurring in a weight

increment. It also requires the access to both sides of the joint narrowing the design freedom. The thermal expansion difference between components, as well as the humidity contributes also for poor joints quality [85, 89, 95, 96].

Riveting is other well-known mechanical fastening method. Depending on the type of rivet, it mainly consists in an introduction of a rivet into the component joint in order to fix both parts together. Among the wide range of riveting methods, self-pierce riveting is one of those most used in the automotive industry. It is based on a mechanical deformation of both materials to be joined during its penetration. Only one single operation is required even entailing high punching forces (approx. 40kN) [97].

Blind rivet requires a previous hole made through the components, which makes it less attractive for the automotive industry. The rivet is inserted and mechanically deformed in order to fix the parts together. Besides its ease of use, riveting leads to stress concentrations next to the holes region [89, 97].

Overmoulding consists in a process where the final part is assembled during the injection, i.e. both injection and assembly steps happen at once. It consists in the incorporation of an element inside the mould which is up to be involved by the polymer. The overmoulded element should contain interlocking geometries which may be achieved through special surface treatments, roughness, holes or indentations. Some authors have been trying this process through many techniques including multicomponent injection moulding. This joining method has many advantages, among them, the possibility of not having assembly operations contributing for the reduction of hand labour, materials and energy. Besides that, it allows the combination of different material properties in one single piece. However, some parts become more complex to be overmoulded, requiring extra treatments which may invalidate the non-existence of an assembly process in terms of time and costs. Also depending on the design requirements of the parts, the existence of holes may not be advised [98-101].

Clinching and riveting technologies can offer flexibility and low cost results but they must be avoided when aesthetical surface requirements are pursued, like Class A surface quality. Thus, considering the objectives of this work, these joining methods were not explored due to possible plastic deformations that might be caused by the process itself. On the other side, overmoulding offers some potential of being explored and was even tested, however it was found that it carries some risks and costs than could not be covered by the available budget. Supplementary work can be found elsewhere [102].

Welding is an alternative methodology to mechanically assembled joints. It consists in creating a joint where materials are joined through chemical bonds under localized heat and

pressure relying only on the natural tendency of atoms or molecules to attract one another and bond. This joining method has increased in parallel to the increasing use of plastics in the automotive industry. There are three welding types and they are based on the heating source: conductive, electromagnetic or frictional. Conductive heat welding is based on simple heat transfer by contact, while electromagnetic welding is based on heat transfer by convection or conduction. Friction welding is based on a relative movement and contact pressure of the parts to be joined.

Several welding technologies are currently available, among them friction stir welding (with linear or orbital vibration), spin welding, hot plate, electromagnetic, ultrasonic, infrared, laser and forced mixed extrusion technique. For instance, orbital friction stir welding, usually controlled through computer, presents an affordable technology with acceptable cycle times and some studies argue that it is even preferable over linear vibration and ultrasonic welding, once it does not decrease the strength of the welded components [70]. On the other hand, some studies reveal that, depending on thermoplastic specimens, resistance welding is preferred over friction stir welding by not causing internal microstructural damaging [103]. Some of them are more used within the automotive industry by presenting enhanced flexibility, reduced complexity and cycle times like fusion and resistance welding [85]. On the other hand, others are yet to be deeply explored in this area, even being known by their wide range of applications and finishing quality. However, due to the lack of compatibility with the molecular structure of PDCPD, this assembly methodology was not explored within this work.

Adhesive bonding arises as an alternative to mechanical or welded joints. It consists in a process of joining materials with aid of a substance able to hold materials together. Normally the materials to be joined are called adherents while the bonding material is the adhesive. It basically consists in a surface preparation of adherents through degreasing followed by the adhesive application and posterior joining of adherents under some pressure. Nearly all the types of materials can be bonded by adhesives. Such attributes have contributed for its use in the automotive industry[2] [97, 104-107]. In fact, adhesives have improved dramatically over the last decade and today the adhesive market inside the

[2] The use of adhesives in the automotive industry was firstly demonstrated in 1982 by Rover on a prototype called ECV3. It was a four-seater family car prototype built using an aluminum space frame chassis, co-developed with Alcan, and was the first ever bonded structure. Its body was made of polyurethane reinforced reaction injection moulding (PU-RRIM)). This trend was followed by other automotive manufacturers in specific vehicles like Jaguar XJ220, Ford AIV, Lotus Elise, and Honda NSX.

automotive sector accounts for 2 to 3 billion euros. It may be less than 10% of the global adhesives market but industry experts forecast the amount of glue used per car may grow by at least a third over the next 5 to 10 years [108].

The adhesives can be divided in four main categories: sealants, low strength adhesives, medium strength adhesives and high strength adhesives, being sealants and high strength adhesives the most used ones in the automotive industry.

Sealants have the aim of protecting the components from dust or even corrosion. They are usually applied after the assembly in body joints, spot welding and hem flanges. Anti-flutter, for instance, is a type of low strength adhesive and is applied between inner and outer panels acting like a soft elastic, adding stiffness and reducing the vibration effect between them. From the high strength adhesives we can find EP, PU and methacrylate (MMA). EP adhesives guarantee the stiffest bond and a great joint stability. Therefore, they are used where great loads are applied. It also offers good aesthetical results. The PU adhesive is used where elasticity requirements prevail i.e. where the absorption of vibrations and shocking is needed. The MMA presents a trade-off between EP and PU adhesive characteristics [109-111]. An example of the application of MMA in the automotive industry with enhanced lightweight results can be seen in the Lamborghini Murcielago (Figure 2.11). This vehicle has carbon epoxy panels bonded to a metallic chassis (steel and lightweight alloys) and the bonding time accounts for 30min cured at room temperature (RT) for about 2h.

Figure 2.11 – Murcielago body with carbon fibre panels bonded to a tubular steel frame [109].

The major advantages of adhesive bonds are the ease of manufacturing, allowing the possibility of bond dissimilar materials with improved aesthetical appearance and better stress distribution over the joint area. No holes are required to execute the adhesion and it even allows the combination of thin and flexible adherents. Besides that, it is one of the most satisfactory joining methods when reduction of weight is required. Disadvantages are associated to the need for preparing the adherent surface before preform the adhesion and to the difficulty of disassembling, when required. In terms of mechanical performance the adhesives may suffer from environmental conditions such as heat or humidity [105, 112, 113] and they act better only under shear loadings. Stiffness prediction is also difficult to obtain due to the large number of variables such as adhesive modulus, fillet and joint geometry, as well as bond line thickness. In fact, bond line thickness has generated motivation for research, once an understanding of the adequate thickness can guide the selection of an optimal bond line [114]. Some studies argue that lap shear strength decreases as the adhesive thickness increases [115-117], while others reported significant strength improvement with increasing thickness [106, 118, 119] or even no significant effect [120, 121]. Other authors argue that is just related to interface stresses [122] and coexistence of shear and peeling stresses in the joint [123]. Additional research based on linear elastic fracture mechanics test to characterize the crack propagation resistance of joints up to 3mm thick found an optimum joint thickness around 0.5mm [124].

In addition, adhesives do not properly combine with oiled parts that come from production, requiring post-process treatments like cataphoresis where washing, degreasing and additional corrosion resistant layers are applied. It also presents some disadvantages regarding to crash tests where they have tendency to peel during the adherent's deformation. In terms of manufacturability, it may require longer cycle times for curing and, because they are conventionally applied through robots, no much more than 3.000 units can be expected per year. Adhesives also present high buying and disposal costs, once dismantling, with the current available technologies, becomes challenging, ending always with unclean separations or undesirable gases from heat application [3, 86, 89, 107, 111, 115, 125-127].

2.5. Cost engineering

In a recent study, using a 2011 Honda Accord sedan as baseline vehicle, to evaluate the potential weight and cost savings by using alternative structural materials it was concluded that making a car entirely in Al would cut weight by 35% with $927 cost penalty. In contrast,

a car using a combination of advanced steel, Al, and polymers in strategic locations would cut weight by 24.5% with $319 cost penalty. A CFRP intensive vehicle would cut weight by half, but it would have $2.700 cost penalty [128, 129]. These conclusions can be obtained using a cost engineering tool, which allows measuring the costs of a product or service. These analyses are based in mathematical models which, depending on the complexity, may provide the total investment, breakeven values, and total manufacturing times by correlating materials, part attributes, manufacturing conditions and processes. These models are especially relevant for the automotive industry which is always seeking for new designs, materials and process technologies with reduced manufacturing costs [35, 130].

In spite of several models have been proposed, none have been widely disseminated and among the variety of mathematical models that may be adopted, within this work, there is the Process-Based Cost Model (PBCM), which consists in a mathematical transformation that accounts the manufacturing process conditions giving an output of cost. In order to build a PBCM, those elements that directly affect the cost must be isolated and the model shall be built backwards i.e. from the objective to the input that can be controlled [131-137].

Three main steps must be performed to build a cost model, and they are the following:

1 – Identify the relevant cost elements. Depending on each objective, the cost elements may vary in terms of importance, so that, they must be isolated according to the metric being pursued and they must be separated in two: fixed and variable. Fixed costs are those independent of output, which remain constant such as rents, buildings, manufacturing equipment, among others. Variable costs are those that vary according to the output and are commonly wage, materials, energy, etc.

2 – Establish contributing factors. After the selection of the most appropriated cost elements, the contributing factors must be established. They are those correlated to the manufacturing steps required to produce a part, like stamping forces, injection pressures, among others.

3 – Correlate process operations to cost and use. A list of contributing factors must be transformed into their costs, which may be done by determining the required quantity and its unit price, just like material cost. The same must be done for an equipment cost, which may be calculated through its overall cost and use factor required to produce a part.

2.5.1. Process-based cost modelling

As said before, a PBCM consists in a mathematical model which allows correlating part geometry, attributes and manufacturing conditions with an output of cost. This is a chain of events computed in such a way that all the variables associated to a part and manufacturing operation interferes with each other. In order to accomplish the objectives of this work, a cost model was developed and is detailed in the next few pages.

2.5.1.1. Main cost equations

All the costs are separated by variable and fixed according to the each element. Thus, the total cost per piece $C_{i,Total}$ for a given component or assembly is the sum of its associated cost elements, as may be seen in equation (2.1):

$$C_{i,Total} = C_{i,Variable} + C_{i,Fixed} \quad (2.1)$$

where,

$C_{i,Variable}$ are the variable cost elements

$C_{i,Fixed}$ are the fixed cost elements

Thus, variable and fixed costs are the sum of these elements considered for a hypothetical model, as may be seen through the equations (2.1.1) and (2.1.2).

$$C_{i,Variable} = C_{i,Material} + C_{i,Energy} + \cdots C_{i,n} \quad (2.1.1)$$

$$C_{i,Fixed} = C_{i,Equipment} + C_{i,Auxiliary} + \cdots C_{i,n} \quad (2.1.2)$$

Conventionally, cost models are based in a desired annual production volume input which is defined according to the volume that is intended to be sold $PV_{Saleable}$ in suitable conditions (without defects). Thus, in order to obtain each of these elements as cost per part, the annual cost of each element must be divided by the saleable annual production volume as shown in equation (2.2).

$$C_{i,El} = AC_{i,El} / PV_{Saleable} \quad (2.2)$$

where,

$AC_{i,El}$ is the annual cost associated with a given element El

$PV_{Saleable}$ is the annual production volume required for, i

The total cost of each element is the sum of those element costs calculated for each stage of a manufacturing process. For example, for a stamped part, costs would be calculated for the blanking operation (stage j = 1) and subsequent shaping operation (stage j = 2). These two sets of costs would be summed for the total stamping cost assessment according to the equation (2.3):

$$C_{i,El} = \sum_{j=1}^{n} C_{i,El}^{j} \quad (2.3)$$

where,

n is the total number of stages in the process

The effective production volume is an important variable used to calculate several cost elements, once it represents the number of gross units that must be produced to accomplish the desired number of saleable parts $PV_{Saleable}$. Once that, in process stage, j, a certain percentage of production might be rejected, x_j, the effective production volume at any stage j, $PV_{Effective}^{j}$ is calculated through the next equation (2.4).

$$PV_{Effective}^{j} = PV_{Effective}^{j+1}/(1 - x_j) \quad (2.4)$$

where,

for the final stage, when $j = n, PV_{Effective}^{j+1} = PV_{Saleable}$ it is possible to estimate the operating volume for any antecedent stage in terms of net desired output, $PV_{Saleable}$. The magnitude of flow changes from one step to the next due to the number of parts rejected at each step of the chain. Thus, the magnitude of that output, assuming that each step operates to satisfy the demand of the next, is established by its own yield and the production volume of those steps subsequent to it.

2.5.1.2. Variable cost equations

The variable costs for each stage are projected based on the effective production volume required for that same stage, but are allocated according to the net output of the process chain, as obtained through the previous equation (2.4). For instance, material accounting is based on the design of the component, the raw material price and the yield associated to each process and it may be divided in three main equations (2.5, 2.6 and 2.7). The gross material unit cost at stage j, $C_{i,Material}^{j,gross}$ is calculated using the following equation:

$$C_{i,Material}^{j,gross} = Total\ material_{Mass} \times U_{Material} \quad (2.5)$$

where,

$Total\ material_{Mass}$ is the total material mass required to produce a part. For example, in a stamping process, the total material mass accounts for a metal sheet weight before its shaping and trimming stages.

$U_{Material}$ the unit cost of the material, conventionally measured in €/kg

The annual material cost, for stage j, can be calculated according to the following equation:

$$AC^{j}_{i,Material} = C^{j,gross}_{i,Material} \times PV^{j}_{Effective} \quad (2.6)$$

The calculation of material costs in the assembly model is altered due to the fact that in assembly processes the material is usually some type of consumable. The calculation for annual material usage for assembly j, $AC^{Assm}_{i,Material}$ is calculated through the following equation:

$$AC^{Assm}_{i,Material} = \sum_M \sum_b U_M * PV_{i,Effective} * \gamma_{b,M} \quad (2.7)$$

where,

U_M is the unit cost of material M

$\gamma_{b,M}$ is the material usage per assembly of material M for joining method b

Energy consumption can be calculated from theoretical energy requirements for a part processing or, more correctly, including cycle times, press sizes and real world energy inefficiencies. In some cases, if needed, a linear regression with energy consumption versus press size is also acceptable. More simply, the energy cost for a process stage can be calculated as the product of the energy usage for the equipment at that stage and the unit cost of energy. This is shown through equation (2.8):

$$AC^{j}_{i,Energy} = E^{j} \times U_{Energy} \times PV^{j}_{Effective} \quad (2.8)$$

where,

E^j is the energy usage per unit for the machine at stage j

U_{Energy} is the unit cost of energy in €/kWh.

Other variable cost, for instance, is the labour cost, which is a function of the wages paid, the number of labourers necessary to run the process, the paid operating time and productivity efficiency. The labour cost is divided, this way, in two main equations (2.9 and 2.9.1):

$$AC_{i,Labor}^{j} = N_{Labor}^{j} \times U_{Labor}^{j} \times T_{Labor}^{j} \quad (2.9)$$

where,

N_{Labor}^{j} is the number of labourers required for that stage

U_{Labor}^{j} is the unit cost of labour usually in €/hr

T_{Labor}^{j} is the amount of total paid labour time required for that stage

Conventionally, the total paid labour time, T_{Labor}^{j} is accessed by calculating the total time available to work in one single year and can be described by the equation (2.9.1).

$$T_{Labor}^{j} = \frac{PV_{Effective}^{j} \times Cycle\ time^{j} \times \mathrm{D}_{Labor}^{j}}{\Gamma_{Labor}^{j}} \quad (2.9.1)$$

where,

$Cycle\ time^{j}$ is the amount of time required to produce one batch of parts per stage

D_{Labor}^{j} is the percent of labourers dedicated time to process stage j

Γ_{Labor}^{j} is the percent of labour efficiency

2.5.1.3. Fixed cost equations

As mentioned before, the fixed costs are those independent on the output volume. Fixed costs are usually divided in two groups: on one hand, those which are based in one-time capital payments and, on the other hand those which represent recurring payments. Recurring payments, like building rent, are easily annualized or converted to any pertinent time period basis, however those one-time based, require its cost spreading by the whole production phase of a given part. This ways, the annual cost for any given fixed cost element is calculated using equation (2.10).

$$AC_{i,Fixed}^{j} = R_{El}^{j} \times LR^{j} \tag{2.10}$$

where,

$R_{i,El}^{j}$ represents the annualized investment cost for a given resource

LR^{j} the number of parallel sets required to produce the component

For an effective cost projection of a manufacturing equipment, its cash flows shall be allocated to specific components and process stages according to the operating time. Given that capital equipment tends to have a usable lifetime greater than one product life cycle, these costs are also modelled as uniformly distributed over the equipment lifetime. To take into account the opportunity cost of having funds invested in capital equipment; a capital recovery factor is commonly used. Thus, the annual assigned cost for a given resource, R_{El}^{j}, for process stage j is shown in equation (2.10.1).

$$R_{El}^{j} = I_{El}^{j}\left[\frac{(d(1+d)^{S_{El}})}{((1+d)^{S_{El}}-1)}\right] \tag{2.10.1}$$

where,

I_{El}^{j} is the required investment for the fixed cost element for process stage j

d is the periodic discount rate

S_{El} is the usable lifetime over which the investment should be distributed. The usable lifetime may be different for each of the cost elements i.e. tool lifetime is usually in line with the product lifetime itself, once it is only used to produce that same product. On the other hand, equipment lifetime is usually higher, once it can be used to produce more than one type of product.

Equipment is a type of one-time payment and it should be annualized over the number of productive years. This productive life is usually longer than the number of years over which an individual product is made, thus, it is useful for models to incorporate equipment cost by compute how many pieces of equipment, working in parallel, are required to produce a specified number of parts in the required time period. The number of parallel lines required to produce a given production volume for process stage j, LR^j, is calculated using equation (2.10.2):

$$LR^j = reqLT^j / availLT^j \tag{2.10.2}$$

where,

$availLT^j$ is the available production time for process stage j

$reqLT^j$ is the time required to produce the necessary quantity of parts in stage j.

If a fixed cost is dedicated, LR^j is rounded to the next highest whole number (i.e., the entire yearly cost is attributed to the component even if there is only fractional usage). If the fixed cost is non-dedicated, it is assumed that fixed cost element is shared with some other product, and, this ways the fractional usage is attributed to the component. For the purpose of this work, only tooling costs are dedicated while all other fixed cost elements are non-dedicated. The investment required is projected based on the number of lines or equipment required. Besides that, in some cases, for a given main equipment investment, there is a corresponding investment in an auxiliary equipment. Consequently, in the absence of detailed production facility information auxiliary equipment costs can be estimated as a fixed percent of the main machine cost.

Other elementary cost is the overhead. It is a cost of operational overhead, including all those resources not directly involved in manufacture, is a figure which can be difficult to relate to features of a process, but which can represent a significant expenditure. One

approach is to estimate this cost using a burden rate which is applied against the magnitude of the other fixed costs.

Available time is fundamental to production cost. It represents the time when the work can be performed. It is obtained by multiplying productive working hours per day by the number of working days per year. Thus, the available production time for process stage *j* can be obtained with equation (2.11):

$$availLT^{j} = ODY \times (DS \times (ST - NO - MB - UDS^{j})) \quad (2.11)$$

where,

ODY is the operating days per year,

DS, is the number of daily shifts,

ST, is the number of working hours per shift.

NO, is the time when there is no operations or breaks per shift,

MB, is the time dedicated to maintenance operations per shift,

UDS^{j}, is the time of unplanned downtime that may occur per shift for a stage j. This time is dependent on the type of equipment or machine used.

Last but not least, the time required to produce the necessary quantity of parts for stage j, $reqLT^{j}$, can be calculated using equation (2.12)

$$reqLT^{j} = Cycletime \times PV^{j}_{Effective} \quad (2.12)$$

where,

$Cycletime$, is the time to produce a part. It is determinant for many elements of manufactured part cost. For fixed costs, cycle time influences the number of parallel streams

necessary to achieve a specified production volume. Similarly, variable costs, like labour and energy, are directly dependent on the time it takes to complete the production process. Besides that, in some processes, cycle time is proportionally dependent from a given part properties. This value may be achieved by several ways, among them, through approximation or, more rigorously, through the measurement of a chain of events that are required to produce a part in a stage.

2.6. Environmental concerns

Current car manufacturing including press, body, painting and assembling may consume up to 700kWh/vehicle, what is about 9 to 12% of the total manufacturing cost, and the electricity consumption average in vehicle assembly plants is about 80kWh/car, just for welding's stage [9, 12, 138-141]. However, the energy consumed during the vehicle operation phase is the most predominant during overall life cycle, accounting for 85 to 92% of the total, depending on the environmental properties of the materials, the manufacturing process used and vehicles weight. Reducing the vehicles weight can in fact to reduce the environmental impact, as it has a direct relation to increased fuel efficiency and reduction of the total energy consumption over its life cycle [46, 142-144]. This is proven by additional studies that, based on materials substitution for a lift gate inner, found that, although Al production is about 10 times more energy-intensive than steel, the total life cycle energy consumed by Al is less than that of conventional steel of about 1.8 GJ/vehicle, being the most difference at the vehicle operation phase due to improved fuel economy obtained from light weighting [144].

Besides manufacturing and vehicle operation phase present the highest environmental impact, recycling has also a measurable impact over vehicles life cycle. For instance, in a waste management study, it was estimated that approximately 1.9 to 2.3 million tons of automotive residues are generated annually which accounts for 10% of the total number of hazard wastes and up to 60% of the total shredding wastes [111].

Among the several material types used within a vehicle, composites and polymers arises as great contributors for the environmental impact. At present there are very limited commercial recycling operations for main stream composite materials due to technological and economic constraints even existing several recycling types such as mechanical, thermal and chemical. Mechanical recycling allows shredding and gridding in order to facilitate the subsequent screening to separate fibre from resin. The thermal processing uses high

temperature between 300 and 1.000ºC to decompose the resin and separate the fibres which are regenerated while the secondary fuel or thermal energy can be obtained through pyrolysis, gasification or combustion. The chemical recycling is based in depolymerisation but presents lack of flexibility, generating waste chemicals with increased environmental impacts [3, 52].

Besides the previous recycling technologies being also available for polymers, these are still not proper recycled due to technological, political and economic barriers. Inadequate labelling, sorting technologies and concerns with efficacy and appearance of recycled plastics, or even difficulties to efficiently identify among many different plastics types. Polymers still end up regularly in landfills [145]. In addition, once polymers presented a growth of about three times over the last 30 years, the demand for petroleum/virgin resins has also increased leading for a great environmental impact special caused by the intensive energy required for extraction and refinement [146-149].

This situation leads to an increasing public and legislation awareness over environmental impact and consequently significant pressure in the automotive industry to come up with more environmental friendly vehicles. It is expected that legislation will continue to affect automotive industry by changing the future design and the development and use of new materials and manufacturing technologies. Among all legislations, the most influential is the End of Life Vehicles (ELV) Directive 2000/53/EC and it was considered within this research study for project evaluation. This directive states that all EU members must ensure that ELVs are transferred for Authorized Treatment Facilities (ATF) in order to correctly proceed to the depollution, dismantling and deregistration, while automotive manufacturers are encouraged to reduce the hazardous substances and increase the use of reusable and recovery components up to 95% and the reuse and recyclable ones up to 85% after 1st January 2015 [47, 111]. Figure 2.12 depicts a representative diagram of the Directive 2000/53/EC.

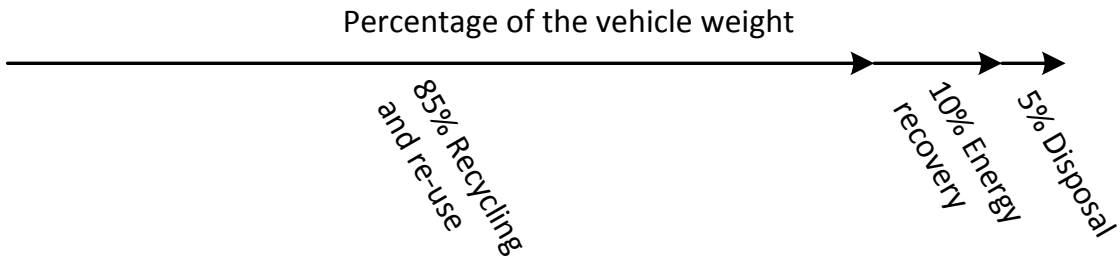

Figure 2.12 – ELVs Directive EU 2000/53/EC objective.

2.6.1. Life cycle analysis

To come up with environmental studies such as those stated previously, a Life Cycle Assessment (LCA) was built. LCA is a method to account for the environmental impacts associated with a product or a service from its origins to the end of life. According to ISO 14001 [150] an LCA can be divided into three main phases: (a) Production phase, including energy requirements for primary and secondary materials used and all the processes involved in manufacturing them into a finished product; (b) Use or operation phase, including the energy, fuel and emissions over the entire lifetime of the product; (c) End-of-life phase, including the energy used in disposal of the discarded product and whatever energy is gained from its recycling. In other words, it takes into account all energy and material flows through the production, use and end of life with aim of identify the sources that most contribute for the environment impact. An LCA may have different outputs types, being CO_2 emissions and energy consumption the most common. [12, 140, 151, 152]. Lifecycle assessment is currently used in the automotive industry too, in order to measure the energy required during the complete life of a car. The automotive LCA model can be summarized into four main stages: raw material processing, manufacturing, use and reclaim, as can be seen through Figure 2.13 [140, 153-156].

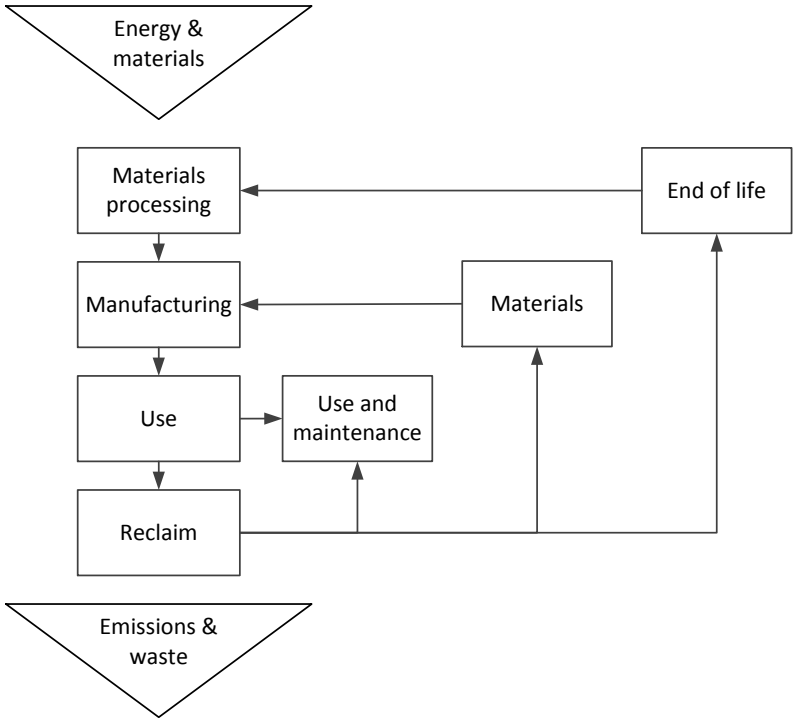

Figure 2.13 - Vehicles life cycle [140].

2.6.1.1. Life cycle assessment equations

For this specific work, only energy was measured, since the CO_2 emissions may vary from energy source and its own efficiency. Thus, the total energy required for the life cycle of the bonnet is obtained thorough a sum of the energy required over the four stages presented before in Figure 2.13 and it can be seen through the following equation (2.13):

$$Energy_{Total} = Energy_{Materials\ processing} + Energy_{Manufacturing} + Energy_{Use} + Energy_{Recycling} \quad (2.13)$$

where,

$Energy_{Materials\ processing}$, is the energy required to process the materials, including extraction.

$Energy_{Manufacturing}$, is the energy required for the production of a given component.

$Energy_{Life}$, is the energy spent during its useful life.

$Energy_{Recycling}$, is the energy spent or gained from the recycling process. At the end of a product life, several recycling strategies are available, among them reuse, recycling, down cycling, combustion (for energy recovery) and landfill. For all types, energy spent/recovered from recycling can be achieved through equation (2.14):

$$Energy_{Recycling} = Energy_{disposal} + Energy_{End\ of\ life} \quad (2.14)$$

where,

$Energy_{disposal}$, is the energy required for collection and sorting, which depending on the materials, it might include, at most, one collection and two sorting phases. For collection, primary and secondary sorting energy calculation, factors of 0.2, 0.3 and 0.5 are respectively attributed. Thus, the total disposal energy is obtained by multiplying the mass of the part/material by the factor in which is being processed. For parts/materials being

landfilled, the $Energy_{Recycling} = Energy_{disposal}$, since no additional sorting phases are required.

$Energy_{End\ of\ life}$, is the end of life of the part or material. For instance after collection and sorting phases, parts or materials might be down cycled and reintroduced in the life chain with inferior quality or incinerated in order to allow recovering energy from them. For down cycle and heat recovery, the following equations (2.15) and (2.16) shall be adopted, respectively:

$$Energy_{End\ of\ life} = \beta \times \left(Energy_{Recycling} - Energy_{Embodiedmaterial}\right) \times Mass \quad (2.15)$$

where,

β, is the nominal down cycle factor, as 0.5 for metals and 0.2 for plastics [157].

$Energy_{Recycling}$ is the energy required on recycling,

$Energy_{Embodiedmaterial}$ is the energy embodied on the material,

$Mass$, is the mass of part.

$$Energy_{Incineration} = -H_{Combustion} \times Mass \times Efficiency_{Combustion} \quad (2.16)$$

where,

$-H_{Combustion}$, is the material heat energy (MJ/kg),

$Mass$, is the mass of part,

$Efficiency_{Combustion}$, is the combustion efficiency (0.25) [158].

2.7. Objectives of the work

The enhancement achieved by using PDCPD as exterior material in EVs, in both physical and economical ways becomes the main objective of this research. For this a PMH automotive bonnet based in PDCPD and metal assembled through an adhesive bonding was created. By going through of all development process, an answer to the following objectives is aimed to be found:

1. **Is PDCPD a promising material to fabricate the exterior body panels for EVs subject to low production volumes?**

As promising material, metrics like cost and weight shall be obtained in order to compare it with current market solutions.

2. **Since PDCPD requires attachment to other stiffer materials, can it be attached to a stamped part with a cost efficient result and what are the economical limits?**

Metrics like cost and assembly cost penalty shall be compared to current market solutions.

3. **What are the environmental penalties of the solution pursued?**

This objective aims to achieve and measure metrics related to energy demanding and CO_2 emissions during the life cycle of the technology developed herein.

4. **Is this solution adequate for the new end of life vehicles legislations?**

Fourth objective aims to understand if the PDCPD adoption is in line to the latest environmental legislations.

3. Bonnet development

The design and development of an automotive exterior body panel based in a polymer-metal hybrid configuration (PMH), containing polydicyclopentadiene (PDCPD) and stamped metal is covered in this section. For this, the bonnet from the MobiCar depicted in Figure 3.1, was selected to be fabricated due to economic reasons and lower analysis complexity in what respects to the structural requirements [159].

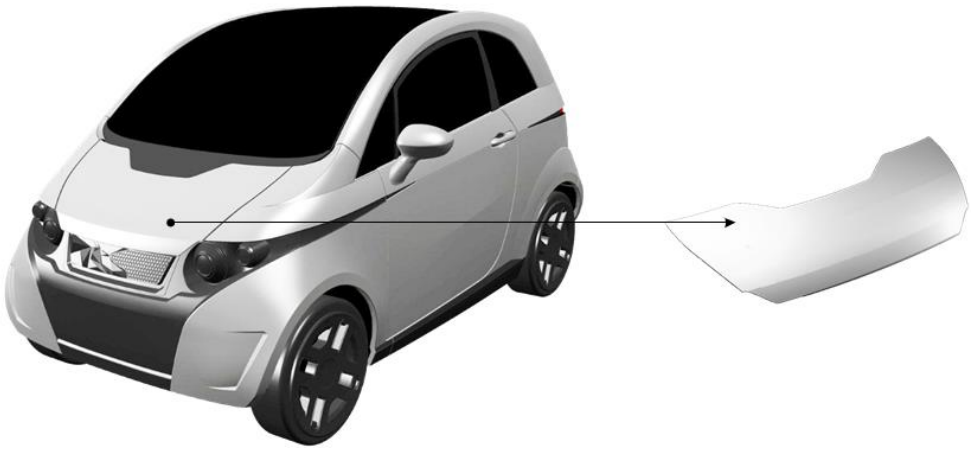

Figure 3.1 – MobiCar and bonnet.

Materials used in the bonnet development whether polymeric or metallic, including adhesives are firstly introduced in this section. Their mechanical properties are identified and then used in finite element analysis (FEA) simulations during the design and optimization phases. Design phase count on the development of three frames and subsequent selection of the most adequate geometry. This geometry was then enhanced during an optimization phase.

Bonnet prototyping section covers the development of both panels (interior and exterior) and its assembly. The interior panel was manufactured through metal stamping, while the exterior panel was manufactured through reaction injection moulding (RIM) and

both were assembled through adhesive bonding. Tools used on the bonnet prototyping are also described within this section.

Prototype validation was performed in two ways, dimensionally and mechanically. A 3D scanning equipment allowed to make a dimensional control over the metallic frame, while a mechanical testing machine together with a positioning structure allowed to perform a mechanical analysis by imitating the same conditions adopted in the FEA simulations.

In order to initiate the bonnet development, the following objectives where defined:

1. Minimize weight - The development should consider a lightweight design with less features possible and shall be assembled in such fashion that its weight increment remains the lowest.

2. Maintain an adequate structural performance - The mechanical properties of the components should be kept according to the structural quality requirements imposed by Centre of Excellency and Innovation for Mobility Industries (CEIIA).

3. Minimize assembly operations - By reducing the number of assembly operations it is expected to decrease both production costs and cycle times.

4. Minimize costs - Cost is one of the most important issues to be analysed herein, once low production volumes are inherent to this kind of vehicles. Thus, the costs of the explored technologies shall remain cost efficient at 10.000 units per year.

5. Reduce environmental impact – Environmental impact must be kept as low as possible, however, once the materials and the manufacturing technologies have already been nominated, it becomes pertinent to measure their impact and compare them with other solutions.

3.1. Materials selection and testing

According to the objectives of the project and consortium, available suppliers and budget, PDCPD, steel and aluminium (Al) were predefined as materials to be explored. Nowadays, there are two main PDPCD suppliers: one is Metton America, existing since 1995 and the other is Telene that exists since 2000 resulting from and joint venture of BFGoodrich and Advanced Polymer Technologies [5].

As Telene is the CEIIA´s dicyclopentadiene (DCPD) supplier, it was also adopted in this work. Taking into account the availability and the variety of Telene products, Telene 1650 series A and BK was selected due to its balanced properties between density, cycle time and mechanical properties.

Once the consortium of this project is composed also by a company with a wide experience in metal stamping (INAPAL-Metal), steel and Al became the materials choice for the bonnet reinforcement, while stamping the main process to fabricate it. Thus, steel EN10152 DC04+ZE and Al alloy AW5754-H111 were used in this study due to their availability and adequate mechanical properties on both structural and deep drawing formability, which are high demanded for this type of automotive components manufacturing.

Several adhesives were thought to be used in the assembly but only epoxy (EP) (Araldite 2015 from Huntsman) and methacrylate (MMA) (M7-15 from Crestabond) were considered, due to their inherent properties and respective supplier's availability. In order to select the most adequate they were tested with the materials previously mentioned.

3.1.1. Polydicyclopentadiene

Current technical data sheet from Telene 1650A/BK series ensure 43MPa and 1.87GPa of tensile strength and tensile modulus respectively as can be observed in Table 3.1 [160, 161]. However, due to some processability variations and uncertainty, these values were reviewed by recurring to PDCPD samples testing.

Table 3.1 – Technical data from Telene 1650A/BK.

PROPERTY	VALUE
Density [kg/m^3]	1030
Tensile strength [MPa]	43
Tensile modulus [GPa]	1.9
Poisson's ratio [v]	0.39
Thermal expansion coefficient	90×10^{-6} ºC^{-1}

In order to carry on the PDCPD tests, the standards for determining tensile strength of rigid plastic (ASTM D 638) were reviewed. Five specimens were machined from a rigid block made from a standard mixture of DCPD A and BK components (3a,4,7,7a-tetrahydro-4,7-methanoindene). Figure 3.2 shows the geometry of the specimens where *La*=200mm, *w*=10mm and *ta*=5.5mm.

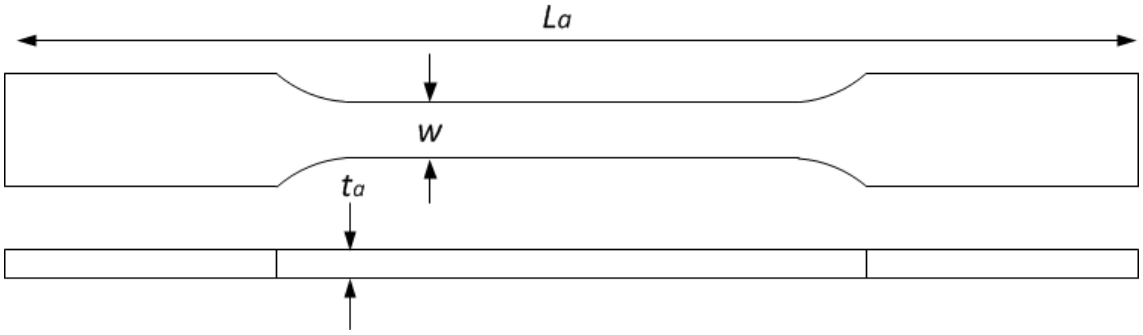

Figure 3.2 - Specimen geometry for the tensile test in accordance to standard.

Specimens were submitted to tensile tests in an Universal machine system Shimadzu AG-X-100KN with a load cell of 100kN. A 50mm extensometer was applied and the speed test was set to 2mm/min. The specimens were placed in the machine with 100mm distance between grips. Table 3.2 shows all the values obtained with this material.

Table 3.2 – Specimens results.

SPECIMENS	THICKNESS [mm]	WIDTH [mm]	MAX σ [MPa]	*E* [GPa]
1	5,55	9,91	45,06	2.01
2	5,47	9,94	41,70	1.93
3	5,56	10,00	44,87	2.03
4	5,57	9,96	43,91	1.92
5	5,54	9,92	44,56	2.03
Mean	5,54	9,95	44,02	1,98

An average value of 44.02MPa and 1.98GPa was found for the max tensile strength and tensile modulus respectively, which are slight higher than those defined by Telene. Poisson's ratio was not measured due to equipment limitations. Considering this, the technical data sheet information (Table 3.1) may be accepted as consistent for this research work being

these values considered for FEA simulations. Additional charts related to this test can be found in the Section A of the Appendices.

3.1.2. Metals

Metals are commonly used within the automotive industry and are currently well defined, not requiring, for the aim of this research work, additional tests. Thus, metals are only described herein by their own properties.

Steel EN10152 DC04+ZE is a carbon steel coated with a zinc layer ensuring good corrosion resistance. It has also excellent weldability due to the uniformity and regularity of the zinc coating. Tables 3.3 and 3.4 show the chemical composition and mechanical properties of this steel grade which can be obtained elsewhere [161, 162].

Table 3.3 – EN10152 DC04+ZE chemical composition.

CHEMICAL ELEMENT	PERCENTAGE [%]
Carbon (C)	0.08
Manganese (Mn)	0.40
Phosphorus (P)	0.03
Sulphur (S)	0.03
Silicon (Si)	0.03

Table 3.4 –Properties used in this work for steel EN10152 DC04+ZE.

PROPERTY	VALUE
Density [kg/m^3]	7850
Tensile strength [MPa]	360 – 510
Tensile modulus [GPa]	210
Poisson's ratio [v]	0.30
Thermal expansion coefficient	13×10-6 ºC^{-1}

Al alloy AW5754-H111 presents excellent corrosion resistance especially to salt and polluted atmospheres being specially indicated for vehicle bodies and shipbuilding. Its

chemical structure and mechanical properties are presented in Tables 3.5 and 3.6 and can be obtained elsewhere [163].

Table 3.5 – AW5754-H111 chemical composition.

CHEMICAL ELEMENT	PERCENTAGE [%]
Magnesium (Mg)	2.60 - 3.60
Manganese +Chromium (Mn + Cr)	0.10 – 0.60
Manganese (Mn)	0.0 – 0.50
Silicon (Si)	0.0 - 0.40
Iron (Fe)	0.0 - 0.40
Chromium (Cr)	0.0 - 0.30
Zinc (Zn)	0.0 - 0.20
Titanium (Ti)	0.0 - 0.15
Copper (Cu)	0.0 - 0.10

Table 3.6 – Properties used in this work for aluminium AW5754-H111.

PROPERTY	VALUE
Density [kg/m^3]	2660
Tensile strength [MPa]	190 – 260
Tensile modulus [GPa]	68
Poisson's ratio [v]	0.30
Thermal expansion coefficient	24×10^{-6} ºC^{-1}

3.1.3. Adhesives

The two adhesives selected for this work (MMA Crestabond M715 and EP Araldite 2015) might behave differently when in contact to different adherents and these values can be found elsewhere [164, 165]. A summary of the adhesive strength demonstrated by each supplier for a single lap joint test is presented in the Table 3.7.

Table 3.7 – Adhesives performance over different adherents in single lap joint testing.

ADHERENT	CRESTABOND M715 [MPa]	ARALDITE 2015 [MPa]
Steel	19	20
Aluminium	21	17
Polymers[3]	14	<5
Glass fibre	<10	<10

Besides the existing information covering several material types, lack of information with PDCPD adherents and the specific metals used in this work have triggered this analysis. In addition, once it is known that adhesives might require metal treatments, like cataphoresis, in order to eliminate possible oiled surfaces, some treated adherents were also tested in order to evaluate such conditions.

Single lap joint tests were carried out. The standards for determining the shear strength of adhesively bonded plastic (ASTM D 3163-01) and adhesively bonded metal specimens (ASTM D 1002-01) where reviewed and the results were obtained with the following expression (3.1), which represents the average shear stress for a single lap joint [166]:

$$\tau = \frac{F}{La \cdot w} \tag{3.1}$$

where,

F is the load

La is the length

W is the width of the joint

[3] It includes an average value for polymers like ABS, PVC, PMMA, Polycarbonate, Polyamides and Acrylic.

This expression does not predict the bending effects resulting from the deformation of the substrates, which demanded the fabrication of compensated ones, as shown in Figure 3.3. Thus, an increment of thickness on the substrates grip zone was created in order to reduce the axial stress resulting from a non-uniform shear deformation.

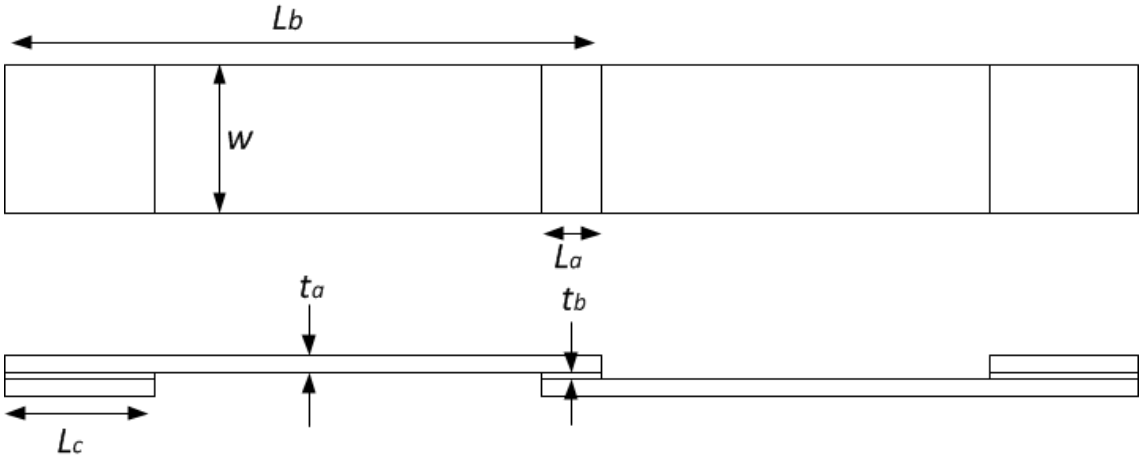

Figure 3.3 - Specimen geometry for adhesive testing.

Five different specimen types were fabricated for each of four types of substrate materials: steel; treated steel, Al and PDCPD. Twenty five PDCPD substrates were produced through milling from a rigid block with two different thicknesses: 7mm and 3mm. Table 3.8 shows the specimens configuration. The thicker specimen (7mm) was used to form a mono-material joint, and the thinner (3mm) was used for a hybrid joint. Forty substrates of steel were cut from a sheet through guillotine cutting. Half of them were submitted to a cataphoresis treatment. For the Al substrates also twenty five were cut from a metal sheet by guillotine cutting.

Table 3.8 – All substrates dimensions and quantity produced.

		DIMENSIONS [mm]					
QUANTITY	**MATERIAL**	***W***	L_a	L_b	L_c	t_a	t_b
20	PDCPD	25	10	100	25	7	0.3
5	PDCPD	25	10	100	25	3	0.3
20	Steel	25	10	100	25	1.4	0.3
20	Treated steel	25	10	100	25	1.6	0.3
25	Aluminium	25	10	100	25	2	0.3

For all substrates, manual abrasion through sand paper *P100* with subsequent manual degreasing was applied. For PDCPD substrates was adopted a manual degreasing with 96° ethylene alcohol while for metallic subtracts was adopted a manual degreasing with acetone. For hybrid specimens only degreasing was adopted. For all adhesive thickness, 0.3 mm was considered, which allowed accomplishing the manufacturer recommendation of using a glue thickness between 0.1 mm and 1mm. This value is also mentioned in several other relevant studies [106, 115-122, 124]. An adhesive overlap bonding (*La*) of 10mm was created in all specimens in order to facilitate the adhesive strength once shorter joints contribute to most reliable results [167].

Different curing times are advised by manufacturers. The EP gel time is about 30 to 40 minutes, while MMA gel time is about 10 to 20 minutes, considering a 1:1 mixing ratio. Also the fixture time is different, varying from 4 to 6 hours for EP and 30 to 45 min to MMA. For this work, the cure of all specimens was performed at room temperature for 5 days before testing.

All specimens were named based on its configuration in order to simplify data analysis. Their reference names were based in the first adherent material plus the adhesive plus the second adherent material. Steel adherents were named as “ST”, and those submitted to cataphoresis were named as “KTL”. PDCPD was named as “DC” and aluminium as “AL”. The adhesives were named according to the manufacturer name, being MMA Crestabond M7- 15 named as “C715” and EP Araldite 2015 as “A2015”. A summary of the all configurations is presented in the Table 3.9.

Table 3.9 – Specimens reference.

SPECIMEN	FIRST SUBSTRACT		ADHESIVE		SECOND SUBSTRACT	
REFERENCE	MATERIAL	THICKNESS [mm]	TYPE	THICKNESS [mm]	MATERIAL	THICKNESS [mm]
STA2015ST	Steel	1,4	Epoxy	0,3	Steel	1,4
STC715ST	Steel	1,4	MMA	0,3	Steel	1,4
KTLA2015KTL	KTL	1,6	Epoxy	0,3	KTL	1,6
KTLC715KTL	KTL	1,6	MMA	0,3	KTL	1,6
ALA2015AL	Aluminium	2	Epoxy	0,3	Aluminium	2
ALC715AL	Aluminium	2	MMA	0,3	Aluminium	2
DCA2015DC	PDCPD	7	Epoxy	0,3	PDCPD	7
DCC715DC	PDCPD	7	MMA	0,3	PDCPD	7
ALC715DC	Aluminium	2	MMA	0,3	PDCPD	3

The specimens were tested at room temperature in an Universal testing machine Shimadzu AG-X-100KN, using a 100kN load cell with a span distance of 140mm between supports and 1mm/min speed. All specimens presented coherent results regarding to the type of failure obtained. Only one sample had failure on the substrate side. A mixture of cohesive and adhesive failure was identified in whole mono-material Al samples. Table 3.10 and Figure 3.4 show the various type of failure achieved in the tests.

Table 3.10 – Tensile test results (SF) is the substrate failure, (CF) is the cohesive failure, (AF) is the adhesive failure).

	SPECIMEN NUMBER				
REFERENCE	**1**	**2**	**3**	**4**	**5**
STA2015ST	AF	AF	AF	AF	AF
STC715ST	CF	CF	CF	CF	CF
KTLA2015KTL	CF	CF	AF	CF	CF
KTLC715KTL	CF	CF	CF	CF	CF
ALA2015AL	CF+AF	CF+AF	CF+AF	AF	CF
ALC715AL	CF+AF	CF+AF	CF+AF	CF+AF	CF+AF
DCA2015DC	CF	CF	CF	CF	CF
DCC715DC	CF	CF	CF	CF	CF
ALC715DC	CF	CF	AF	SF	CF

The whole steel sample bonded with EP presented strength values of about 10 to 14MPa while MMA presented 10 to 15MPa. MMA presented also larger deformations than the EP (approx. 0.5mm). The adherents submitted to the cataphoresis treatment have shown the biggest increment in adhesive bond strength. A maximum of 25MPa was obtained, which is the best case studied. It can be concluded that, besides requiring additional processes, cataphoresis is highly advised, once it provides a substantial strength increment of about 40% comparing to non-treated steel.

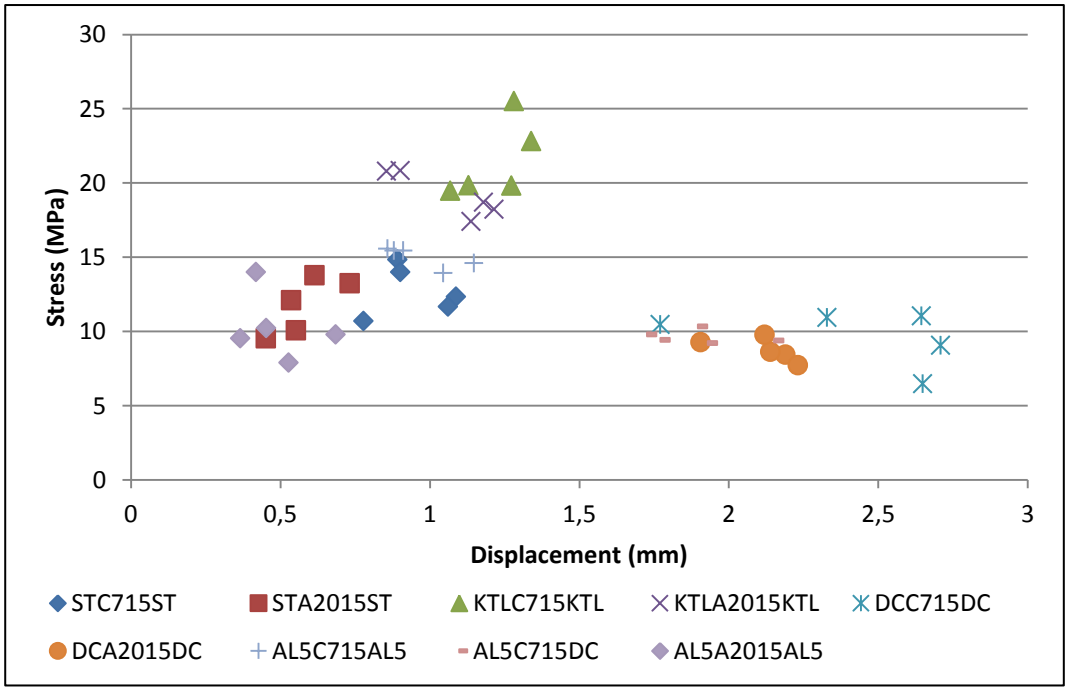

Figure 3.4 - Results overview.

Values between 14 to 16MPa of shear stress were obtained with the Al AW5754-H111 substrates, while with PDCPD only 8 to 11MPa were obtained. Still, with PDCPD samples, deformations of about 2.5mm were measured, being PDCPD itself responsible for 1.05mm of these 2.5mm due to its low Young Modulus. The PDCPD elongation (δ) was obtained using the following equation (3.2).

$$\delta = \frac{FL}{EA} \tag{3.2}$$

where,

F is the maximum force recorded (2500N)

L is the length between grips accordingly to the Figure 3.3

E is the Young Modulus of PDCPD presented in the Table 3.1

A is the cross section area of the specimen according to Figure 3.3.

Hybrid specimens presented shear stress values around 10MPa, which are similar to the mono-material PDCPD joints. The displacement was again about 2mm mainly due to the lower Young Modulus of the PDCPD. Furthermore, considering that the hybrid joints were only degreased and no significant difference in the joint strength was observed, abrading might be redundant for this type of applications.

It may be seen that MMA adhesive presented about 10 % more of shear strength in all specimen types comparatively to the EP adhesive. It presented also shorter curing times at room temperature becoming preferable over EP in terms of manufacturing.

For the development of the bonnet presented in this work, the reference values used to calculate the adhesive bonding area were based on the PDCPD interface properties which present the weaker joint interface. The values adopted can be found in the following Table 3.11. Additional info related to this test can be found in the Section B of the Appendices and elsewhere [168].

Table 3.11 – Properties of materials used in FEA.

PROPERTY	CRESTABOND M7-15
Density [kg/m^3]	1.000
Tensile strength [MPa]	10

3.2. Bonnet design

As the exterior panel of the bonnet presents lower dimensions (1090mm×550mm×80mm) and will have much lower weight than that of other conventional vehicles (approx. 40% to 50% lower), it was decided not use a too much complex methodology to assess the best frame geometry. Thus, the methodology adopted was only divided in two different phases: frame design and optimization.

Frame design consisted in the development of three different geometries through computer aided design (CAD) CATIA V5 software, by taking into consideration the mostly common used designs, mechanical stiffness required by different loading conditions and available manufacturing technologies. Those geometries were simulated using a FEA software (Abaqus) in order to assess which one enables accomplishing quality structural requirements with minimum weight. The geometry selected within the design phase was then optimized by using also CATIA V5 and Hyperworks software. By the end, and still in the optimization phase, there was the need of evaluate the assembly. Thus, the minimum adhesive area required to ensure the minimal structural integrity under thermal expansion was calculated.

Six different types of mechanical simulations, similar to those performed by Ultralight Steel Auto Body Organization (ULSAB) [169] to optimize automotive steel structures, were used to support frame development. For each type of mechanical simulation, a minimum stiffness target was defined as result from a 100N applied load. This consisted in a slope of a straight line force versus displacement that corresponds to the elastic behaviour of the bonnet when the force is applied from 0 to 100N and they can be understood through the following Figure 3.5 and Table 3.12 and Section C of the Appendices.

Front beam test consisted in a bending load (A) applied to the front part of the bonnet, while hinges (point 1 and 2) were fixed in all 6 degrees of freedom (DOF) (fixed in 123456 = fixed in XYZRXRYRZ) and the bumpstop zone (point 3 and 4) fixed only in Z. Side and rear beam tests, present similar boundary conditions while withstanding with loads applied over that same beams (B and C, respectively).

Torsion test consisted in an applied load (D) on one frontal corner of the bonnet. Contrary to the previous configurations it is only supported by one frontal bumpstop in the opposite corner of that load (point 3). This bumpstop is also fixed in Z sense. Hinges (point 1 and 2) were also fixed in all DOF.

The over-opening test consisted in a load (F) forcing the bonnet to open more than it is prepared to do, while hinges (point 1 and 2) are fixed in all DOF. Here, no bumpstops were

used. The lateral test consists in a load (E) applied on the striker, aiming to simulate a non-linear closing behaviour, i.e. a closing movement that disrespects the hinges rotation axis. In this test, hinges were fixed in all six DOF and no bumpstops were used too.

PDCPD, steel and Al properties applied within the simulations were defined according to the previous Tables 3.1, 3.4 and 3.6. Quadratic shell elements were used in all simulations.

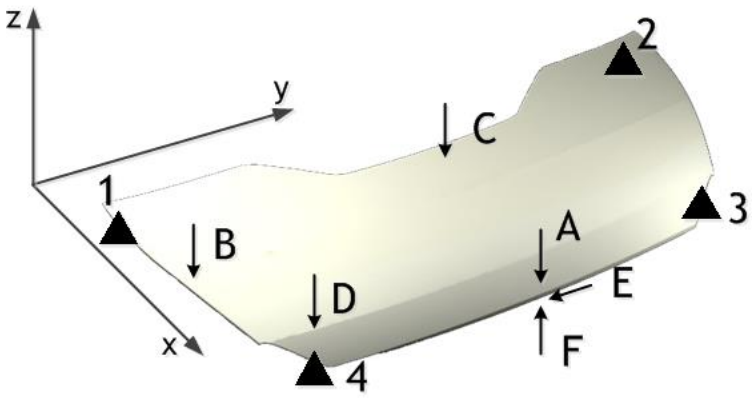

Figure 3.5 – FEA testing configuration.

Table 3.12 – Structural objectives for bonnet design and optimization phases.

		BOUNDARY CONDITION [DoF]				
TEST TYPE	**LOAD**	**ZONE 1**	**ZONE 2**	**ZONE 3**	**ZONE 4**	**TARGET [N/mm]**
Front beam	A	1,2,3,4,5,6	1,2,3,4,5,6	3	3	100
Side beam	B	1,2,3,4,5,6	1,2,3,4,5,6	3	3	100
Rear beam	C	1,2,3,4,5,6	1,2,3,4,5,6	3	3	100
Torsion	D	1,2,3,4,5,6	1,2,3,4,5,6	3	-	6
Lateral	E	1,2,3,4,5,6	1,2,3,4,5,6	-	-	100
Over-opening	F	1,2,3,4,5,6	1,2,3,4,5,6	-	-	10

3.2.1. Frame design

Figure 3.6 shows the three different geometries developed by using MobiCar exterior bonnet panel as base reference. The first design (F1) corresponds to the geometry of a

conventional frame usually applied to withstand the flexural and torsional loading conditions imposed with the minimum required displacements. While second frame (F2) may be considered an attempt to reduce weight relatively to F1, the third design (F3) corresponds to a strategy that is expected to better accomplish all imposed targets under loading conditions, especially under torsion. For all designs, a "U" section beam was adopted.

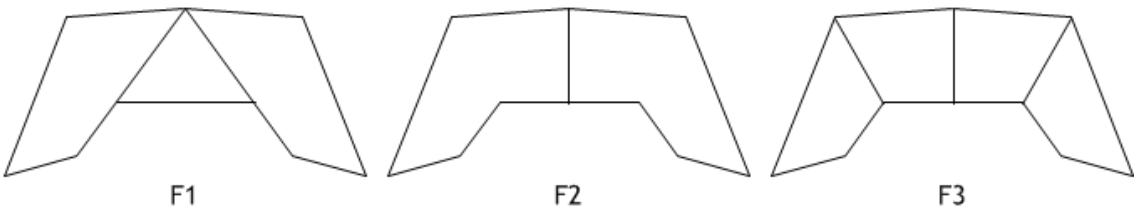

Figure 3.6 – Three frame designs analysed for the bonnet (F1, F2 and F3).

From these three frame designs, six different configurations were obtained by only varying the "U" section depth from 10 to 30 (mm), and the material thicknesses of 0.8 and 1.2 (mm). In such conditions, the 18 different versions of the steel frames resulting from the combination of attributes shown in Figure 3.7 were analysed.

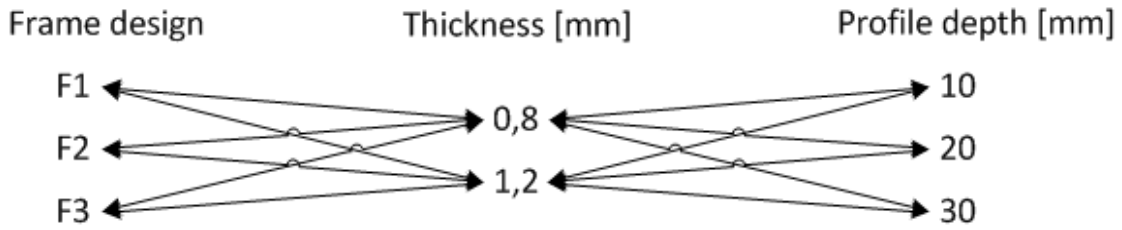

Figure 3.7 – Frames design diagram.

Only steel was used in this phase once it was enough to evaluate the most appropriated frame design. Besides that, from all test configurations previously described, only front, side, rear and torsion were performed, since they are the ones that act exclusively over the structure. In order to simplify the analysis, one array of numbers from 1 to 6 was attributed to each configuration accordingly to Table 3.13. Configuration 1, for example, corresponds to a frame with a cross-section having 0.8 mm of thickness by 10 mm of depth. As may be seen, identical configurations were used in all three frames. Table 3.13 also presents the bonnets

weights calculated using the materials densities shown in previous Tables 3.1 and 3.4 (PDCPD and steel densities 1030 kg/m^3 and of 7850 kg/m^3, respectively). This allowed understanding that frames F2 and F3 correspond to the lightest and heaviest solution, respectively. Table 3.14 presents the number of elements and nodes adopted for this testing phase.

Table 3.13 – Frame configurations and weight.

	CONFIGURATIONS [THICKNESS × DEPTH] [mm]					
FRAME DESIGN	**1**	**2**	**3**	**4**	**5**	**6**
	[0.8×10]	[0.8×20]	[0.8×30]	[1.2×10]	[1.2×20]	[1.2×30]
F1 weight [kg]	2,67	3,00	3,34	3,40	3,90	4,40
F2 weight [kg]	2,54	2,85	3,15	3,21	3,66	4,12
F3 weight [kg]	2,71	3,05	3,40	3,46	3,97	4,49

Table 3.14 – Number of elements and nodes.

FRAME DESIGN	Elements	Nodes
F1	7151	6772
F2	6854	6499
F3	7167	6781

Figure 3.8 shows that configurations 1 and 4 present values below the targets corresponding to the front, rear and torsion behaviour. It means that higher thicknesses or deeper sections are required here. Nevertheless it is possible to select a configuration from the other array of configurations. Thus, it is appropriate to select the configuration number 2 from the frame design F1, once it presents the lowest weight with all targets accomplished.

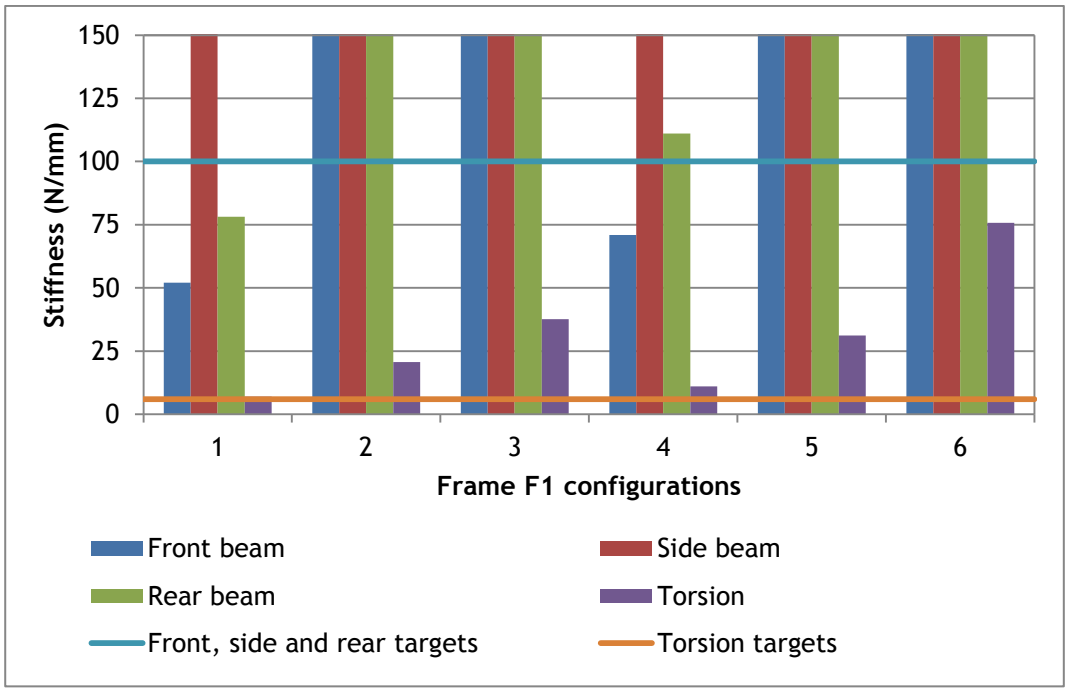

Figure 3.8 – Stiffness obtained with Frame F1.

With the frame design F2, closer results were obtained as may be seen in Figure 3.9. The same configurations 1 and 4 presented values under the structural targets. Even presenting an overall decrease of performance compared to frame design F1 all the other configurations still remain adequate. This leads again to selection of the configuration number 2 from frame design F2 since accomplish all the stiffness targets.

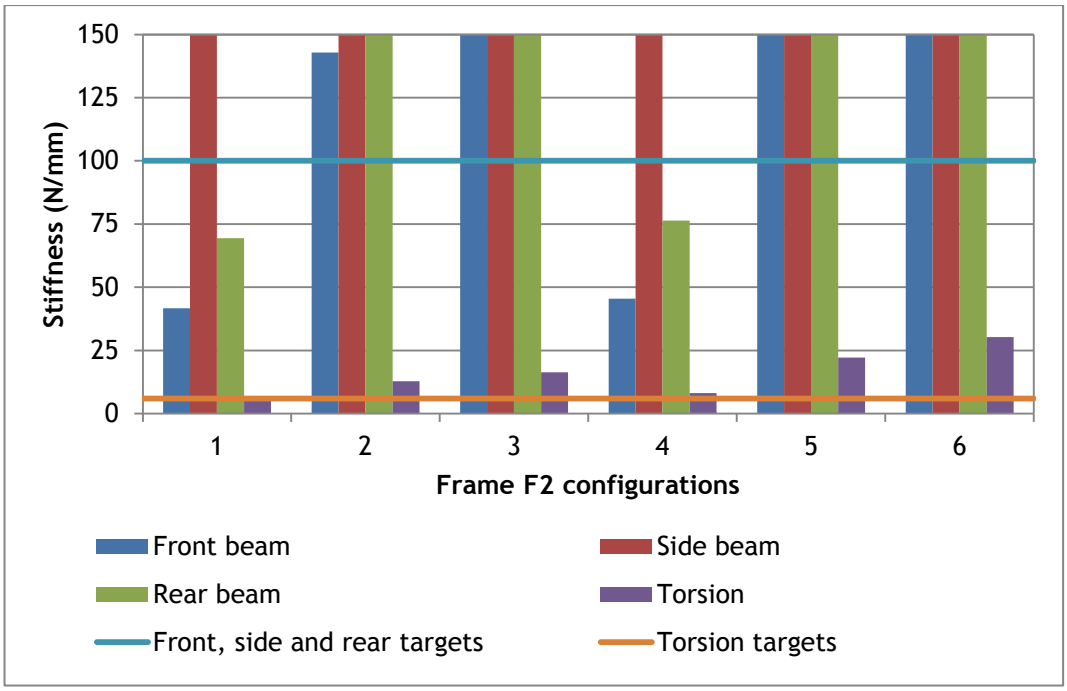

Figure 3.9 – Stiffness obtained with Frame F2.

For the frame design F3, the same range, of low values, was presented by 1st and 4th configurations, as may be seen in Figure 3.10. However, not counting on the front beam test, this frame design F3 presented better mechanical responses of the three frames. Although its good structural performance, this frame presented always the highest weight values along all configurations. As example, a visual of the results obtained with Frame 1, 2 and 3 under the torsion test are represented in the Section D of the Appendices.

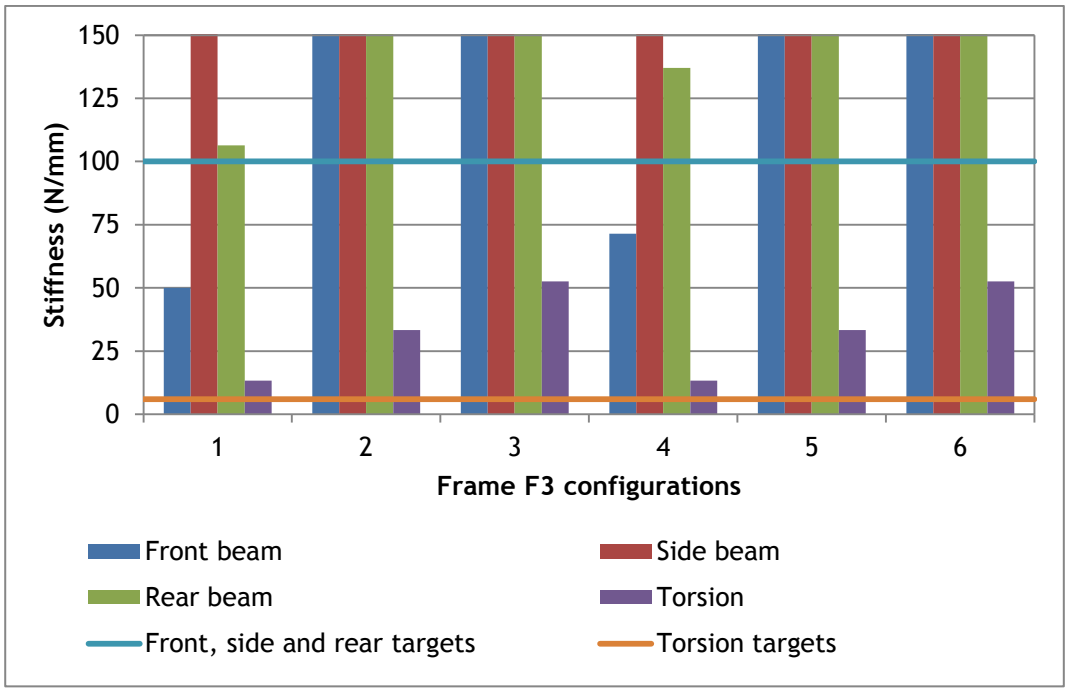

Figure 3.10 – Stiffness obtained with Frame F3.

Taking into account all the results presented herein, the frame design F2 with the configuration number 2 was selected by presenting the lowest weight and accomplishing all the structural targets. Considering this choice, an optimization phase took place where the previous geometry was converted into a frame capable of being manufactured as can be seen in Figure 3.11. Here, concerns with the stampability were taking into account. Bending degrees were kept as high as possible, while special care was taken on the important features such as the striker and hinges support zone.

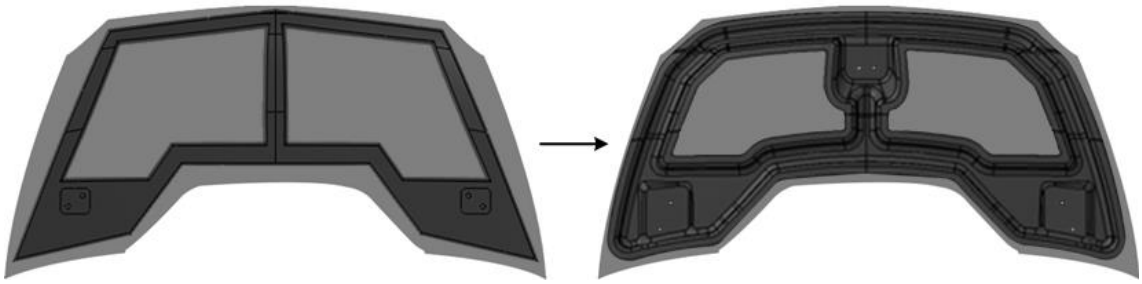

Figure 3.11 – Discretized frame converted to a detailed frame (version F2.0).

3.2.2. Optimization

First optimization phase consisted in an empirically evaluation of the detailed model previously designed (F2.0). Several changes were performed even before the second FEA phase as may be seen in Figure 3.12. A new frontal area section, smaller striker and hinges areas, inner perimeter configuration, as well as the elimination of the central beam were performed as an attempt to reduce weight. An increment of area was only performed in the back corners of the bonnet in order to increase local stiffness. This configuration ended up with 3.15kg.

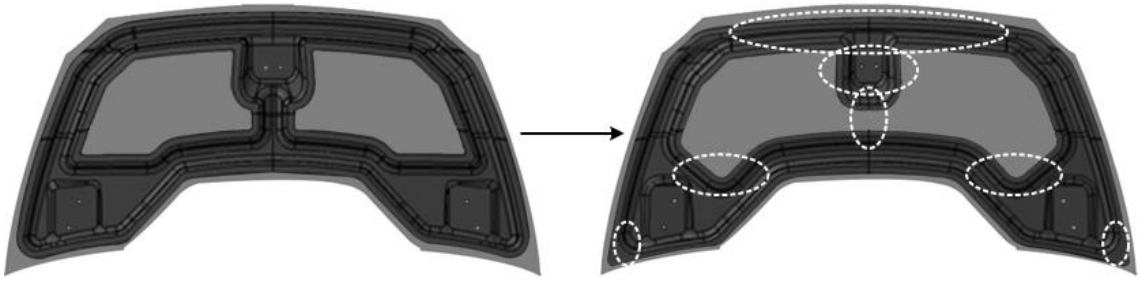

Figure 3.12 – Bonnet version F2.0 and F2.1 respectively.

Still in the optimization phase and due to the need of come up with more realistic results within this phase, the hinges were added to the model in order to simulate all parts acting as a single system. However, once hinges present an articulated configuration (as can be observed in Section C of the Appendices), it is expected a considerable loss of mechanical performance, so that, both tests (with and without hinges) were carried out within this phase. In addition, and contrary to the design phase, over opening and lateral tests were also carried out.

Therefore the frame F2.1 was submitted to FEA and the following results, presented in Figure 3.13 were obtained. The front, rear, over opening and lateral mechanical simulation did not present adequate results. An average of 30% less than required was observed. Regarding to the same tests performed with no hinges only frontal beam and lateral tests presented inadequate stiffness. The loss of structural integrity provoked by the hinges is even more perceived in the rear beam, over opening and lateral tests. Due to the small longitudinal dimension of the bonnet, it has been found that geometry accomplishes both side and torsional stiffness targets in more than 50% from required.

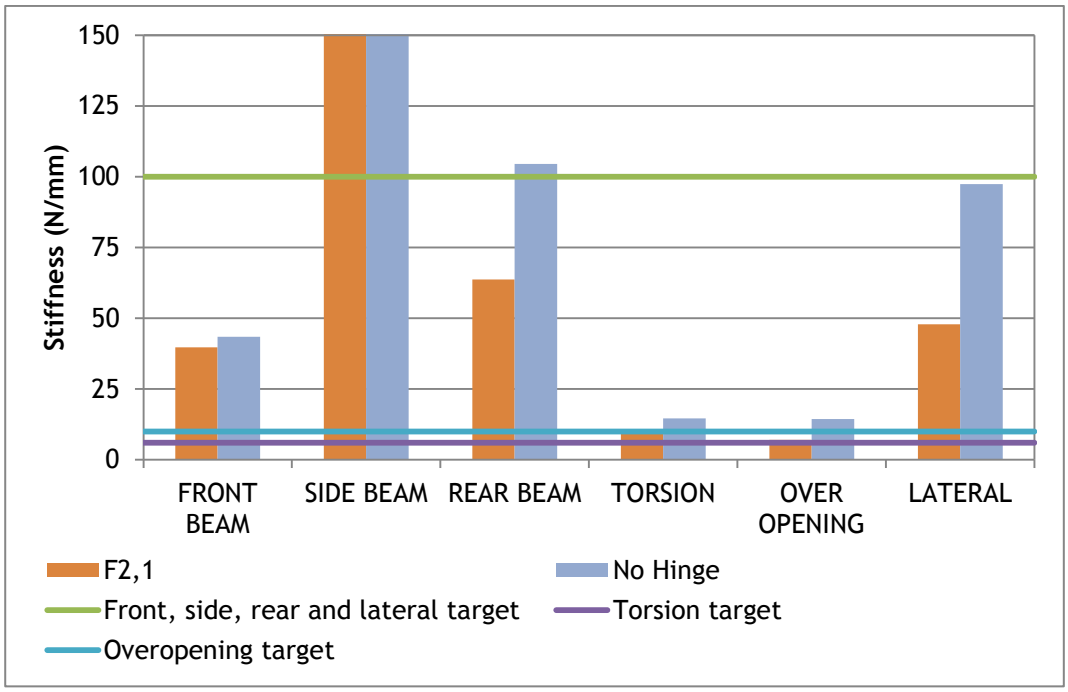

Figure 3.13 – Bonnet version F2.1 results.

A redesign of the frame F2.1 was necessary due to the inappropriate structural results obtained. Thus, as may be seen in Figure 3.14 a central section was created to improve rigidity and force distribution from striker to rear beam areas. Such increment resulted in a weight of 3.17kg.

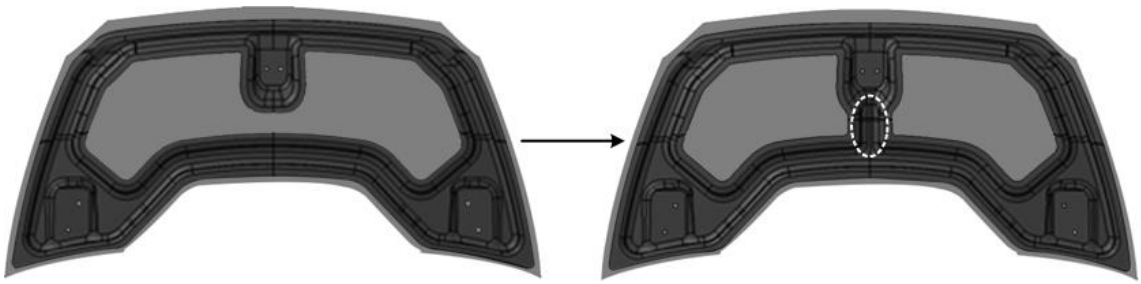

Figure 3.14 – Bonnet version F2.1 and F2.2 respectively.

With these design changes, the following results depicted in Figure 3.15 were obtained. Similarly to the previous frame F2.1, the front, rear, over opening and lateral tests presented results under the target. Only small improvements were spot even with the reintroduction of

the central beam. The tests without hinges have also presented results under the target on both front and rear beams.

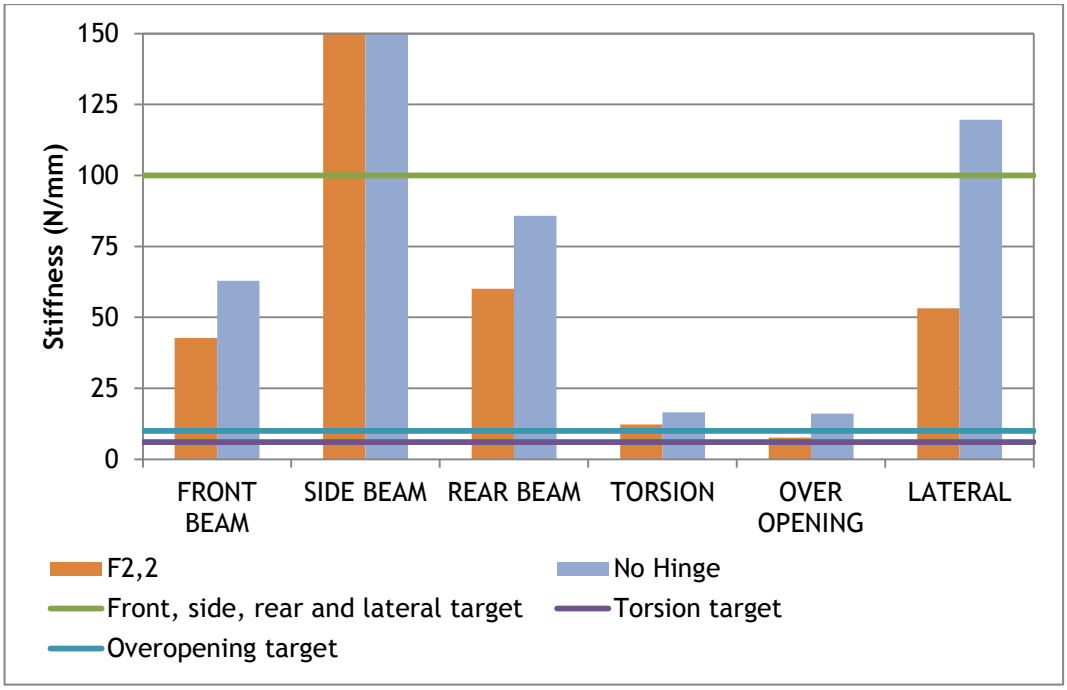

Figure 3.15 – Bonnet version F2.2 results.

Last results required a redesign, where the front beam was increased in both width and section depth as may be seen in Figure 3.16. Such design variations gave place to the frame version F2.3 which presented a final weight of 3.32kg.

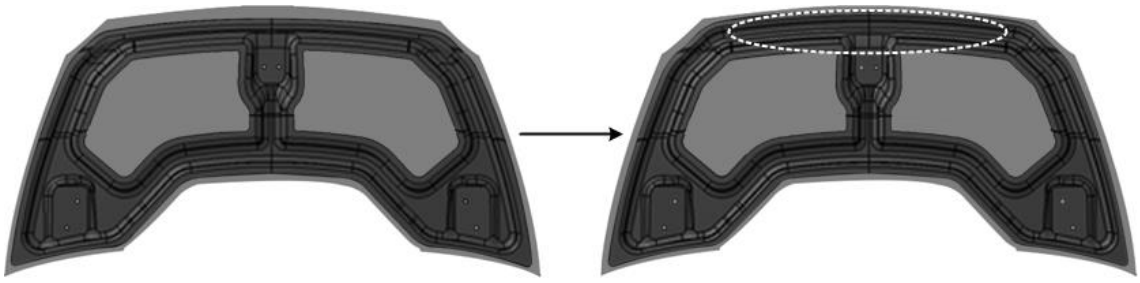

Figure 3.16 – Bonnet version F2.2 and F2.3 respectively.

Such design change contributed for a substantial stiffness increment in the front beam as may be seen in Figure 3.17. It has also contributed for residual stiffness increment in rear beam, once they are connected by the central beam. The over opening and lateral test also presented slightly improvements. This version was able to reach all the imposed structural targets without the hinges being used.

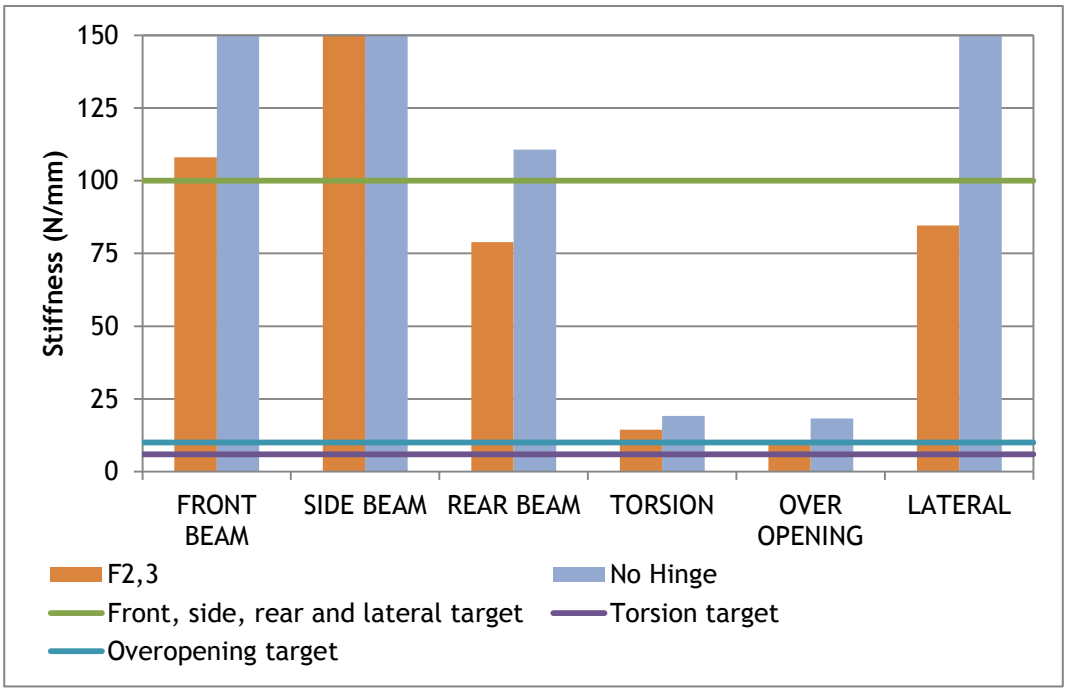

Figure 3.17 – Bonnet version F2.3 results.

In order to improve the frame a little bit more, a last design change took place as may be seen in Figure 3.18. The rear beam was increased in both width and depth directions and two indentations were created in the central beam in order to increase stiffness. Therefore, the last frame version (F2.4) ended up weighing 3.35kg.

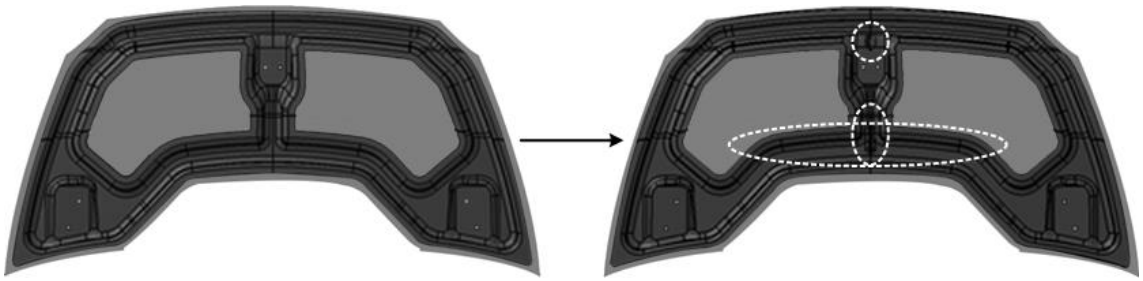

Figure 3.18 – Bonnet version F2.3 and F2.4 respectively.

After run the simulations some improvements were obtained and only rear beam and lateral tests remain under the target as may be seen in Figure 3.19. Both have presented stiffness values of 13.5% and 6.5% less than the requirement, respectively. However, such values were within an acceptable margin, once the hinge contribution for the stiffness loss of the assembly was 31% on the rear and 60% on the lateral tests. Thus, it was considered that additional geometry changes would incur in an excessively dimensioned frame and consequent weight penalty, so that, no further iterations were performed.

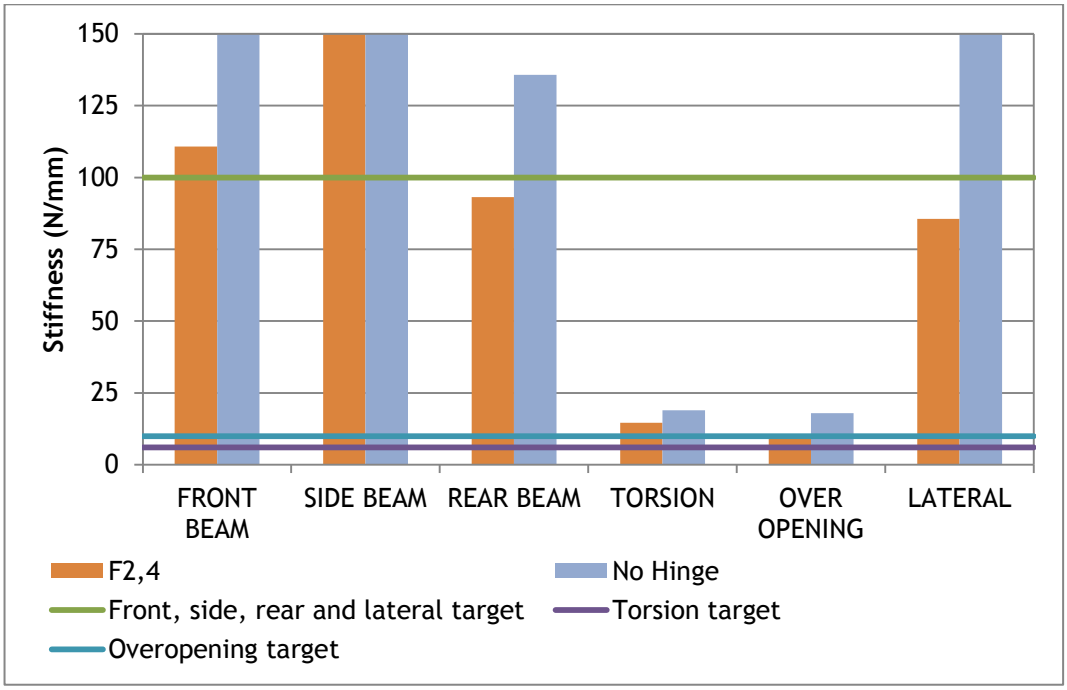

Figure 3.19 – Bonnet version F2.4 results.

As an attempt to understand what can be achieved in terms of stiffness and weight by using Al, it was created and additional frame version counting on a similar geometry to frame

F2.4 but with a thickness increment (from 0.8 to 1.5mm) and the mechanical properties of the Al. It was named of F2.4.1. This frame was then simulated under the same conditions of the steel frames. This version ended up weighing 2.63kg and presented results above the target in the front, side and torsion beams as can be seen in Figure 3.20. In the rear beam, over-opening and lateral tests an average of just 7% under the target was obtained. With no hinge, no results under the target were obtained.

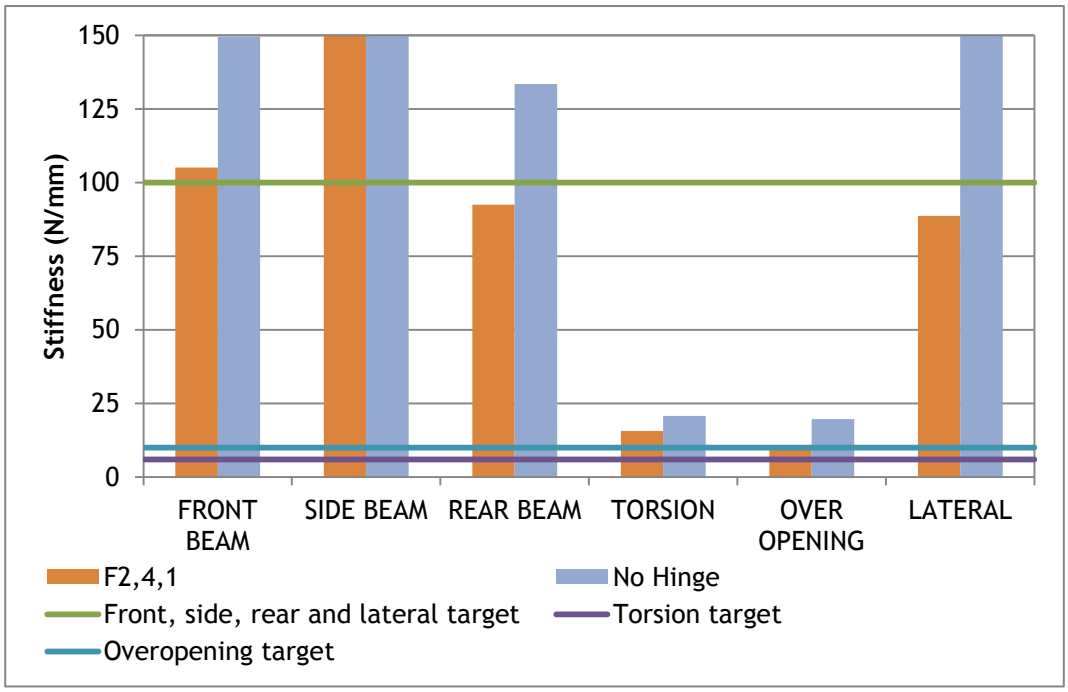

Figure 3.20 – Bonnet version F2.4.1 results.

With the aim of improving the values under the target, a new version F2.4.2 was also created. This frame version, count on the same configuration of frame version F2.4.1 but with a thickness increment (from 1.5 to 2mm) which has contributed to achieve 3kg. Besides FEA revealed an improvement on overall frame stiffness, the lateral test still presented values of about 5% under the target, as may be seen in Figure 3.21.

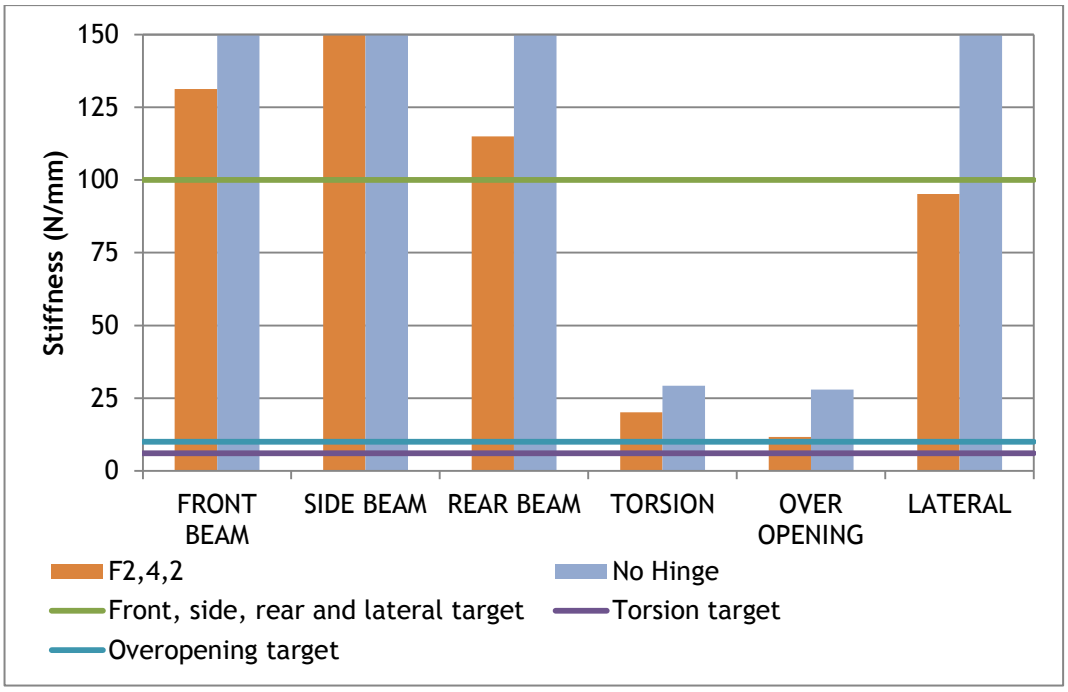

Figure 3.21 – Bonnet version F2.4.2 results.

Comparing those bonnets (F2.4 and F2.4.1) similar results may be seen, with slightly improvements in torsion, over opening and lateral tests of 8%, 84% and 26% respectively, as may be seen through the Figure 3.22. Regarding to the front, side and rear beam tests, no stiffness gain was observed.

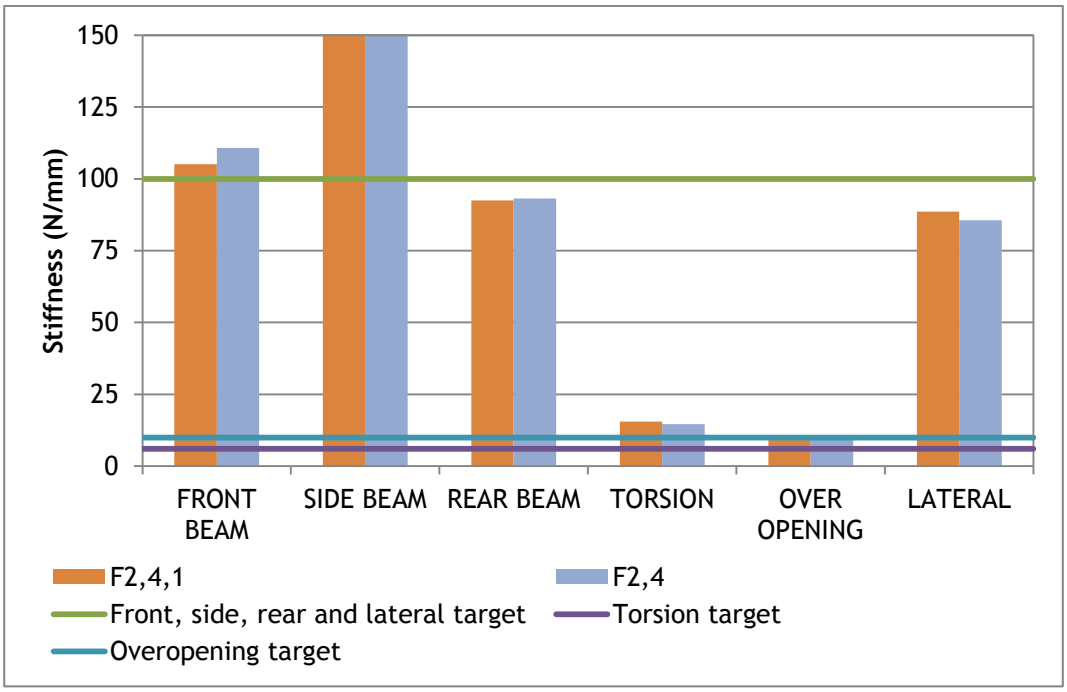

Figure 3.22 – Bonnet version F2.4 and F2.4.1 results.

Figure 3.23 presents only the weights of the bonnets that have presented acceptable structural results. Bonnet with a frame version F2.4.1 presented the lowest weight, while the F2.4 presented the highest weight. Besides bonnet with the frame F2.4.2 presenting a much higher thickness than F2.4, it has still presented lower weight remaining the most preferable in terms of structural results.

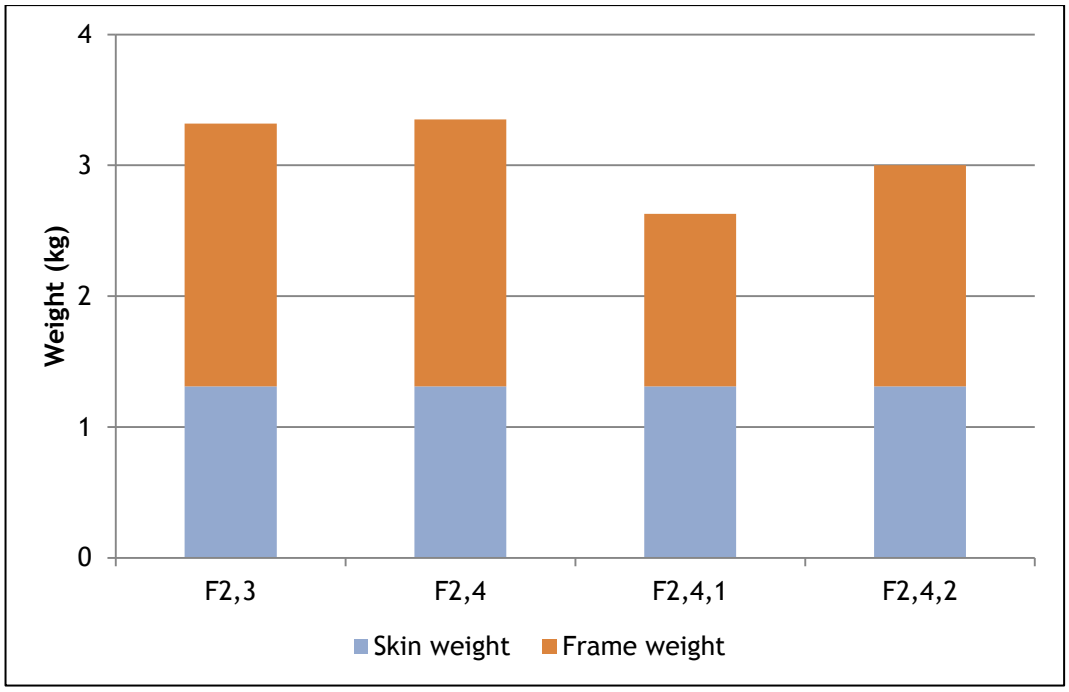

Figure 3.23 – Weights of the acceptable tested bonnets.

3.2.2.1. Adhesive track validation

After the optimization phase, it was necessary to verify the joint size in order to assemble them in a reliable way. A two-dimensional (2D) CAD analysis was done once it provides enough accuracy to evaluate the performance of the joint. To do this a cross section *AA* was created in the bonnet as can be seen in Figure 3.24 and Figure 3.25 and the data, presented in Table 3.15 was used to calculate the assembly strength.

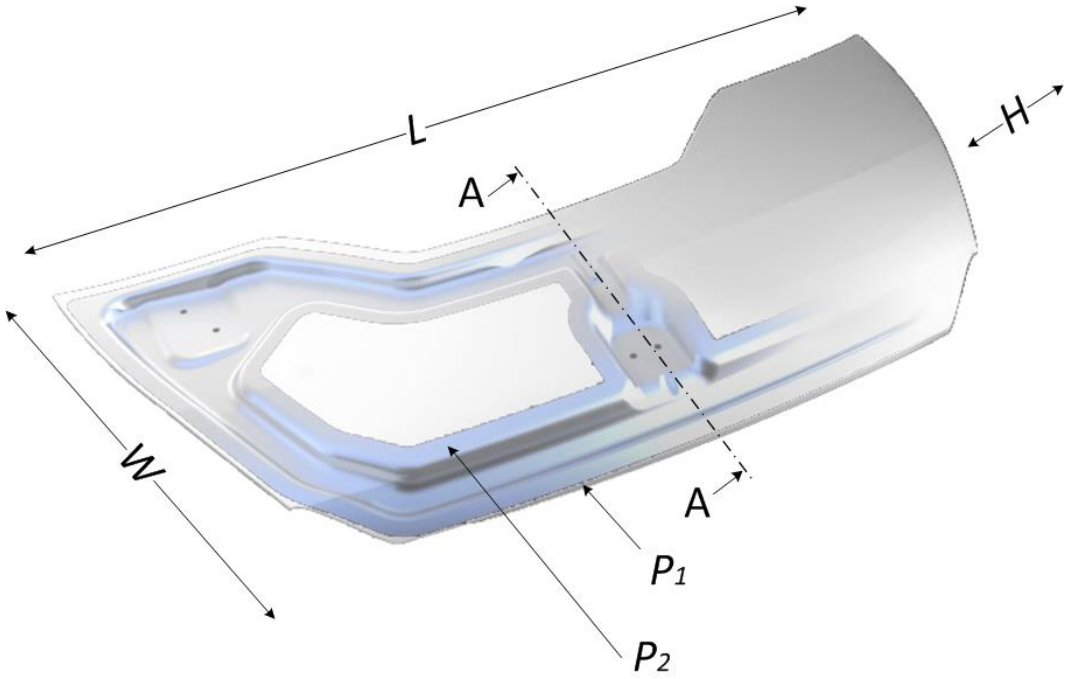

Figure 3.24 - AA section cut used for the assembly analysis.

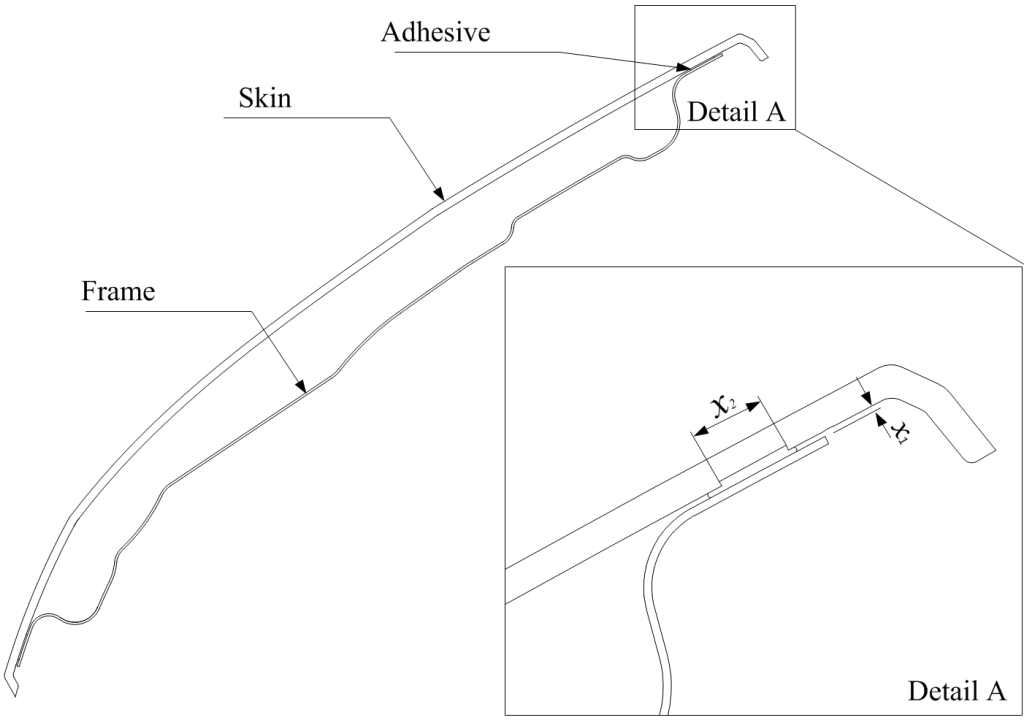

Figure 3.25 - AA section view.

Table 3.15 – Bonnet geometrical characteristics.

		FRAME		SKIN
SYMBOL	**PARAMETERS**	**STEEL**	**ALUMINIUM**	**PDCPD**
L	Length [mm]	1070	1070	1090
W	Width [mm]	524	524	550
H	Height [mm]	80	80	66
-	Thickness [mm]	0,8	1,5	3
P_1	Exterior perimeter [mm]	2960	2960	N/A
P_2	Interior perimeter [mm]	1934	1934	N/A
-	Volume (CAD output) [mm^3]	260330	488120	1277820

To improve accuracy and minimize material losses, a small gluing track needs to be created in the PDCPD skin with the desired bonding thickness of 0.3 mm (same tested thickness in the section 3.1.3 Adhesives) along the exterior perimeter P_1 (2690mm). Thus in order to find the optimal width of the adhesive track x_2 (Figure 3.25), it was necessary to implement some structural targets.

As no minimum disassembling strength is apparently known, for quality issues it was assumed that the assembly must withstand the uniform distributed shear load resulting from stress developed in the PDCPD skin due to the different thermal expansion coefficient of the materials to be joined. Thus, for this analysis, was considered an average temperature variation of 65° C since car body shells may experience a temperature variation between -40° till +90° degrees Celsius [105]. In such case, the normal stress developed in PDCPD skin (σ_{skin}) may be calculated by:

$$\sigma_{skin} = (\alpha_{PDCPD}^{T} - \alpha_{steel}^{T}) \times \Delta T \times E_{PDCPD} \quad (3.3)$$

where,

α_{PDCPD}^{T} is the PDCPD thermal expansion coefficient of 90×10^{-6} °C^{-1} (Table 3.1)

α_{steel}^{T} is the steel thermal expansion coefficient of 13×10^{-6} °C^{-1} (Table 3.4)

ΔT is the variation of temperature of 65°C

E_{PDCPD} is the PDCPD Young modulus (Table 3.1)

Then, by considering the thickness of the PDCPD skin, $t_{skin} = 3mm$, the uniform shear loading, q, developed along the bonnet external perimeter was determined as:

$$q = \sigma_{skin} \times t_{skin} \tag{3.4}$$

resulting in a uniform shear loading of 28.5 N/mm along the bonnet external perimeter (2960 mm), which means a total uniform shear loading (Q) between the steel frame and PDCPD skin of 84kN.

Considering that the bonding was made with the MMA adhesive Crestabond M7-15 which presents approximately 10MPa of shear strength with PDCPD substrates, according to the previous analysis (in section 3.1.3. Adhesives) and the shear loading Q = 84 kN between the steel frame and the PDCPD skin as well as a Safety Factor (SF) of 1.5, the minimal adhesive area may be calculated through the following equation (3.5):

$$a_{min} = \frac{Q}{\tau_{adhesive}} \cdot SF \tag{3.5}$$

where,

Q, is the uniform shear loading

$\tau_{adhesive}$, is the shear loading of the adhesive

A value a_{min} of 12666 mm^2 was obtained and the minimal adhesive width (x_2) required can then be calculated through equation (3.6):

$$x_2 = \frac{a_{min}}{P_1} \tag{3.6}$$

where,

P_1 = is the exterior perimeter of the bonnet, as stated in Table 3.14.

With this, a value of 4.28 mm was obtained for x_2. As a result, no more design changes were performed over the frame and skin. A technical drawing of the final bonnet geometry can be found in the Section E of the Appendices.

3.3. Prototyping

Bonnet prototyping was divided in three parts. Firstly, frame was developed through stamping and in order to meet the objectives of this work it was thought to fabricate one of the most lightweight frames (F2.4.1 or F.4.2) in detriment of the steel ones. The frame prototyping was then followed by the skin manufacturing through RIM and by the assembly through adhesive bonding. This section presents these three steps including also the development of the prototyping tools.

3.3.1. Frame

Four different stamping tools (T1, T2, T3 and T4) were designed and tested by one element of the consortium and the results were obtained only as an output. The stamping tools can be seen in Figure 3.26 and the results in Section F of the Appendices. A brief summary can be read in the following paragraphs.

Tool configuration T1 represents a conventional stamping tool with an interior and exterior matrix to work on a double phase press. T2 is quite similar to configuration T1, but contains additional grooves to hold the metal sheet in place and also to avoid slippery. Stamping tool T3 is also similar to configuration T1 but contains only a single part matrix. Configuration T4 is the same configuration of T1 but contains clamping corners to grab the metal sheet in that same zone.

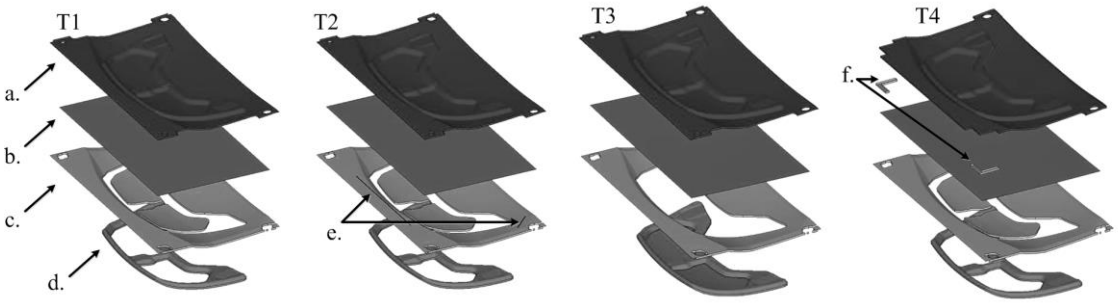

Figure 3.26 – Stamping tool versions to simulate (T1, T2, T3 T4). (a) is the punch, (b) is the metal sheet, (c) is the binder blank, (d) is the matrix, (e) are the grooves and (f) are the clamping corners.

In order to carry on the analysis, three softwares were used: Hypermesh v12.0 for the pre-process, LS Dyna 971 as solver and Hyperview v12.0 for the post process. As mentioned before only Al configuration was simulated since it presented lighter results comparatively to steel. Thus, two analyses for each stamping mould were conducted, each one running with two different Al thicknesses (1.5 and 2.0mm corresponding to frames F2.4.1 and F2.4.2, respectively) and the results were plotted in a forming limit diagram (FLD).

The forming limit curve (FLC), which provides information on the maximum stress the metal can undertake, was set between 2% of material elongation (to reduce springback) and a maximum of 3% of thickness increment (to prevent wrinkle). The FLC was plotted in a two-dimensional coordinate system, with the major strain plotted on the y-axis and the minor strain plotted on the x-axis. Results show the behaviour during the binder blank closing (c), stamping and subsequent cut. Table 3.16 presents a summary of the stamping simulation results.

The simulation with tool T1 with 2mm and 1.5mm Al sheet thickness revealed adequate strain in great part of the component without fissure risk. In both cases the maximum thickness decrease was about 10% and any zone subject to compression presented a thickness increment bigger than 3%. However some risk of wrinkle exists in the frontal and central zones, as well as in the back corners of the component during the initial phase of stamping. The maximum force obtained to stamp the frame using tool T1 was 1559kN for the 2mm sheet thickness and 1265kN for the 1.5mm sheet thickness.

Tool T2 revealed adequate strain in great part of the component without fissure risk in both 2mm and 1.5mm Al sheet thickness. In fact, the use of grooves contributed for the reduction of compression area as well as for the reduction of overall wrinkle risk. However some risk of wrinkle still exists in the frontal and central zones, as well as in the back corners

of the component. The maximum force obtained to stamp the frame using tool T2 was 1661kN for the 2mm sheet thickness and 1337kN for the 1.5mm sheet thickness.

After T3 simulation with both Al sheets (2mm and 1.5mm) no significant improvements were spot comparatively to tool T1. Only a slight reduction on the maximum force required to stamp the frame was obtained with this tool. This way, 1558kN are required to shape a 2mm Al sheet thickness and 1256kN to shape a 1.5mm Al sheet thickness.

Tool T4 revealed a substantial reduction on the wrinkle risk on the frontal and central frame zones due to the application of constraints in the frontal corners. However some wrinkle risk still remains next to the hinges zone. The maximum force obtained to stamp the frame using tool T4 was 1577kN for the 2mm sheet thickness and 1279kN for the 1.5mm sheet thickness.

Table 3.16 – Stamping simulation results.

ALUMINIUM	STAMPING FORCE [kN]			
SHEET THICKNESS [mm]	T1	T2	T3	T4
1.5	1265	1337	1256	1279
2.0	1559	1661	1558	1577

In summary, all tested versions suggested adequate strain in the majority of the frame area without fissuring risk. The most critical point is located next to the striker where the highest thickness reduction is seen. The frontal zone as well as corners next to the hinges presented wrinkle risk especially due to the lack of physical constraint during the initial stamping phase. The use of grooves can improve the quality of the part allowing higher control on local wrinkles propagation. The displacement limitation on the exterior edges of the metal sheet in the beginning of the stamping revealed to be ideal in order to control the wrinkles. However the increment of complexity in the tool does not result in a great improvement leading to the selection of the stamping tool T1.

Tool T1 was manufactured using carbon steel grade DIN 1.1191. Due to time issues, a 2mm gap stamping tool was supplied on time in detriment of a 1.5mm. The tool was setup in a double phase hydraulic press from Ona-pres type EMD-30-1.2-l with 3.000 kN of capacity and 33.4kW of power according to Figure 3.27 and 3.28.

Figure 3.27 – Stamping tool punch and matrix setup in the press.

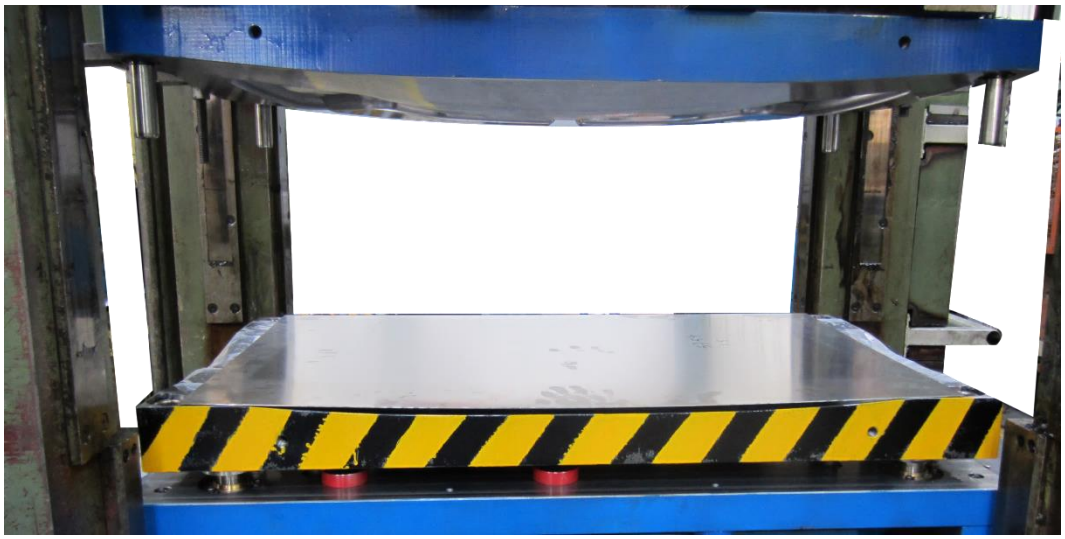

Figure 3.28 – Aluminium sheet placed over the stamping tool.

Due to the fragility of the tool surface and the need to extract several samples with acceptable quality, it was lubricated and covered with a plastic film before each stamping stroke. Each stamping stroke took 10 seconds plus lubrication and film covering leading to a total cycle time of 2 minutes. Two labours were also required for this process. Eight samples of 2mm were stamped and all have presented acceptable quality results comparable to the stamping simulations previously performed. After trimming with the desired shape, a constant 1.64Kg was measured in all samples.

3.3.1.1. Dimensional control

For frame scanning and inspection was used the hardware Comet L3D 2M, Aicon Studio DPA PRO Standard Plus. For post processing was used the software Comet Plus 9.62 and Delcam Powerinspect 5.040. For results visualization was used Inspect Plus 5.22, Tebis 3.4, CATIA V5 and Rapidform 2006.

According to Figure 3.29, an interval between 1.7mm and 2mm was measured in almost all area of the frame. 95% of the frame came up from the stamping with a thickness of 1.9mm accounting only for a 0.05% of thickness reduction. The lowest thickness value (1.3mm) was measured next to the striker zone, where the deep pressing operation caused high strain deformations.

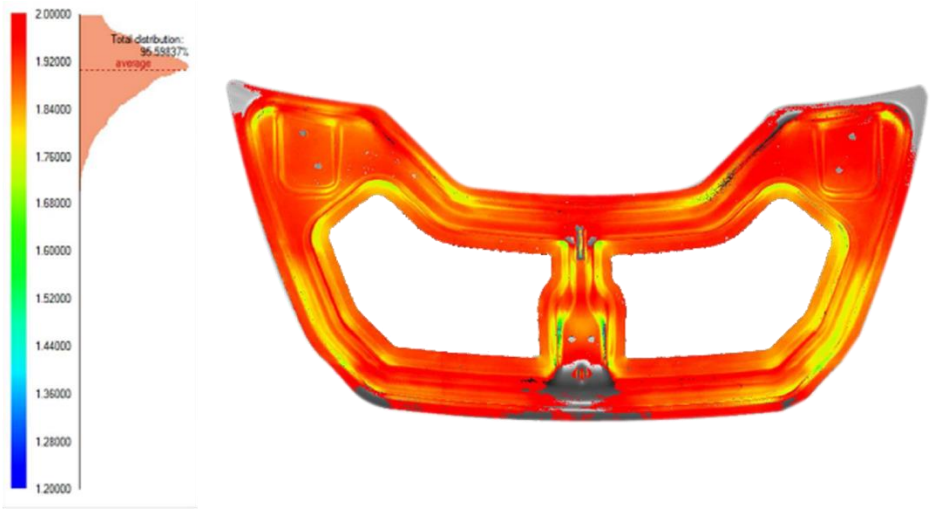

Figure 3.29 – Thickness control results.

Geometrical analysis has shown a max deviation of 2.7mm, in both +Z and –Z axis senses, comparatively to the CAD model, as may be seen in Figure 3.30. While rear part of the frame presented positive deviations, the frontal part presented negative deviations. The striker and hinges zones, as well as great part of the inner perimeter presented almost none deviation.

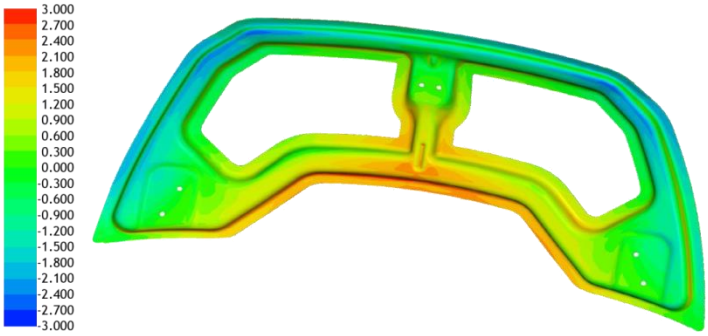

Figure 3.30 – Geometry deviation results

3.3.2. Exterior panel

A mould was developed from a 5853 Al alloy block containing two parts: a cavity and a core as can be seen in Figure 3.31. The partition line was created wilfully with the bonnet edge and the runner was placed in the back part of the mould taking advantage of it inclined geometry. From the conventional mixing geometries [170], the dipper type was adopted due to lower complexity of the part. A dam gate was also included in order to contribute for a uniform mould filling. A gasket was placed along the cavity perimeter in order to be compressed during the injection and minimize material losses. Vent and flash zones were also introduced. Vents avoid trapping air inside the mould which contributes to increase polymer pressures while preventing unfilled zones or bubbles. In areas where excessive venting is needed, a reservoir was milled. This reservoir does not necessarily need to be filled, but it will allow a safety buffer to solve venting issues. Flash zones leave excessive material to go out with a reduced thickness allowing, this way, an easy finishing operation.

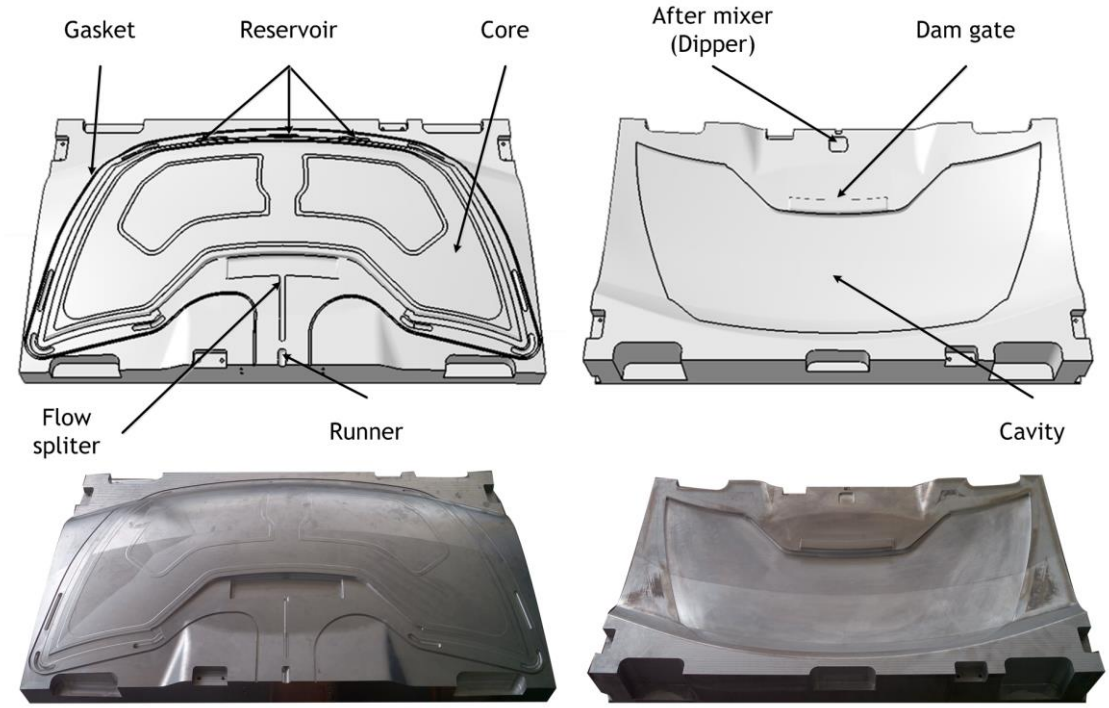

Figure 3.31 – Virtual and real mould, core and cavity respectively.

Conventional RIM moulds present heating channels which are filled with hot water in order to keep the mould with a desirable temperature (approx. 60 to 80ºC). However in this specific work, budget availability as well as the reduced number of runs necessary for this project did not justified this feature. Thus, mould was pre-heated through conduction till the desired temperature, between 60°C and 80 °C and was then setup into a 150ton force hydraulic press Findout, with 5.5kW of power. A RIM machine Ecomaster 100/50 from OMS Group was then connected to the mould as may be seen in Figure 3.32.

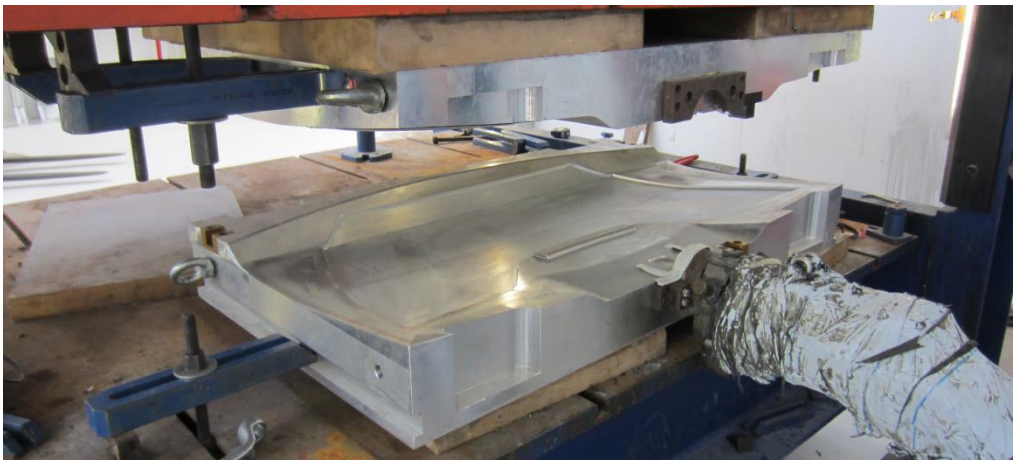

Figure 3.32 – Injection mould core and cavity connected to the RIM machine.

This specific RIM machine works with a 38kW power and an injection rate interval of 150 to 1500g/sec depending on the production requirements. For this case study an injection rate of 550 g/sec was adopted with a 1:1 mixing ratio for both DCPD liquid resins (Telene 1650 series A and BK; 275g/sec for each component), and a mixture pressure of 100bars. DCPD is commonly supplied in two separated components A and B. DCPD resins were at room temperature during the process (21ºC at the moment of this work).

Three samples were injected. First injection served to evaluate cycle time, cure and mixing rate by applying just 1 sec to the machine parameters. A part with 0.550kg was obtained, as can be seen in Figure 3.33. Two minutes were considered enough for the cure. Figure 3.34 presents injection 2 and Table 3.17 shows the weights obtained with the injections. No dimensional control was made over the exterior body panel once the elevated flexibility of PDCPD would lead to misleading dimensions.

Figure 3.33 – Injection 1.

Figure 3.34 – Injection 2.

Table 3.17 – Injection results.

INJECTION	INECTION TIME [sec]	CURING TIME [sec]	WEIGHT BEFORE TRIMING [kg]	WEIGHT AFTER TRIMING [kg]	CONDITION
1	1	120	0.550	-	nOK
2	2.9	120	1.55	1.45	OK
3	3.2	120	1.70	1.60	OK

3.3.3. Assembly

A positioning JIG was designed and developed by INAPAL-Metal using CATIA V5. It was conceived containing a rectangular metallic base with 1210mm by 654mm as may be seen in Figure 3.35. Several clips were attached to the base and they served to hold the bonnet in place during the adhesive curing. Several frame supports were placed under the striker and hinges zone while four positioners were placed in the front and rear part of the bonnet in order to prevent its slide during the adhesive application.

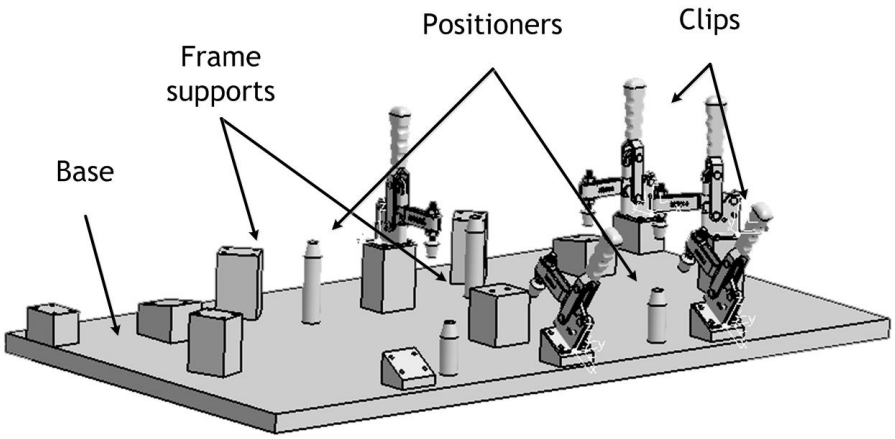

Figure 3.35 – CAD of the JIG for adhesive bonding.

The assembly was manually processed for this prototype and consisted in three steps. Firstly, the frame was positioned in the JIG, secondly the adhesive and anti-flutter were sprayed over the exterior and interior perimeter track of the metallic frame, respectively. In the end, the exterior panel was placed over the frame and it was held by closing the clips. These steps are illustrated in Figure 3.36. The clips provided a uniform pressure during the adhesive cure. After 15min (Crestabond M7-15 curing time) bonnet could be extracted from the JIG. Considering the reduced number of skins produced previously in RIM process, only two successful assemblies were performed. Both presented a final weight of 3.20 and 3.35kg.

Figure 3.36 – Adhesive bonding assembly steps.

3.4. Mechanical testing

Mechanical tests similar to those simulated through FEA were performed in order to validate the bonnet. Taking into account the complexity of the tests, bonnet geometry and available equipment, only front, side, rear beams and torsion tests were considered to be replicated. Taking into account the testing machine architecture, the bonnet positioning and boundary conditions, as well as the direction of the loads, the interface depicted in Figure 3.37 was developed, which counts on the use of Rexroth Al profile with a squared section of 40mm.

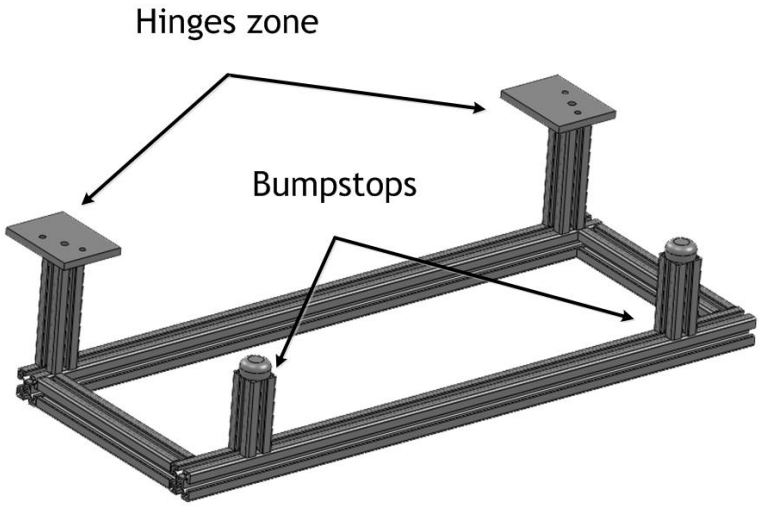

Figure 3.37 – Interface for bonnet mechanical tests.

3.4.1. Test procedures

Firstly, the bonnet was fastened to the interface through the use of bolts in the hinges zone while the frontal zone was simply supported by the bumpstops. Then, two AML/E LVDT displacement sensors were attached to the interface. One was placed next to the hinges in order to control unexpected displacements since no great displacement is expected in that same zone. The other LVDT was placed in the centre with the aim of recording the displacement in the middle area of the bonnet. This setup can be seen through Figure 3.38 and 3.39. Secondly, the interface was placed on the testing machine and the puncture device range was verified. In the end, four circles were delineated on the top of the bonnet for right puncture positioning, as may be seen in the Figure 3.40.

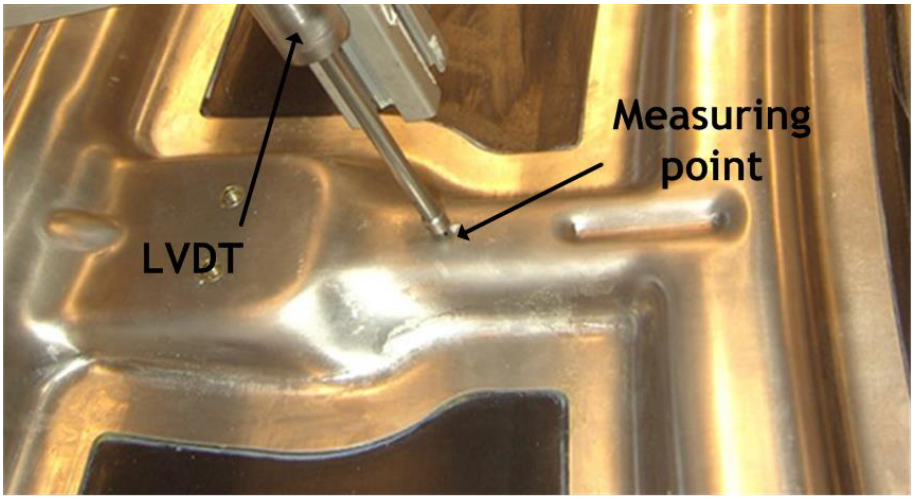

Figure 3.38 – LVDT in centre position.

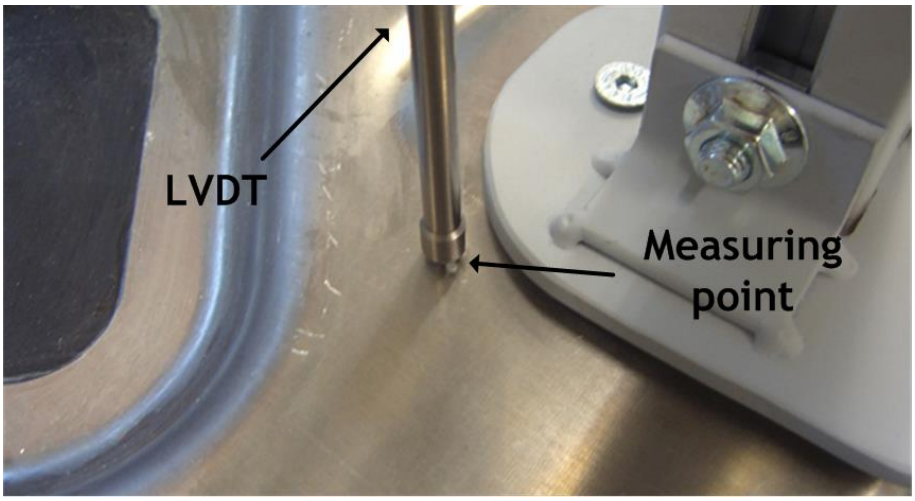

Figure 3.39 – LVDT in hinges position.

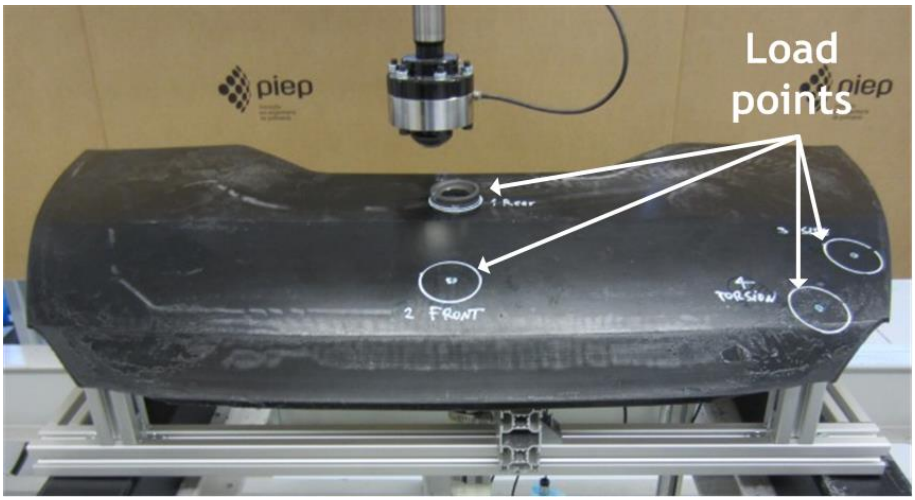

Figure 3.40 – Puncture positioning setup.

In the end, a testing program was designed using Dyna Tester software as can be seen in Figure 3.41. A testing configuration with two ascendant and descendent loading magnitudes was defined (a ramp from 0N to 100N with a subsequent pause, a second ramp from 100N to 200N with subsequent pause and two more descendant ramps with inverse behaviour). The displacement was measured with the load cell and LVDTs. A load cell of 20kN and a contact kneecap of 50mm diameter were used acting at 2N/sec.

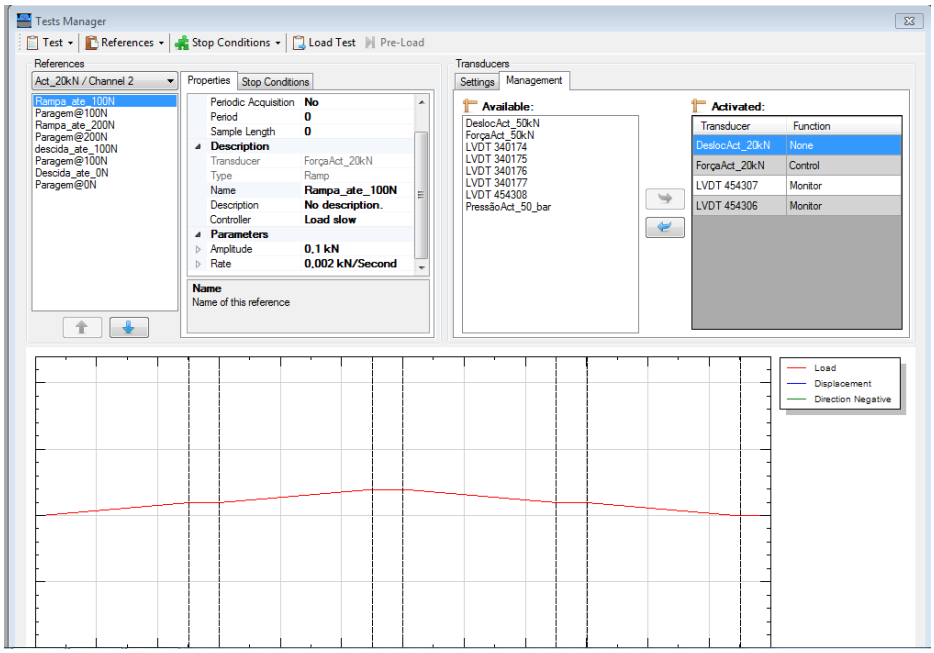

Figure 3.41 – Test configuration.

3.4.2. Results

Front and rear tests presented an apparent regular behaviour along the test, while the side beam and torsion tests presented some slippery mainly due to the curved bonnet geometry. The slippery issue was even more evident on the torsion test where a great displacement difference can be observed between the simulation and the experimental test. Front and rear beam tests, as well as torsion presented stiffness values of 38, 24 and 51 and 86% lower than FEA, as can be seen in Figure 3.42. Nevertheless they were enough to validate the model once all stiffness targets were accomplished. More detailed charts can be found in the Section G of the Appendices.

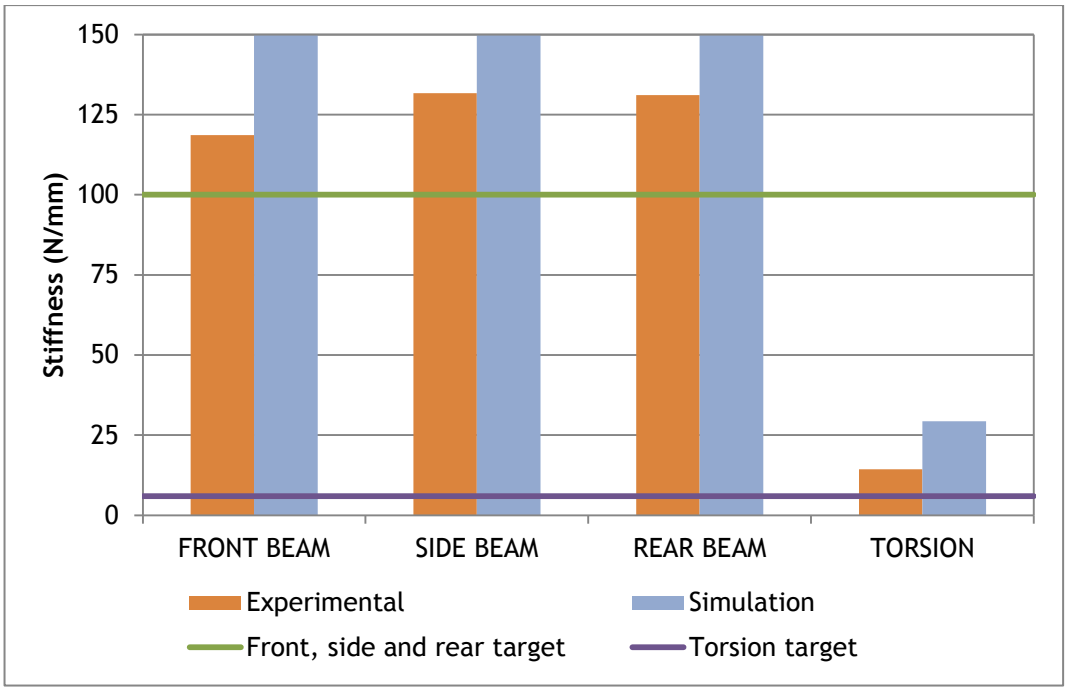

Figure 3.42 – Simulation and experimental results.

4. Manufacturing costs and life cycle analysis of the bonnet

This section shows the cost and environmental impact of the bonnet developed herein and they were obtained through the Process-Based Cost Model (PBCM) and Life Cycle Assessment (LCA) models depicted in Figure 4.1. Both cost and environmental impacts were calculated according to a mass production scenario and they were compared to the costs of a conventional bonnet configuration, i.e. as they had both exterior and interior panels in metal. This was done with the aim of understanding the actual magnitude of the obtained results.

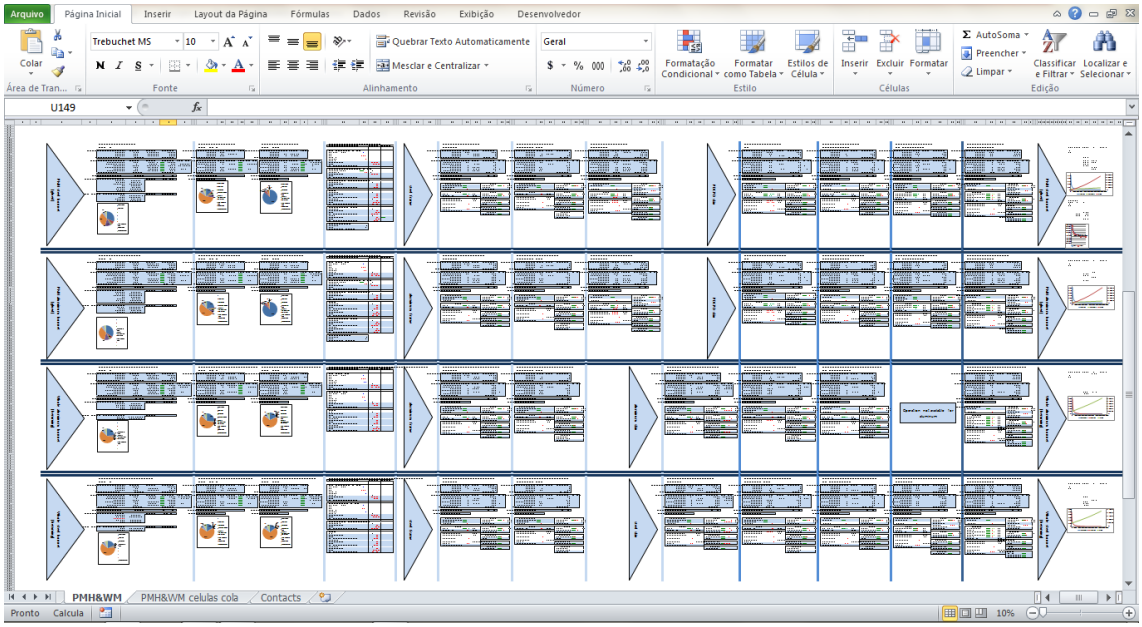

Figure 4.1 – Process-Based Cost and Life Cycle Assessment model.

4.1. Manufacturing costs

This analysis compares four different bonnet types: two bonnets containing a polymer-metal hybrid (PMH) configuration and two other containing a whole metal (WM) configuration. In order to simplifying data, bonnets where named as Bonnet1, Bonnet2, Bonnet3 and Bonnet4, as can be seen in Figure 4.2.

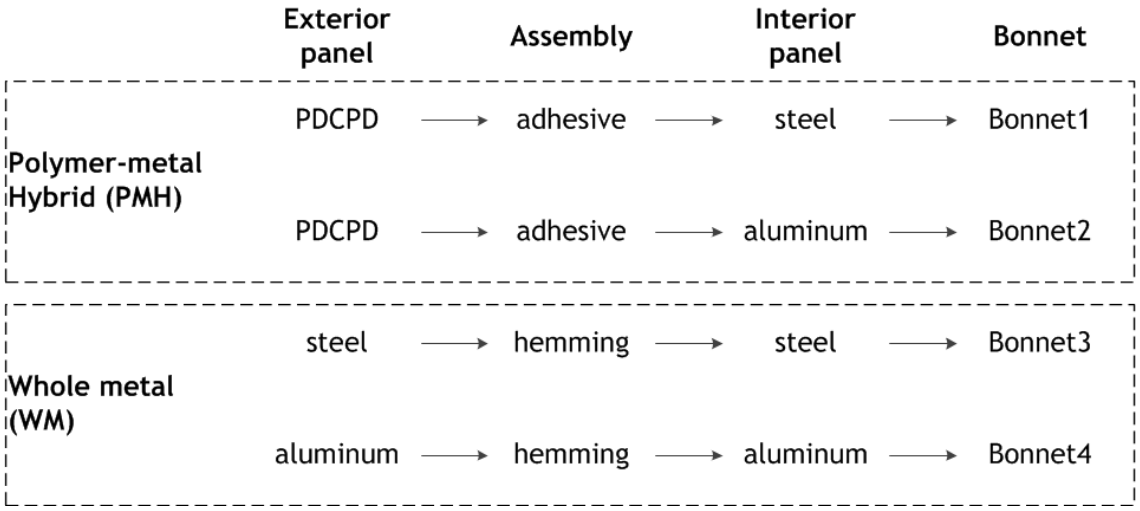

Figure 4.2 - Configuration and identification of the studied bonnets.

Each group (PMH or WM) is intended to be produced according to two different manufacturing chains with different processing stages, as can be seen in Figure 4.3 and 4.4 and Tables 4.1 and 4.2.

PMH bonnets start with the frame manufacture, where a metal coil whether in steel or aluminium (Al) is trimmed, stamped and then submitted for a surface treatment like cataphoresis. It allows having a suitable surface condition during the adhesive bonding operation. Skin manufacturing starts also in raw but in a liquid state inside a barrel (dicyclopentadiene (DCPD)), which is subsequently injected into the mould using a reaction injection moulding (RIM) equipment. This is then submitted to finishing operations where the flash is removed. By the end, frame and skin are assembled through adhesive bonding with successively painting.

Within WM group, while the frame is produced as the previous described manufacturing chain, skin tends to adopt a metallic manufacturing environment, being shaped through the same manufacturing stages used for the frame.

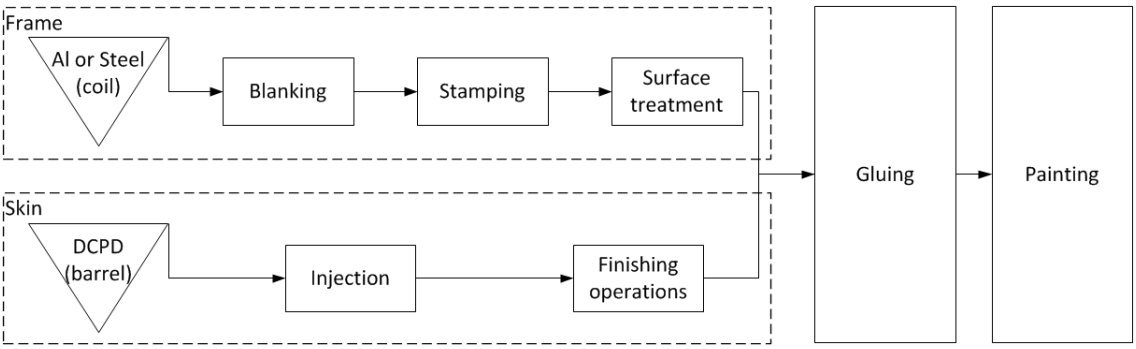

Figure 4.3 - Manufacturing diagram for PMH bonnets.

Table 4.1 – Manufacturing stages for PMH bonnets.

PART	REFERENCE	STAGES	DEPENDENCE
Frame	a	Blanking	Start
	b	Stamping	a
	c	Surface treatment	b
Skin	d	Injection	Start
	e	Finishing operations	d
	f	Assembly	c and e
	g	Painting	f

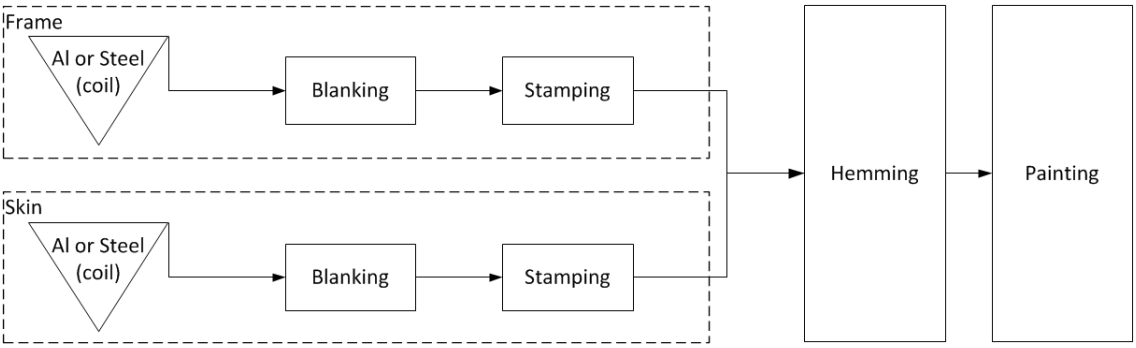

Figure 4.4 - Manufacturing diagram for WM bonnets.

Table 4.2 – Manufacturing stages for WM bonnets.

PART	REFERENCE	STAGES	DEPENDENCE
Frame	a	Blanking	Start
	b	Stamping	a
Skin	c	Blanking	Start
	d	Stamping	c
	e	Assembly	b and d
	f	Painting	e

Comparing both manufacturing chains, it may be concluded that WM bonnets will require less stages since processes like finishing or surface treatment are not applicable. As a result, the total cost for the complete bonnet may be achieved through the equation (4.1):

$$C_{bonnet} = C_{frame} + C_{skin} + C_{assembling} + C_{painting} \quad (4.1)$$

where,

C_{frame} is the frame total cost

C_{skin} is the skin total cost

$C_{assembling}$ is the assembling total cost

$C_{painting}$ is the painting total cost

4.1.1. Process-based cost model inputs

Costs related to marketing and advertising, product development, taxes, packaging, waste disposal and warehousing were not considered since they do not have a great contributing factor for the cost delta pursued within this study. Assuming that the entire bonnet is manufactured and assembled in one single facility, no transportation costs were also considered. Therefore, only those elements enumerated in Table 4.3 were considered.

Table 4.3 – Costs elements used.

VARIABLE COSTS	FIXED COSTS
Main Materials	Main Machine
Consumables	Auxiliary Equipment
Energy	Tooling
Labour	Fixed Overhead
	Building
	Maintenance

Inputs were obtained by measuring comparable processes within an industrial environment, while tooling and equipment costs were provided by the consortium involved in this research work. Stamping tools cost differ according to the materials to be stamped (Al or steel) and they require different number of stamping phases to shape the parts because they have different geometries i.e. once the skin geometry is less complex, than the frame, it would require less stamping phases to go from a flat sheet to the intended shape, including edge trimming. Table 4.4 presents both tooling costs and necessary stamping phases.

Table 4.4 - Tooling costs and required stamping phases.

TOOL	COST [€]	STAMPING PHASES
Blanking cut tool	100.000	-
Stamping tool for steel frame	700.000	5
Stamping tool for aluminium frame	900.000	5
Stamping tool for a steel skin	900.000	4
Stamping tool for an aluminium skin	1.100.000	4
Injection mould for polydicyclopentadiene skin	15.000	-
Jig for frame positioning	60.000	-

Table 4.5 presents the shaping processes for both skin and frame. 5 and 10sec per stroke were considered for blanking and stamping, respectively. Thus, the complete cycle time for stamping can be achieved through a function of those 10sec and the number of stamping phases presented in the previous Table 4.4.

RIM process behaves in a different way. Here the RIM cycle time x_1 is obtained through a function of the shot rate, the mass of the part to be produced and the subsequent curing

time (as previously shown, in the section 3.3.2 Exterior panel). Equation (4.2) expresses this reasoning:

$$x_1 = Injection_{time} = \frac{Part_{Mass}}{Shot\ rate} + Curing_{time} \quad (4.2)$$

where,

$Part_{Mass}$, is the mass of the part (Table 4.10).

$Shot\ rate$, is the shot time per kg, which according to the previous section, 3.3.2 Exterior panel, was 550g/sec.

$Curing_{time}$, is the required time for the polymerization occur inside the mould. For this work, 2min of curing time were considered which is also in line with the previous section 3.3.2 Exterior panel.

Table 4.5 – Shaping and cutting operations.

	STAGE		
ELEMENTS	**BLANKING**	**STAMPING**	**RIM**
Main machine cost [€]	1.000.000	2.500.000	135.000
Energy consumption rate [kWhr]	20	200	55
Space required [m^2]	20	30	30
Workers	1	2	2
Unplanned downtime [hr/shift]	0.1	0.1	0.1
Cycle time [sec]	5	10	x_1

A robotic cell was assumed for adhesive application and hemming but with different speed rates, since robots perform the task in a different way. For finishing, a manual operation was considered. The cycle time x_2 for these operations was obtained by simply multiplying the bonnet exterior perimeter (P_1) (previously defined in Table 3.13 as 2960mm) and the operation rates stated in Table 4.6.

Table 4.6 – Assembling and finishing operations.

	GLUING	FINISHING	HEMMING
Cell cost [€]	300.000	5.000	400.000
Energy consumption [kWhr]	20	2	20
Space required [m^2]	20	20	20
Operation rate	100 mm/sec	20 mm/sec	50 mm/sec
Workers	1	1	1
Total downtime [hr/shift]	0.1	0.1	0.1
Cycle time [sec]		x_2	

Table 4.7 presents cataphoresis and painting cell parameters used for PMH bonnet versions. Thus, before any assembly step, the stamped frame is submitted to the cataphoresis where a 20μm layer is applied over its surface. This process is divided in seven steps as may be seen in Figure 4.5. It starts with degreasing and washing operations with subsequent painting. It ends up with the drying and polymerization operations which conventionally occur during 30min at 180° C [171]. 40min of cycle time were considered for the whole chain of events. 10 parts can be produced at once.

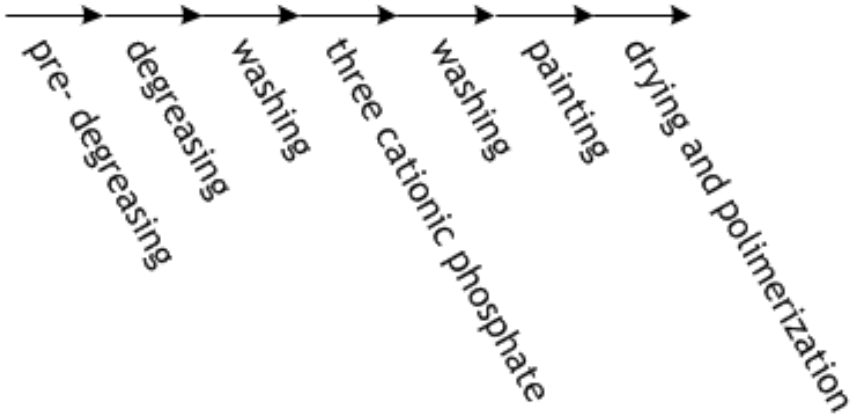

Figure 4.5 - Cataphoresis process steps.

Painting time x_3 is obtained by multiplying the area to be painted and the painting operation rate. Besides the existence of a wide choice of painting options for the automotive body panels, the painting stage selected herein presents a three layer application (primer, base and clear coats) for the WM bonnets and a two layer application (base and clear coats)

for the PMH bonnets. An acrylic based solvent was selected for both primer and clear coats, while polyester based water was selected as base coat. This is a combination that less contributes for the environmental impact and may be found elsewhere [12]. 70% effective transfer efficiency (ETE) without reclaim was also considered for all painting layers.

Table 4.7 – Surface treatment and painting operations.

	CATAPHORESIS	**PAINTING**
Cell cost [€]	400.000	15.000
Energy consumption [kWh]	50	15
Gas Consumption [m^3/h]	20	11
Space required [m^2]	200	40
Operation rate	-	1 m^2/min
Workers	3	1
Total downtime [h/shift]	0.1	0.1
Cycle time [sec]	40	x_3

Tables 4.8, 4.9 and 4.10 present the information related to materials, general data and the detailed weights for each bonnet configuration. It includes the cost of the materials introduced previously within the section 3.1 Materials Selection, as well as the painting and cataphoresis coatings cost. It includes also the curing times expected for the adhesive bonding and the layer thickness applied during the painting operations.

Table 4.8 – Material costs.

MATERIAL	€/kg	kg/m^3	-
Steel [DC04+ZE]	0,90	7.850	-
Aluminium [AW5754 H111]	3,50	2.660	-
DCPD [Telene 1650]	9	1.030	-
CONSUMABLES	**€/kg**	**kg/m^3**	**CURING TIME [sec]**
Adhesive contact [Terostat 3216]	35	1.000	N/R
Adhesive [Crestabond M7-15]	38	1.000	900
INK	**€/kg**	**kg/m^3**	**LAYER [µm]**
Electro coat	15	950	20
Primer [Acrylic solvent based]	35	950	25
Basecoat [Polyester water based]	27	950	25
Clearcoat [Acrylic solvent based]	43	950	45

Table 4.9 – General data.

GENERAL INPUTS	VALUE
Annual Production Target [#/year]	10.000
Interest Rate [%]	10
Product life [years]	5
Wage [€/hr]	4,50
Energy cost [€/kWhr]	0,16
Gas cost [€/m^3]	0,50
Building Costs [€/m^2]	200
Building Life [years]	40
Equipment life [years]	20
Overhead burden [%]	10
Operating Days [days/year]	240
Number of shifts [#]	1
Working Hours per Shift [hr]	8
No operations, breaks, etc. [hrs/shift]	1
Maintenance [hrs/shift]	0,1
Equipment & Building Maintenance [%]	10

Table 4.10 – Bonnet specifications.

PARAMETERS	BONNET1		BONNET2		BONNET3		BONNET4	
	PDCPD	Steel	PDCPD	Al	Steel	Steel	Al	Al
Thickness[mm]	3	0.8	3	1.5	0.8	0.8	1	1.5
Weight[kg]	1.31	2.04	1.31	1.32	2.67	2.04	1.13	1.32
Assembly type	Adhesive		Adhesive		Hemming		Hemming	
Adhesive weight [kg]	0.01		0.01		-		-	
Cataphoresis [kg]	-	0.01	-	0.01	-	-	-	-
Painting weight [kg]	0.05		0.05		0.07		0.07	
Total weight [kg]	3.42		2.7		4.78		2.52	

4.1.2. Results

According to Figure 4.6, 71% cost decrease can be seen for Bonnet1 and Bonnet2 till 5.000 units produced. Their cost difference percentage tends to decrease from 19 to 12% till 50.000 units produced. After 30.000 units produced, a slightly cost increase may be denoted for both bonnets, which is caused by the additional tooling and RIM equipment required to ensure that annual production volume.

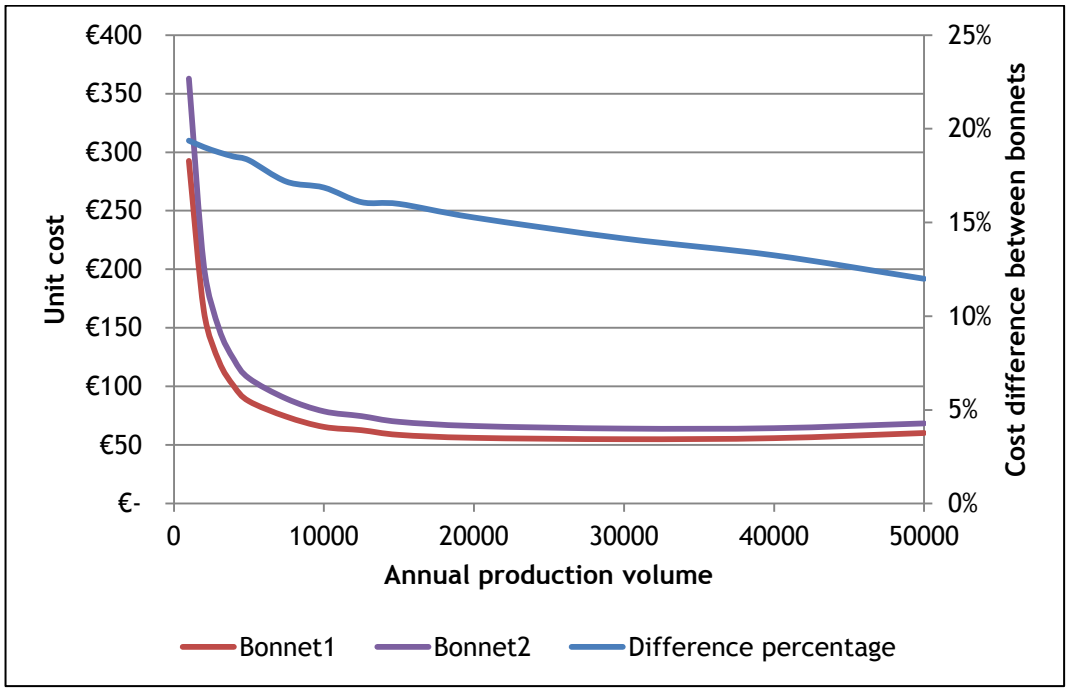

Figure 4.6 - Bonnet1 and 2 cost difference.

WM bonnets presented a different cost projection. According to Figure 4.7, 78% cost decrease can be seen for Bonnet3 and Bonnet4 till 5.000 units produced, however their cost difference percentage increases from 20 to 31% till 50.000 units produced. Contrary to the PMH bonnets, these WM presented a steady cost till 50.000 units.

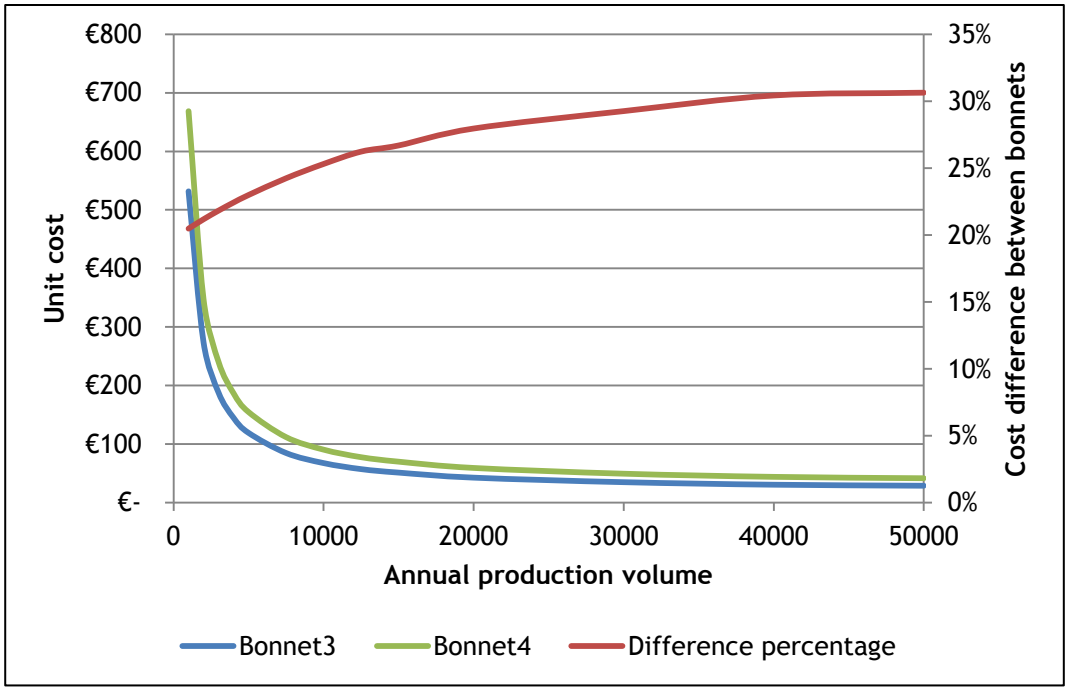

Figure 4.7 - Bonnet3 and 4 cost difference.

Figures 4.8 and 4.9 present the cost efficiency of PMH against WM bonnets in two ways, investment and unit cost respectively. It may be seen that a steel reinforced PMH bonnet tops its cost efficiency at 10.000 units when compared to its equivalent whole steel based. Taking into account that the steel reinforced PMH bonnet is 29% lighter (Table 4.10) than its WM equivalent, the total cost efficiency might be extended if life energy savings were considered (not evaluated within this study). Al reinforced PMH bonnet presents a different projection by reaching its maximum cost efficiency at 15.000 annual units. However considering that its equivalent WM bonnet is 7% lighter, Bonnet2 becomes unsatisfactory after this annual production volume. With this, it may be concluded that, for annual production volumes fewer than 15.000 units, a PMH configuration equivalent to the one developed herein will present a positive outcome. Additional charts with the cost breakdown can be found in the Section H of the Appendices.

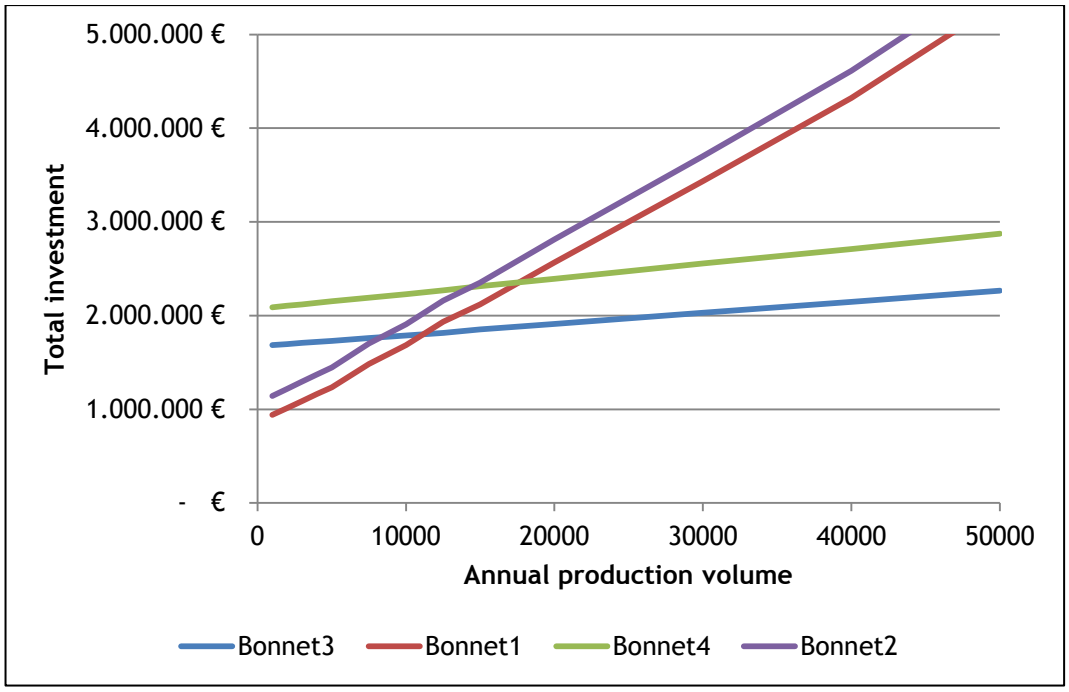

Figure 4.8 - Required investment.

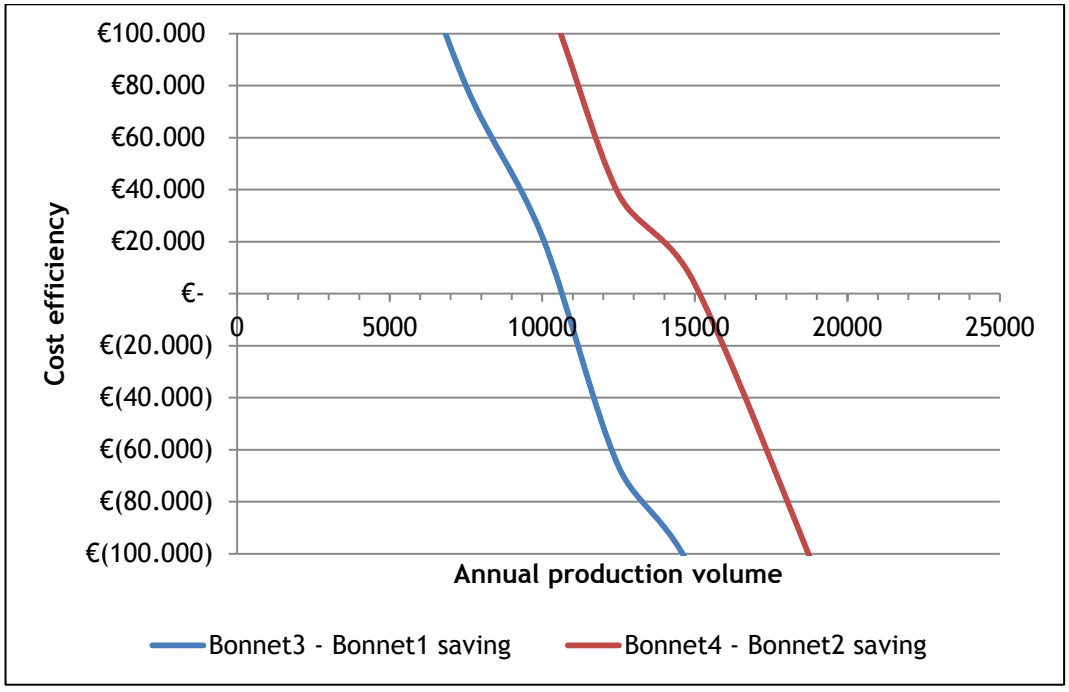

Figure 4.9 - Production volume limit of PMH versus equivalent WM bonnets.

4.2. Life cycle assessment

A Life Cycle Assessment (LCA) was done using energy data from raw material extraction, manufacturing, use and recycling (Figure 4.10). General material databases available elsewhere [157] were accessed for embodied energy data. For manufacturing energy calculation, the power required for each manufacturing stage was considered. For running costs calculation, the general EVs energy efficiency ratio was used too. Recycling energy demand was obtained using estimated values of collection, sorting and disposal as defined previously in 2.6.1.1 Main LCA equations section.

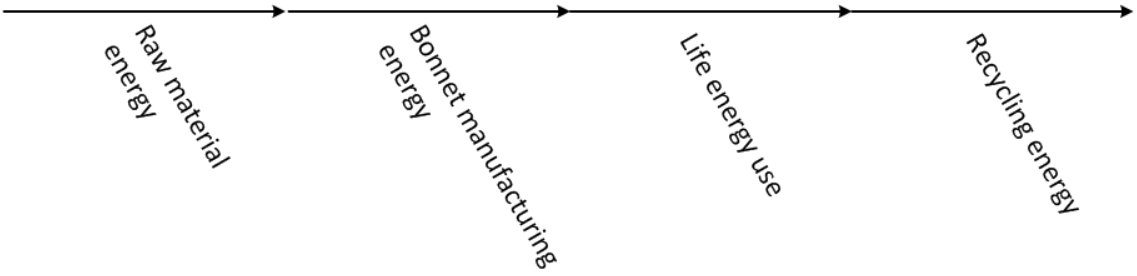

Figure 4.10 – Life cycle analysis framework.

4.2.1. Life cycle assessment inputs

Table 4.11 presents energy data used in the LCA model. The energy value of 6.70 MJ/kWh was considered once it corresponds to the world average energy conversion ratio obtained according to the average of different sources like thermal, nuclear, wind, among others [144, 157, 172].

During data gathering different sources were found presenting different values of embodied energy for Al and steel (203 to 216MJ/kg and 26.5MJ/kg to 35MJ/kg respectively), but as question of conformity, only the values from one single source [157] were considered. See Table 4.12.

In order to obtain the total vehicle energy demand over lifetime, 10 years of use were assumed with an average of 10.000km per year, which was then multiplied by the weight of the bonnet and EV energy efficiency ratio presented in Table 4.13.

Table 4.11 – Electricity and natural gas energy conversion [157, 172].

ENERGY SOURCE	ENERGY CONVERSION
Electricity [MJ/kWh]	6.70
Natural gas [MJ/m^3]	38

Table 4.12 – Materials embodied energy [12, 157].

MATERIAL	EMBODIED ENERGY [MJ/kg]	RECYCLING ENERGY [MJ/kg]	RECYCLING TYPE
Steel	26.5		down cycled
Aluminium	203		down cycled
PDCPD	100	41.8	incinerated
Adhesive	322	-	disposal
Electro coat	100	-	disposal
Primer	275	-	disposal
Basecoat	49	-	disposal
Clearcoat	126	-	disposal

Table 4.13 – Estimated life parameters for MobiCar [158].

VEHICLE PARAMETERS	VALUE
Vehicle lifetime operation [km]	100.000
Vehicle energy consumption [MJ/kg.km]	0.00017

4.2.2. Results

Figure 4.11 shows a summary of the results. It may be seen that both bonnets containing Al require more energy, which has to do with the highly energy demanding process required to extract and refine Al. On the other hand, the embodied energy still presents some "credit" after recycling. This happens especially because Al recycling only takes 5% of its extraction energy. Manufacturing is the second more energy demanding phase of the life cycle, except for the WM steel based version (Bonnet3) which due to its weight, it will require more energy during the vehicle operation than during its manufacturing. Besides that, PMH bonnets have a more energy demanding penalty by requiring a surface treatment

process. For disposal, minor values were achieved since only sorting stages are necessary. In spite of PDCPD contributing for credit by incineration, only a few energy amounts are recovered by bonnet. Additional data can be found in the Section I of the Appendices.

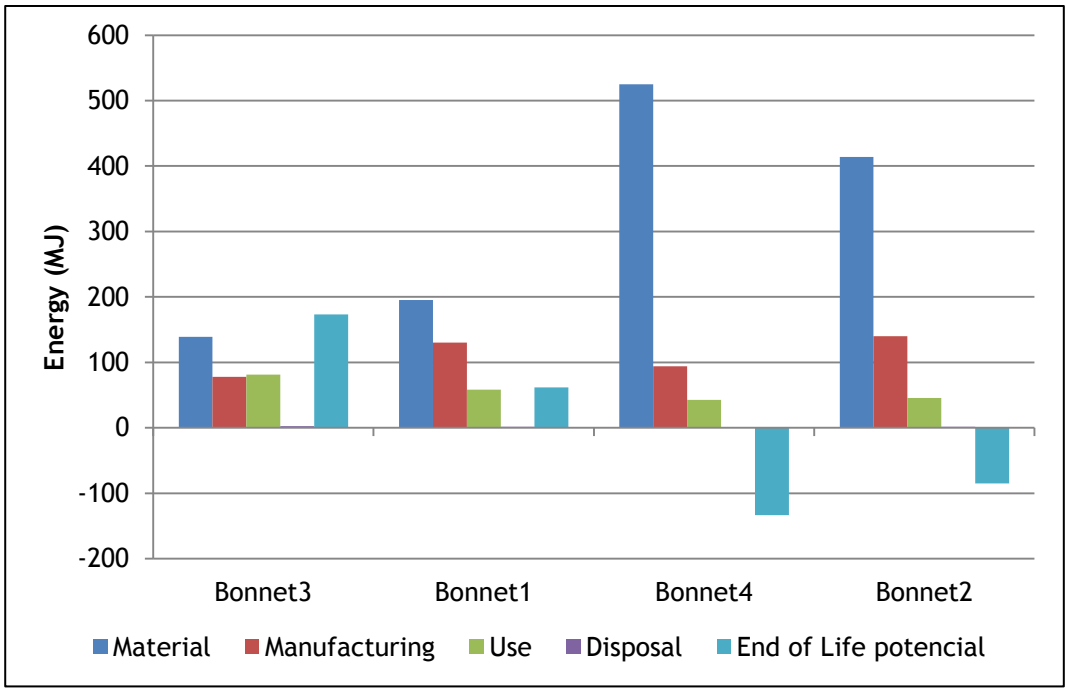

Figure 4.11 – Total energy required and recovered.

4.3. Legislation discussion

According to recycling targets defined by EU directives for 2015, vehicles shall present 95% of recyclable materials. Only 5% can remain as pure waste and be landfilled. With this, concerns to the PDCPD application on vehicle arises since it makes part of those 10 to 15% once it can be recovered as energy or landfilled. Considering that MobiCar presents 8m^2 of exterior surface, the use of PDCPD will account for 17.5kg if the geometry developed herein is used as reference. In addition, once MobiCar belongs to a vehicle category L7 which requires a maximum weight of 400kg, it can be concluded that the use of PDCPD at least in the exterior will hardly exceed 15% of vehicle weight.

5. Conclusion

A new class of vehicles combining improved design solutions, advanced lightweight materials and configurations, cost efficient manufacturing processes and energy efficient propulsion systems, are nowadays desired. However, this new class presents some engineering and economic challenges. The majority of electric vehicles (EVs) still present reduced autonomy range which is reflected in a low demand and consequently in low production volumes, leading to lightweight materials and manufacturing process choice limitations. As a result, this research work aimed to show an innovative solution for exterior automotive body panels by combining low density materials and a cost efficient manufacturing process applicable on low production volumes.

From the development phase it was concluded that a frame with a single central beam would be adequate to ensure the structural stiffness required by Centre of Excellency and Innovation for Mobility Industries (CEIIA). It was also concluded that larger and deeper profile beams are required to ensure adequate stiffness once the polydicyclopentadiene (PDCPD) skin offers little structural improvement. It was also possible to prove by experimental tests that the bonnet developed herein is able to accomplish the structural targets established by CEIIA.

In terms of physical attributes it may be concluded that, for the final bonnet, a minimum weight of 3.35kg may be expected with a 0.8mm thick steel frame and a minimum weight of 2.63kg may be expected with a 1.5mm thick aluminium (Al) frame, both having equivalent stiffness.

From the adhesive track evaluation it was concluded that no additional material on the frame was necessary, since an adhesive bond with 4.28mm would be enough to withstand the maximum thermal expansion deformation.

From the prototyping phase it can be concluded that hydraulic pressing would require 2 persons constantly verifying the process between stampings. This process took about 1 to 2 minutes between each stamping, with the stamping stroke itself only accounting for 10 seconds.

From reaction injection moulding (RIM) process, two parts were extracted in perfect conditions and were enough to accomplish the objectives of the project. The assembly process was the most ease of overtake, not presenting any relevant challenge.

From the cost model it can be concluded that polymer-metal hybrid (PMH) solutions may provide cost efficient results till a maximum of 10.000 to 15.000 annual produced units. This is considered a maximum since alternative materials such as Al can provide lower weight ratio than the PMH bonnet developed herein and thus, become preferable. This section also showed that the use of Al would incur in higher energy impacts since the available extraction technologies currently available are still high energy demanding. However its low density presents lower weights and thus, lowers energy requirements during vehicles life time than versions using steel (Bonnet1 and Bonnet3).

Thus, it can be concluded that PDCPD PMH based exterior body panels can contribute to produce new and exciting automotive designs that with enough structural integrity with lower capital investment and cost efficient result on low production volume vehicles. It can be also concluded that PDCPD based components can ensure acceptable end of life results once a reasonable energy value can be recovered from it. In addition, with reasoning use, PDCPD will hardly exceed the EU targets for vehicles end of life once it makes part of those 10% that can be energetically recovered plus the 5% that can be landfilled.

5.1. Recommendations and future works

Due to the lack of time and budget, several questions remained with no answer and others were raised:

- Other materials, apart from Al and steel could be used to produce the reinforcement for PDCPD.
- The structural reliability of the assembly remains uncertain. Additional simulations or real tests shall be made in order to understand the adhesive acting on PDCPD under different weather and fatigue conditions. Other tests like overall corrosion, vibration and impact could also potentially be made.
- Other techniques like riveting and overmoulding may be explored in the future in terms of cost and reliability by using parts where no aesthetic concerns are involved.
- PDCPD shares the same production infrastructure of Polyurethane (PU) however remains with less market visibility. The PDCPD potential over PU in the automotive industry, in terms of cost, weight and quality might be a useful research work.
- Additional research needs to be done on the PDCPD polymerization with aim of reducing its odour, which is, apparently, a limiting factor on its massive adoption.

References

1. Becker, T., *Electric Vehicles in the United States, A New Model with Forecasts to 2030*, in *Center for Entrepreneurship & Technology (CET), Technical Brief*2009, Center for Entrepeneurship & Technology, Univesity of California: Berkeley.
2. Shinnar, R., *The hydrogen economy, fuel cells, and electric cars.* Technology in Society, 2003. 25(4): p. 455-476.
3. Edwards, K.L., *Strategic substitution of new materials for old: Applications in automotive product development*. Materials & Design, 2004. 25(6): p. 529-533.
4. *Telene brochure*, Rimtec, Editor.
5. Sherman, L.M. *Poly-DCPD RIM shifts into higher gear*. 2002 June 2014]; Available from: http://www.ptonline.com/articles/poly-dcpd-rim-shifts-into-higher-gear.
6. Rosato, D.V., D.V. Rosato, and M.V. Rosato, *2 - Plastic Property*, in *Plastic Product Material and Process Selection Handbook*. 2004, Elsevier: Oxford. p. 40-129.
7. Heskett, J., *Industrial design*. 1980: Oxford University Press.
8. Høyer, K.G., *The history of alternative fuels in transportation: The case of electric and hybrid cars.* Utilities Policy, 2008. 16(2): p. 63-71.
9. Mayyas, A., et al., *Design for sustainability in automotive industry: A comprehensive review.* Renewable and Sustainable Energy Reviews, 2012. 16(4): p. 1845-1862.
10. Bilotkach, V. and M. Mills, *Simple Economics of Electric Vehicle Adoption.* Procedia - Social and Behavioral Sciences, 2012. 54(0): p. 979-988.
11. Shepherd, S., P. Bonsall, and G. Harrison, *Factors affecting future demand for electric vehicles: A model based study.* Transport Policy, 2012. 20(0): p. 62-74.
12. Papasavva, S., et al., *Characterization of automotive paints: an environmental impact analysis.* Progress in Organic Coatings, 2001. 43(1–3): p. 193-206.
13. McAuley, J.W., *Global Sustainability and Key Needs in Future Automotive Design.* Environmental Science & Technology, 2003. 37(23): p. 5414-5416.
14. Sharma, R., et al., *Conventional, hybrid and electric vehicles for Australian driving conditions – Part 1: Technical and financial analysis.* Transportation Research Part C: Emerging Technologies, 2012. 25(0): p. 238-249.

15. Van Vliet, O., et al., *Energy use, cost and CO_2 emissions of electric cars*. Journal of Power Sources, 2011. 196(4): p. 2298-2310.

16. Hodkinson, R. and J. Fenton, *7 - Lightweight construction materials and techniques*, in *Lightweight Electric/Hybrid Vehicle Design*. 2000, Butterworth-Heinemann: Oxford. p. 173-198.

17. Midler, C. and R. Beaume, *Project-based learning patterns for dominant design renewal: The case of Electric Vehicle*. International Journal of Project Management, 2010. 28(2): p. 142-150.

18. Obsession, E. *Electric Cars 2014 — Prices, Efficiency, Range, Pics, More*. 2014 June 2014]; EV News. EV Commentary. Original EV Analysis.]. Available from: http://evobsession.com/electric-cars-2014-list/.

19. Plugincars. *2014 Electric Cars*. 2014 June 2014]; Available from: http://www.plugincars.com/2014-electric-cars.

20. Economist, T., *The electric-fuel-trade acid test*. The Economist, 2009.

21. Tseng, H.-K., J.S. Wu, and X. Liu, *Affordability of electric vehicles for a sustainable transport system: An economic and environmental analysis*. Energy Policy, 2013. 61(0): p. 441-447.

22. Ribeiro, B., F. Brito, and J. Martins, *A survey on electric/hybrid vehicles*. Transmission and Driveline 2010 (SP-2291), 2010. SAE International, 2010-01-0856: p. 133-146.

23. Lieven, T., et al., *Who will buy electric cars? An empirical study in Germany*. Transportation Research Part D: Transport and Environment, 2011. 16(3): p. 236-243.

24. Obsession, E. *Ranking European Countries On 2013 Electrified Car Sales*. 2014 June 2014]; EV News. EV Commentary. Original EV Analysis.]. Available from: http://evobsession.com/ranking-european-countries-2013-electrified-car-sales/.

25. Driscoll, Á., et al., *Simulating demand for electric vehicles using revealed preference data*. Energy Policy, 2013. 62(0): p. 686-696.

26. AVERE. *Immatriculations de véhicules électriques en Europe : +60% en 2014*. 2015 June 2015]; Association nationale pour le développement de la mobilité électrique]. Available from: http://www.avere-france.org/Site/Article/?article_id=5985&from_espace_adherent=0.

27. *Renault ZOE*, 2012: https://www.cdn.renault.com/content/dam/Renault/UK/vehicles/b10-zoe-ph1-2012/zoe-expnav.jpg.ximg.l_full_m.smart.jpg.

28. *Nissan Leaf*: http://cdn2.carbuyer.co.uk/sites/carbuyer_d7/files/nissan-leaf-cutout-2.jpg.

29. ChinaAutoWeb. *2014 EV Sales Ranking*. 2015 June 2015]; A Guide to China's Auto Industry]. Available from: http://chinaautoweb.com/2015/01/2014-ev-sales-ranking/.

30. Association, E.D.T. *Electric Drive Sales Dashboard*. 2015 June 2015]; Promoting electric drive technologies and infrastructure]. Available from: http://electricdrive.org/index.php?ht=d/sp/i/20952/pid/20952.

31. Alcoa, *Body in white concept: Body in white with aluminium sheet metal parts*, Aluminium matter: http://aluminium.matter.org.uk/.

32. Zhang, Y., et al., *Lightweight design of automobile component using high strength steel based on dent resistance*. Materials & Design, 2006. 27(1): p. 64-68.

33. Sherman, A.M., et al., *Automotive Body Materials*, in *Encyclopedia of Materials: Science and Technology (Second Edition)*, K.H.J.B. Editors-in-Chief: , et al., Editors. 2001, Elsevier: Oxford. p. 415-421.

34. *ULSAB - Ultralight Steel Auto Body*. 2013 [cited 2013 March]; Available from: http://www.worldautosteel.org/projects/ulsab/.

35. Roth, R., *Manufacturing Costs of Auto Bodies*, in *Encyclopedia of Materials: Science and Technology (Second Edition)*, K.H.J.B.W.C.C.F.I.J.K.M. Veyssière, Editor. 2001, Elsevier: Oxford. p. 5163-5172.

36. ACC's, *Plastics and Polymer Composites Technology Roadmap for Automotive Markets*, 2014, ACC's. p. 64.

37. Demeri, M.Y., *Advanced high-strength steels; science, technology, and applications*. 2013: ASM International. 301.

38. Wood, K. *Automotive Composites: Taking Subjectivity out of Class A Surface Evaluation*. 2008 June 2014]; Available from: http://www.compositesworld.com/articles/automotive-composites-taking-subjectivity-out-of-class-a-surface-evaluation.

39. Fuchs, E.R.H., et al., *Strategic materials selection in the automobile body: Economic opportunities for polymer composite design*. Composites Science and Technology, 2008. 68(9): p. 1989-2002.

40. Association, T.A., *Aluminum for automotive body sheet panels*, 1998, The Aluminum Association.

41. Miller, W.S., et al., *Recent development in aluminium alloys for the automotive industry*. Materials Science and Engineering: A, 2000. 280(1): p. 37-49.

42. James G.Bralla, *Design for Manufacturability Handbook, Second Edition*. 1999: 1986 The McGraw-Hill Companies, Inc.

43. Roth, R., J. Clark, and A. Kelkar, *Automobile bodies: Can aluminum be an economical alternative to steel?* JOM, 2001. 53(8): p. 28-32.

44. Gunnarsson, L. and E. Schedin, *Improving the properties of exterior body panels in automobiles using variable blank holder force*. Journal of Materials Processing Technology, 2001. 114(2): p. 168-173.

45. Kleiner, M., M. Geiger, and A. Klaus, *Manufacturing of Lightweight Components by Metal Forming*. CIRP Annals - Manufacturing Technology, 2003. 52(2): p. 521-542.

46. Farag, M.M., *Quantitative methods of materials substitution: Application to automotive components*. Materials & Design, 2008. 29(2): p. 374-380.

47. Council, E.P.a., *Directive 2000/53/EC*, E.P.a. Council, Editor 2000.

48. McConnell, V.P., *SMC has plenty of road to run in automotive applications*. Reinforced Plastics, 2007. 51(1): p. 20-25.

49. Kurcz, M., et al., *Replacing Steel with Glass-Mat Thermoplastic Composites in Automotive Spare-Wheel Well Applications*, 2005, SAE Technical Paper.

50. Stauber, R. and L. Vollrath, *Plastics in Automotive Engineering: Exterior Applications*. 2007: Hanser Publishers.

51. Messler, R.W., *Joining Composite Materials and Structures: Some Thought-Provoking Possibilities*. Journal of Thermoplastic Composite Materials, 2004. 17(1): p. 51-75.

52. Yang, Y., et al., *Recycling of composite materials*. Chemical Engineering and Processing: Process Intensification, 2012. 51(0): p. 53-68.

53. Niu, M.C.Y., *Composite airframe structures: practical design information and data*. 1992: Conmilit Press.

54. Ashley, S. *Lightweight carbon-fiber and SMC body panels under development*. 2013 June 2014]; Available from: http://articles.sae.org/12288/.

55. Malnati, P. *Faster cycle, better surface: Out of the autoclave*. 2013 June 2014]; Available from: http://www.compositesworld.com/articles/faster-cycle-better-surface-out-of-the-autoclave.

56. Fit, H.W., *BMW I3*, 2015: http://hdwallpapersfit.com/wp-content/uploads/2015/01/bmw-i3-wallpapers-hd.jpg.

57. Papathanasiou, T.D., *Flow and rheology in polymer composites manufacturing, Vol. 10, Composite Materials Series. Edited by S. G. Advani, Elsevier Science, Amsterdam, 1994, xvii + 607pp., price Dfl325.00/US$185.75. ISBN 0 444 89347 4*. Journal of Chemical Technology & Biotechnology, 1996. 67(1): p. 106-106.

58. *Is RTM ready for mass production?* Reinforced Plastics, 1995. 39(1): p. 26-34.

59. Haider, M., P. Hubert, and L. Lessard, *An experimental investigation of class A surface finish of composites made by the resin transfer molding process*. Composites Science and Technology, 2007. 67(15–16): p. 3176-3186.

60. Li, W. and L.J. Lee, *Shrinkage control of low-profile unsaturated polyester resins cured at low temperature*. Polymer, 1998. 39(23): p. 5677-5687.

61. Hsu, C.P., et al., *Effects of thermoplastic additives on the cure of unsaturated polyester resins*. Polymer Engineering & Science, 1991. 31(20): p. 1450-1460.

62. Davidson, T.A. and K.B. Wagener, *The polymerization of dicyclopentadiene: an investigation of mechanism*. Journal of Molecular Catalysis A: Chemical, 1998. 133(1–2): p. 67-74.

63. Estevez, S.R. and J.M. Castro, *Applications of a RIM Process Model*, in *Polymer Processing and Properties*, G. Astarita and L. Nicolais, Editors. 1984, Springer US. p. 123-130.

64. Yang, Y.-S., E. Lafontaine, and B. Mortaigne, *Curing study of dicyclopentadiene resin and effect of elastomer on its polymer network*. Polymer, 1997. 38(5): p. 1121-1130.

65. Rosato, D.V., D.V. Rosato, and M.V. Rosato, *12 - Reaction Injection Molding*, in *Plastic Product Material and Process Selection Handbook*. 2004, Elsevier: Oxford. p. 406-427.

66. Armitage, P.D., et al., *Modelling and simulation of reactive injection processes*. Computers & Chemical Engineering, 1999. 23, Supplement(0): p. S761-S764.

67. Teixeira, A. and B. Ribeiro, *Use of DCPD-RIM on exterior panels for the automotive industry*. Rapid Product Development Event, 2010.

68. Ng, H., *Studies of reactive polymer processing for dicyclopentadiene RIM and filled epoxy systems*, 1992, Case Western Reserve University.

69. *Nylon RIM Expands into Niche Applications*. 2004 June 2014]; Available from: http://www.ptonline.com/articles/nylon-rim-expands-into-niche-applications.

70. BASF, *Welding technologies for plastics manufacturing : vibration welding of thermoplastics*, B. Corporation, Editor 2003, BASF Corporation. p. 22.

71. Toplosky, V.J. and R.P. Walsh, *Thermal and Mechanical Properties of Poly-Dicyclopentadiene (DCPD) at Cryogenic Temperatures*. AIP Conference Proceedings, 2006. 824(1): p. 219-224.

72. Abadie, M.J., et al., *New catalysts for linear polydicyclopentadiene synthesis*. European Polymer Journal, 2000. 36(6): p. 1213-1219.

73. Barnes, S.E., et al., *Raman spectroscopic studies of the cure of dicyclopentadiene (DCPD)*. Spectrochim Acta A Mol Biomol Spectrosc, 2005. 61(13-14): p. 2946-52.

74. Perring, M., T.R. Long, and N.B. Bowden, *Epoxidation of the surface of polydicyclopentadiene for the self-assembly of organic monolayers*. Journal of Materials Chemistry, 2010. 20(39): p. 8679 – 8685.

75. Kessler, M.R. and S.R. White, *Cure kinetics of the ring-opening metathesis polymerization of dicyclopentadiene*. Journal of Polymer Science Part A: Polymer Chemistry, 2002. 40(14): p. 2373-2383.

76. He, Y., et al., *Preparation and Properties of Polydicyclopentadiene/MMt Nanocomposites Using Supported Tungsten Catalyst*. Polymer-Plastics Technology and Engineering, 2011. 50(11): p. 1103-1108.

77. Weijun Yin Weijun, Y., S. Kniajanski, and B. Amm, *Dielectric properties of polydicyclopentadiene and polydicyclopentadiene-silica nanocomposite*. Ieee International Symposium On Electrical Insulation. Proceedings, 2010: p. 1-5.

78. Constable, G.S., A.J. Lesser, and E.B. Coughlin, *Morphological and Mechanical Evaluation of Hybrid Organic−Inorganic Thermoset Copolymers of Dicyclopentadiene and Mono- or Tris(norbornenyl)-Substituted Polyhedral Oligomeric Silsesquioxanes*. Macromolecules, 2004. 37(4): p. 1276-1282.

79. Démoutiez, F. *Polydicyclopentadiene winning over construction professionals*. 2008 June 2014]; Available from: http://www.jeccomposites.com/news/composites-news/polydicyclopentadiene-winning-over-construction-professionals.

80. Constable, G.S., A.J. Lesser, and E.B. Coughlin, *Ultrasonic spectroscopic evaluation of the ring-opening metathesis polymerization of dicyclopentadiene*. Journal of Polymer Science Part B: Polymer Physics, 2003. 41(12): p. 1323-1333.

81. Industries, O. *PDCPD Molding Overview*. 2013 [cited 2013 23rd of October]; Available from: http://www.osborneindustries.com/dcpd-molding.php.

82. LLC, P., *Kenworth W-900L bonnet*, 2002, Plastics Technology: http://www.ptonline.com/articles/poly-dcpd-rim-shifts-into-higher-gear.

83. *The Elbil Norge*, 2014.

84. Gerstmann, T. and B. Awiszus, *Recent developments in flat-clinching*. Computational Materials Science, 2014. 81(0): p. 39-44.

85. Mucha, J., L. Kaščák, and E. Spišák, *Joining the car-body sheets using clinching process with various thickness and mechanical property arrangements*. Archives of Civil and Mechanical Engineering, 2011. 11(1): p. 135-148.

86. Rotheiser, J., *Joining of Plastics 3E: Handbook for Designers and Engineers*. 2009: Hanser Gardner Publications.

87. Charles, A.H., *Finishing, Assembly, and Decorating*, in *Modern Plastics Handbook*. 2000, McGraw Hill Professional, Access Engineering.

88. Messler Jr, R.W., *The challenges for joining to keep pace with advancing materials and designs*. Materials & Design, 1995. 16(5): p. 261-269.

89. Amancio-Filho, S.T. and J.F. dos Santos, *Joining of polymers and polymer-metal hybrid structures: Recent developments and trends*. Polymer Engineering & Science, 2009. 49(8): p. 1461-1476.

90. Swift, K.G. and J.D. Booker, *Process Selection: from design to manufacture*. 2003: Elsevier Science.

91. Brayton Lincoln, Kenneth J. Gomes, and J.F. Braden, *Mechanical Fastening of Plastics: An Engineering Handbook*. 1984: Taylor & Francis.

92. Parmley, R.O., *Standard handbook of fastening and joining*. 1989: McGraw-Hill.

93. Varis, J., *Ensuring the integrity in clinching process*. Journal of Materials Processing Technology, 2006. 174(1–3): p. 277-285.

94. Busse, S., et al., *Development of a mechanical joining process for automotive body-in-white production*. International Journal of Material Forming, 2010. 3(S1): p. 1059-1062.

95. Abe, Y., K. Mori, and T. Kato, *Joining of high strength steel and aluminium alloy sheets by mechanical clinching with dies for control of metal flow*. Journal of Materials Processing Technology, 2012. 212(4): p. 884-889.

96. Lambiase, F. and A. Di Ilio, *Optimization of the Clinching Tools by Means of Integrated FE Modeling and Artificial Intelligence Techniques*. Procedia CIRP, 2013. 12(0): p. 163-168.

97. Barnes, T.A. and I.R. Pashby, *Joining techniques for aluminium spaceframes used in automobiles: Part II — adhesive bonding and mechanical fasteners*. Journal of Materials Processing Technology, 2000. 99(1–3): p. 72-79.

98. Corporation, G.L.S., *Overmoulding Guide*, 2004.

99. Fetecau, C., D. Dobrea, and I. Postolache, *Overmolding Injection Molding Simulation Of Tensile Test Specimen*. International Journal of Modern Manufacturing Technologies, 2010. 2(2): p. 45-50.

100. J. Zhao, et al., *Over moulding technologies for automotive plastic components manufacturing applications*. SIMTech technical reports, 2008. 9: p. 6.

101. Marta Gomes, Júlio C. Viana, and A.J. Pontes, *Hybrid injection moulding: Overmoulding of metal inserts with pp*. Semana de Engenharia 2010, 2010: p. 8.

102. Camboa, A., et al., *Mechanical analysis of polydicyclopentadiene with metal inserts through flexural load*, in *IRF 2013 - 4th International Conference on Integrity, Reliability and Failure*2013: Funchal/Madeira.

103. Ageorges, C., L. Ye, and M. Hou, *Advances in fusion bonding techniques for joining thermoplastic matrix composites: a review*. Composites Part A: Applied Science and Manufacturing, 2001. 32(6): p. 839-857.

104. Higgins, A., *Adhesive bonding of aircraft structures*. International Journal of Adhesion and Adhesives, 2000. 20(5): p. 367-376.

105. Grant, L.D.R., R.D. Adams, and L.F.M. da Silva, *Effect of the temperature on the strength of adhesively bonded single lap and T joints for the automotive industry*. International Journal of Adhesion and Adhesives, 2009. 29(5): p. 535-542.

106. Xu, W. and Y. Wei, *Strength and interface failure mechanism of adhesive joints*. International Journal of Adhesion and Adhesives, 2012. 34(0): p. 80-92.

107. Packham, D.E., *Adhesive technology and sustainability*. International Journal of Adhesion and Adhesives, 2009. 29(3): p. 248-252.

108. Cremer, A. and V. Bryan. *Rush to lightweight cars boosts adhesive makers*. 2013 June 2014]; Available from: http://www.reuters.com/article/2013/06/05/automotive-glue-idUSL5N0AX2VI20130605.

109. Feraboli, P. and A. Masini, *Development of carbon/epoxy structural components for a high performance vehicle*. Composites Part B: Engineering, 2004. 35(4): p. 323-330.

110. Daggett, S. *A guide to selection of methacrylate, urethane and epoxy adhesives*. 2004 June 2014]; Available from: http://www.compositesworld.com/articles/a-guide-to-selection-of-methacrylate-urethane-and-epoxy-adhesives.

111. Lu, Y., J. Broughton, and P. Winfield, *A review of innovations in disbonding techniques for repair and recycling of automotive vehicles*. International Journal of Adhesion and Adhesives, 2014. 50(0): p. 119-127.

112. Harris, J.A. and P.A. Fay, *Fatigue life evaluation of structural adhesives for automative applications*. International Journal of Adhesion and Adhesives, 1992. 12(1): p. 9-18.

113. Lavery, M., *Sealants in the automotive industry*. International Journal of Adhesion and Adhesives, 2002. 22(6): p. 443-445.

114. Azari, S., M. Papini, and J.K. Spelt, *Effect of adhesive thickness on fatigue and fracture of toughened epoxy joints – Part II: Analysis and finite element modeling*. Engineering Fracture Mechanics, 2011. 78(1): p. 138-152.

115. Grant, L.D.R., R.D. Adams, and L.F.M. da Silva, *Experimental and numerical analysis of single-lap joints for the automotive industry*. International Journal of Adhesion and Adhesives, 2009. 29(4): p. 405-413.

116. Kahraman, R., M. Sunar, and B. Yilbas, *Influence of adhesive thickness and filler content on the mechanical performance of aluminum single-lap joints bonded with aluminum powder filled epoxy adhesive*. Journal of Materials Processing Technology, 2008. 205(1–3): p. 183-189.

117. da Silva, L.F.M., et al., *Effect of material, geometry, surface treatment and environment on the shear strength of single lap joints*. International Journal of Adhesion and Adhesives, 2009. 29(6): p. 621-632.

118. Abou-Hamda, M.M., M.M. Megahed, and M.M.I. Hammouda, *Fatigue crack growth in double cantilever beam specimen with an adhesive layer*. Engineering Fracture Mechanics, 1998. 60(5–6): p. 605-614.

119. Kawashita, L.F., et al., *The influence of bond line thickness and peel arm thickness on adhesive fracture toughness of rubber toughened epoxy–aluminium alloy laminates*. International Journal of Adhesion and Adhesives, 2008. 28(4–5): p. 199-210.

120. Bascom, W.D., et al., *The fracture of epoxy- and elastomer-modified epoxy polymers in bulk and as adhesives*. Journal of Applied Polymer Science, 1975. 19(9): p. 2545-2562.

121. Schmueser, D.W. and N.L. Johnson, *Effect of Bondline Thickness on Mixed-Mode Debonding of Adhesive Joints to Electroprimed Steel Surfaces*. The Journal of Adhesion, 1990. 32(2-3): p. 171-191.

122. Gleich, D.M., M.J.L. Van Tooren, and A. Beukers, *Analysis and evaluation of bondline thickness effects on failure load in adhesively bonded structures*. Journal of Adhesion Science and Technology, 2001. 15(9): p. 1091-1101.

123. Haghani, R., *Analysis of adhesive joints used to bond FRP laminates to steel members - A numerical and experimental study*. Construction and Building Materials, 2010. 24(11): p. 2243-2251.

124. Kin Loch, A.J. and S.J. Shaw, *The Fracture Resistance of a Toughened Epoxy Adhesive*. The Journal of Adhesion, 1981. 12(1): p. 59-77.

125. Kweon, J.-H., et al., *Failure of carbon composite-to-aluminum joints with combined mechanical fastening and adhesive bonding*. Composite Structures, 2006. 75(1–4): p. 192-198.

126. Davies, P., et al., *Influence of adhesive bond line thickness on joint strength*. International Journal of Adhesion and Adhesives, 2009. 29(7): p. 724-736.

127. Beevers, A., et al., *Analysis of stiffness of adhesive joints in car bodies*. Journal of Materials Processing Technology, 2001. 118(1): p. 95-100.

128. Ashley, S. *Lightweight materials compete for automakers' attention*. 2013 June 2014]; Available from: http://articles.sae.org/12090/.

129. Ashby, M.F., *Materials Selection in Mechanical Design*. 2004: Elsevier Science.

130. Roy, R., P. Souchoroukov, and E. Shehab, *Detailed cost estimating in the automotive industry: Data and information requirements*. International Journal of Production Economics, 2011. 133(2): p. 694-707.

131. Shehab, E.M. and H.S. Abdalla, *Manufacturing cost modelling for concurrent product development*. Robotics and Computer-Integrated Manufacturing, 2001. 17(4): p. 341-353.

132. Boothroyd, G., P. Dewhurst, and W.A. Knight, *Product Design for Manufacture and Assembly, Third Edition*. 2010: Taylor & Francis.

133. Wei, Y. and P.J. Egbelu, *A framework for estimating manufacturing cost from geometric design data*. International Journal of Computer Integrated Manufacturing, 2000. 13(1): p. 50-63.

134. Curran, R., S. Raghunathan, and M. Price, *Review of aerospace engineering cost modelling: The genetic causal approach*. Progress in Aerospace Sciences, 2004. 40(8): p. 487-534.

135. Rehman, S. and M.D. Guenov, *A methodology for modelling manufacturing costs at conceptual design*. Computers & Industrial Engineering, 1998. 35(3–4): p. 623-626.

136. Kirchain, R.E., *Cost Modeling of Materials and Manufacturing Processes*, in *Encyclopedia of Materials: Science and Technology (Second Edition)*, K.H.J.B. Editors-in-Chief: , et al., Editors. 2001, Elsevier: Oxford. p. 1718-1727.

137. Johnson, M. and R. Kirchain, *Quantifying the effects of parts consolidation and development costs on material selection decisions: A process-based costing approach*. International Journal of Production Economics, 2009. 119(1): p. 174-186.

138. Mayyas, A., et al., *Using Quality Function Deployment and Analytical Hierarchy Process for material selection of Body-In-White*. Materials & Design, 2011. 32(5): p. 2771-2782.

139. Alonso, E., et al., *Evaluating the potential for secondary mass savings in vehicle lightweighting*. Environ Sci Technol, 2012. 46(5): p. 2893-901.

140. Fysikopoulos, A., et al., *An Empirical Study of the Energy Consumption in Automotive Assembly*. Procedia CIRP, 2012. 3(0): p. 477-482.

141. Galitsky, C., *Energy Efficiency Improvement and Cost Saving Opportunities for the Vehicle Assembly Industry: An ENERGY STAR Guide for Energy and Plant Managers*, 2008.

142. Ashby, M.F. and K. Johnson, *Materials and Design: The Art and Science of Material Selection in Product Design*. 2009: Elsevier Science.

143. Giudice, F., G. La Rosa, and A. Risitano, *Materials selection in the Life-Cycle Design process: a method to integrate mechanical and environmental performances in optimal choice*. Materials & Design, 2005. 26(1): p. 9-20.

144. Das, S., *Life cycle energy impacts of automotive liftgate inner*. Resources, Conservation and Recycling, 2005. 43(4): p. 375-390.

145. Duval, D. and H.L. MacLean, *The role of product information in automotive plastics recycling: a financial and life cycle assessment*. Journal of Cleaner Production, 2007. 15(11–12): p. 1158-1168.

146. Lundquist, L., et al., *3 - Plastics Recovery and Recycling*, in *Life Cycle Engineering of Plastics*. 2000, Elsevier Science Ltd: Oxford. p. 39-75.

147. Denison, R.A., *ENVIRONMENTAL LIFE-CYCLE COMPARISONS OF RECYCLING, LANDFILLING, AND INCINERATION: A Review of Recent Studies*. Annual Review of Energy and the Environment, 1996. 21(1): p. 191-237.

148. Bellmann, K. and A. Khare, *European response to issues in recycling car plastics*. Technovation, 1999. 19(12): p. 721-734.

149. Keoleian Gregory, et al., *Industrial Ecology of the Automobile: A Life Cycle Perspective*, 1997.

150. *ISO 14001:2004, Environmental management systems — Requirements with guidance for use*, 2004.

151. *Measures of Environmental Performance and Ecosystem Condition*, ed. P.C. Schulze. 1999: The National Academies Press.

152. Ashby, M.F., *Chapter 3 - The material life cycle*, in *Materials and the Environment (Second Edition)*, M.F. Ashby, Editor. 2013, Butterworth-Heinemann: Boston. p. 49-77.

153. Mayyas, A.T., et al., *Quantifiable measures of sustainability: a case study of materials selection for eco-lightweight auto-bodies.* Journal of Cleaner Production, 2013. 40(0): p. 177-189.

154. Pennington, D.W., et al., *Life cycle assessment Part 2: Current impact assessment practice*. Environment International, 2004. 30(5): p. 721-739.

155. Sundin, E., *Product and process design for successful remanufacturing*. 2004, Linköping, Sweden: Production Systems, Dept. of Mechanical Engineering, Linköpings Universitet.

156. T. Gutowski, et al., *WTEC Panel Report on: Environmentally Benign Manufacturing (EBM)*, W.T.W.D. International Technology Research Institute, Editor 2001: Baltimore, Maryland, USA.

157. Ashby, M.F., *Chapter 6 - Eco-data: Values, sources, precision*, in *Materials and the Environment (Second Edition)*, M.F. Ashby, Editor. 2013, Butterworth-Heinemann: Boston. p. 119-174.

158. *Cambridge engineering selector (CES) software*, in *CBs sLS (UK): Granta Design Limited, 2000*, b.H.S. Trunmpignton Mews, Cambridge, Editor 2000.

159. Inc., L.E., *An Assessment of Mass Reduction Opportunities for a 2017 – 2020 Model Year Vehicle Program*, 2010, Lotus Engineering Inc.: The International Council on Clean Transportation.

160. *Values data sheet Telene*, T. SAS, Editor. p. 1.

161. Automations Creations, I., *MatWeb the online materials information resource*, 1997, Automation Creations Inc.: Christiansburg, VA.

162. ArcelorMittal. *EN10152 DC04+ZE Carbon Steel*. 2014 June 2014]; E10 Electrogalvanised steels]. Available from: http://fce.arcelormittal.com/prd_web/E10_EN.html.

163. aalco, *Aluminium Alloy*

5754 - H111 Treadplate, a.-T.U.s.l.i.m.-m. stockholder, Editor 2015. p. 2.

164. Huntsman, *Araldite® 2015 - Technical data sheet*, Huntsman, Editor.

165. Adhesives, S.B., *CRESTABOND® M7-15 Methacrylate Structural Adhesive*, S.B.C. LIMITED, Editor 2014, www.scottbader.com.

166. Adams, R.D., J. Comyn, and W.C. Wake, *Structural Adhesive Joints in Engineering*. 1997: Springer.

167. Haghani, R. and M. Al-Emrani, *A new design model for adhesive joints used to bond FRP laminates to steel beams – Part A: Background and theory*. Construction and Building Materials, 2012. 34(0): p. 486-493.

168. Camboa, A., J. Nunes, and F. Alves, *Analysis of polydicyclopentadiene-metal hybrid adhesive joints for automotive exterior body applications*, in *Materiais 2015*: Porto/Portugal. p. 01–80.
169. (ULSAB), U.S.A.B., *UltraLight Steel Auto Closures - Concept Report*, 2000, World Auto Steel
170. BaySystems, *Engineering Polyurethanes - RIM Part and Mold Design Guide*, B.M. LLC, Editor 2008, Bayer.
171. Grupo Kataforesis. *Cataphoresis*. 2011 [cited 2013 June]; Available from: http://www.grupokataforesis.com/engl/procesos/procesos/ktl.html.
172. Ashby, M.F., *Chapter 2 - Resource consumption and its drivers*, in *Materials and the Environment (Second Edition)*, M.F. Ashby, Editor. 2013, Butterworth-Heinemann: Boston. p. 15-48.

Appendices

Section A- PDCPD testing results

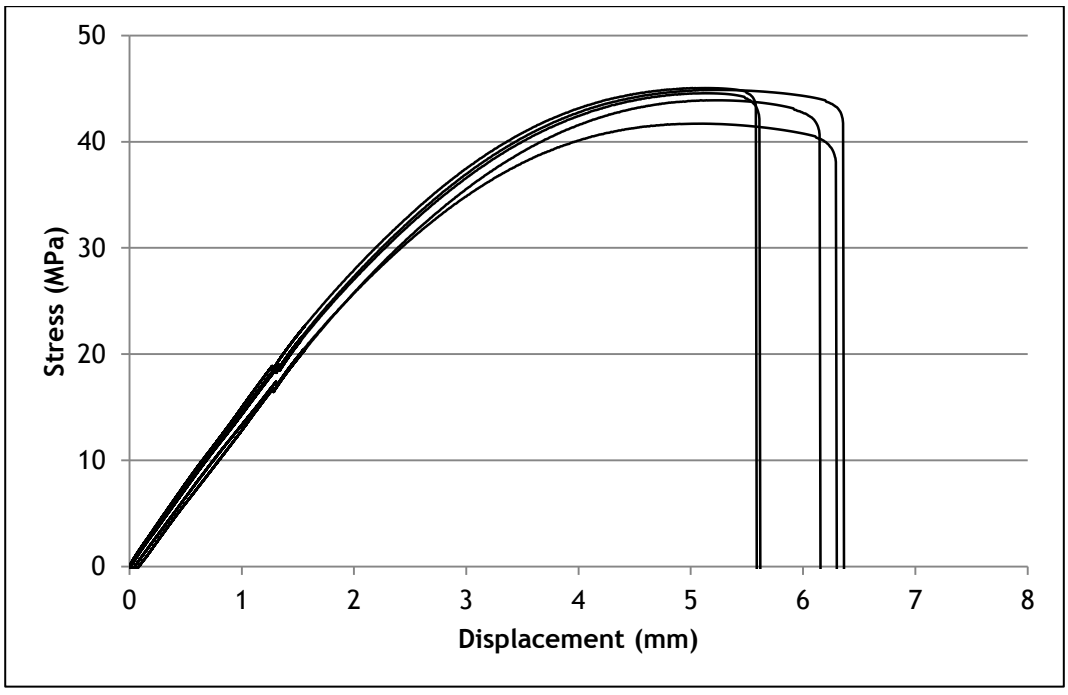

Figure A.1 - PDCPD tensile test results.

Section B - Adhesive testing results

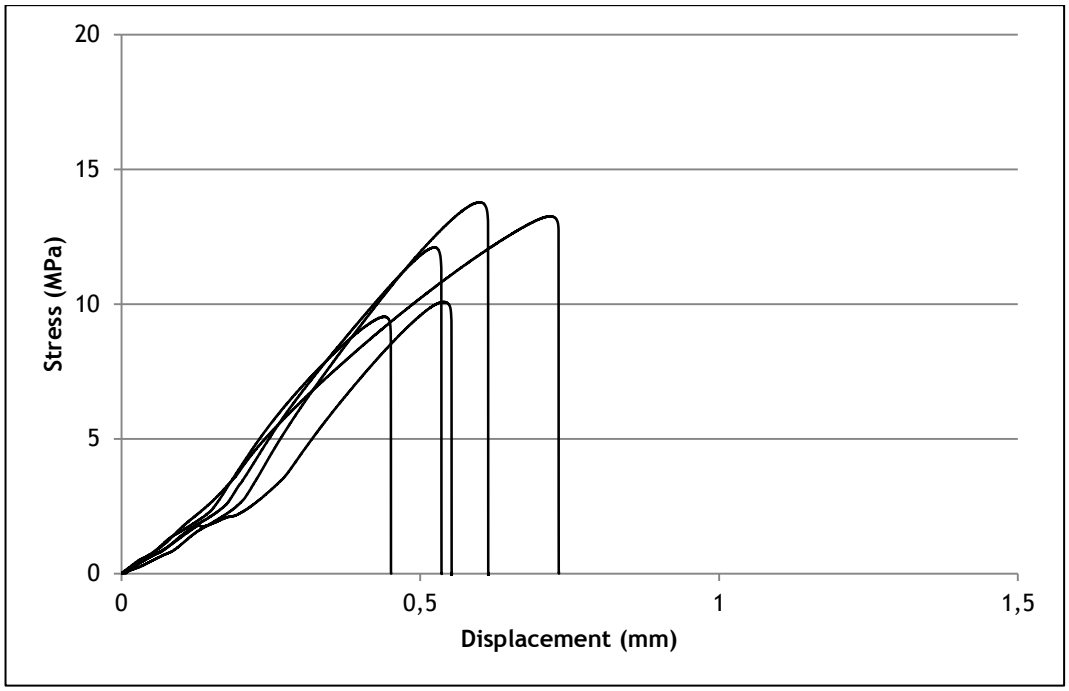

Figure B.2 - Results for steel bonded with epoxy.

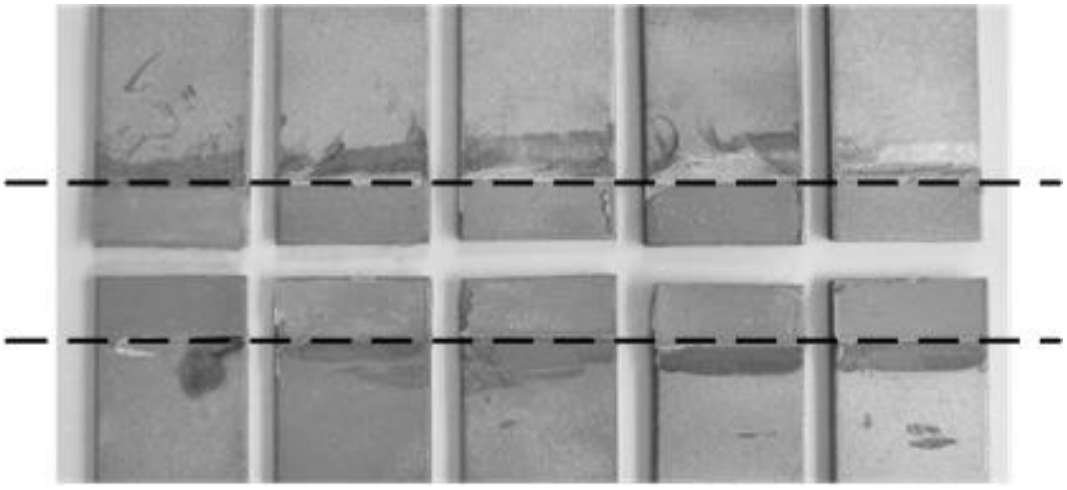

Figure B.3 - Steel specimens bonded with epoxy.

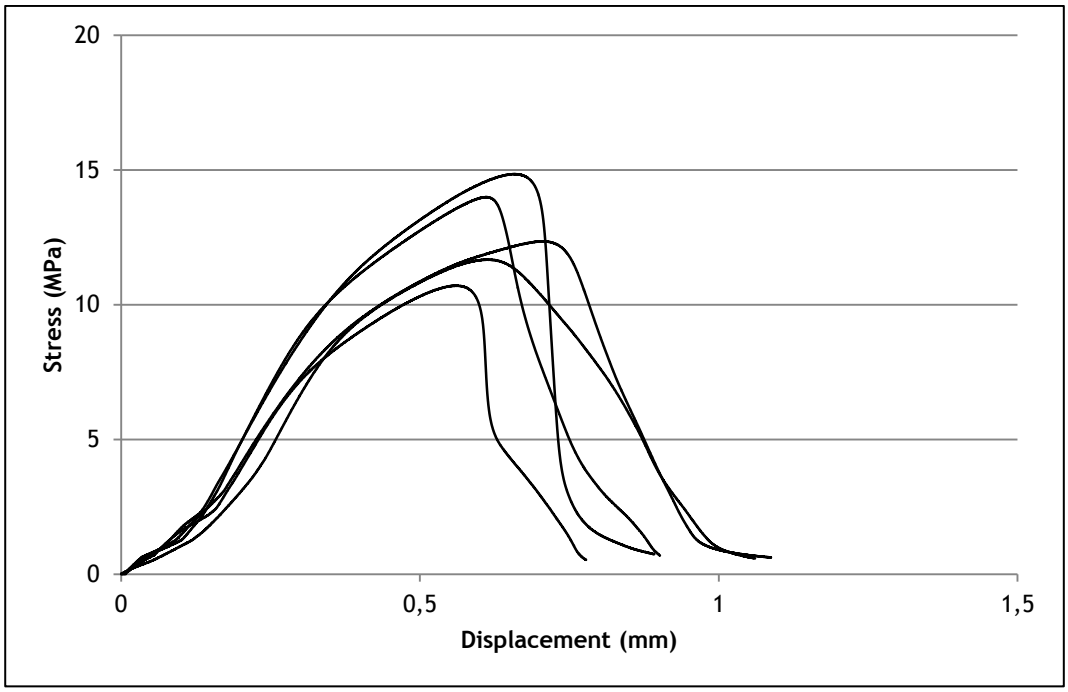

Figure B.4 - Results for steel bonded with methacrylate.

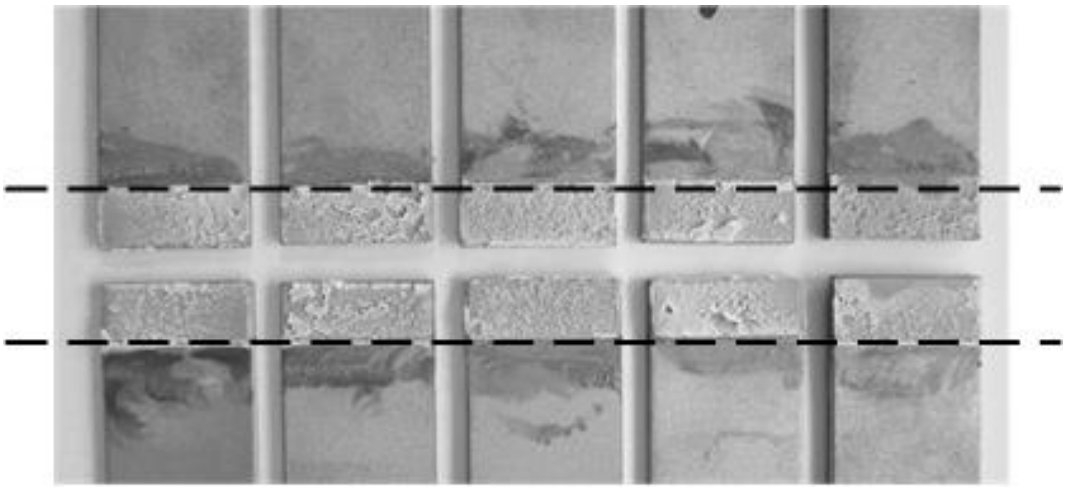

Figure B.5 - Steel specimens bonded with methacrylate.

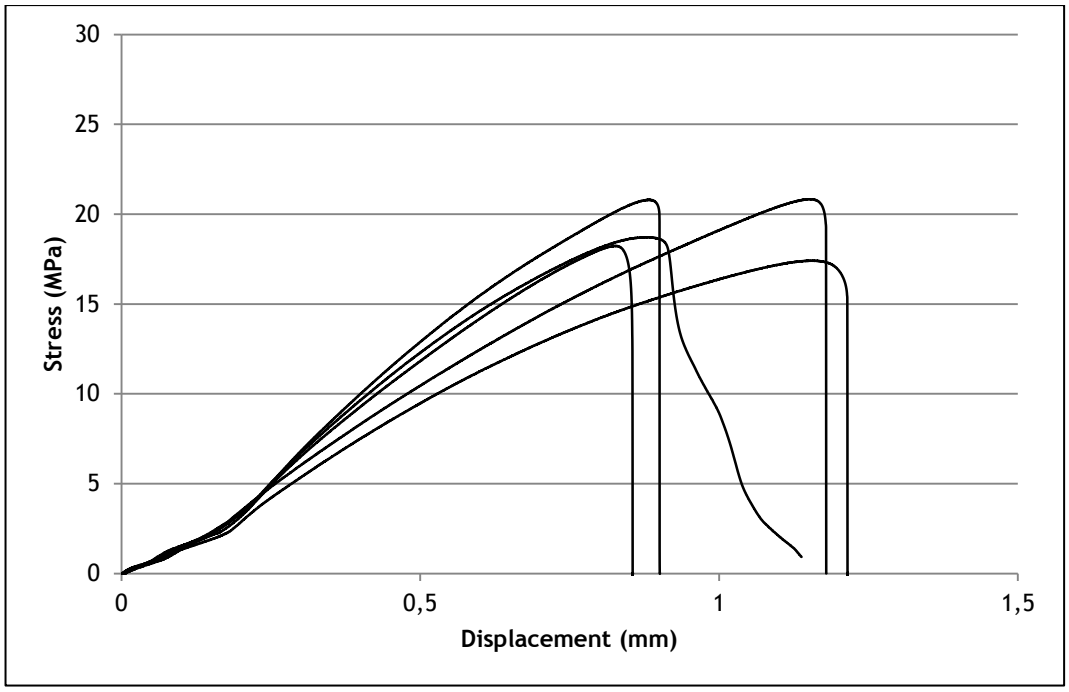

Figure B.6 - Results for cataphoresis bonded with epoxy.

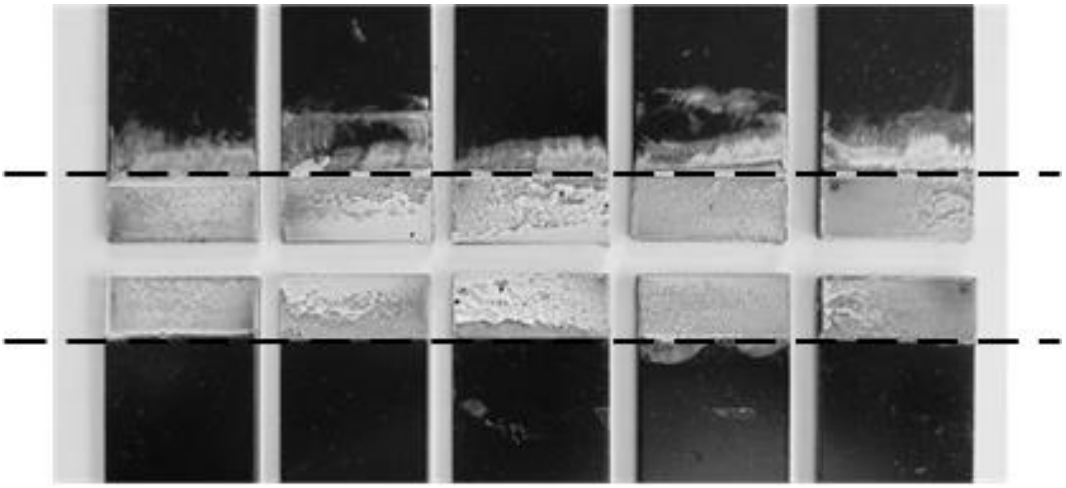

Figure B.7 - Cataphoresis specimens bonded with epoxy.

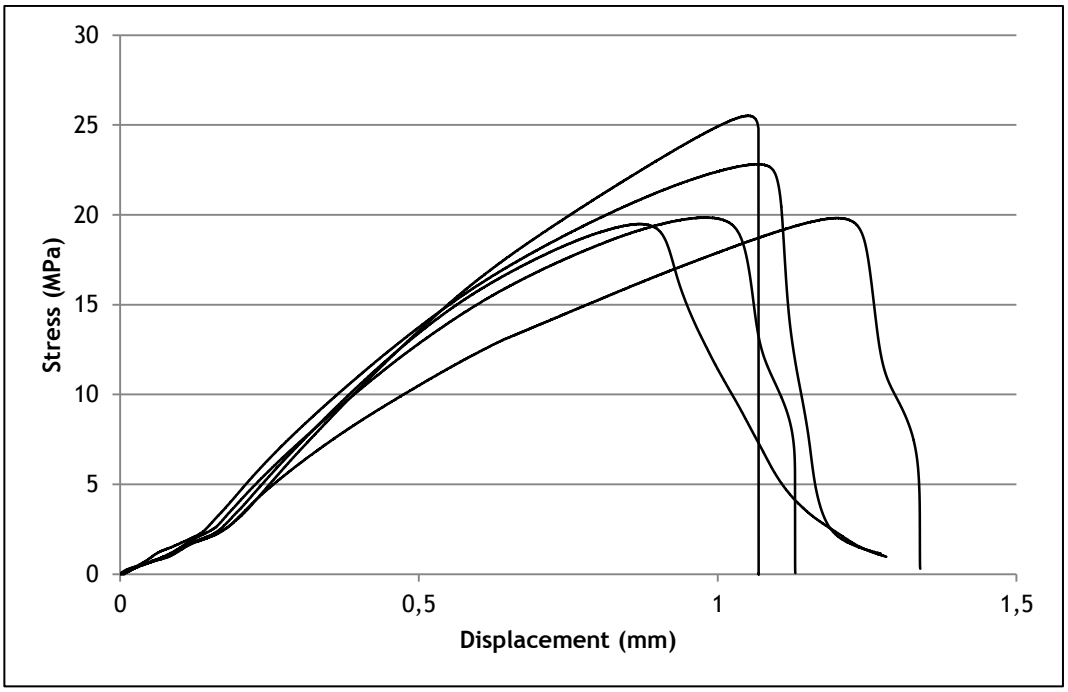

Figure B.8 - Results for cataphoresis bonded with methacrylate.

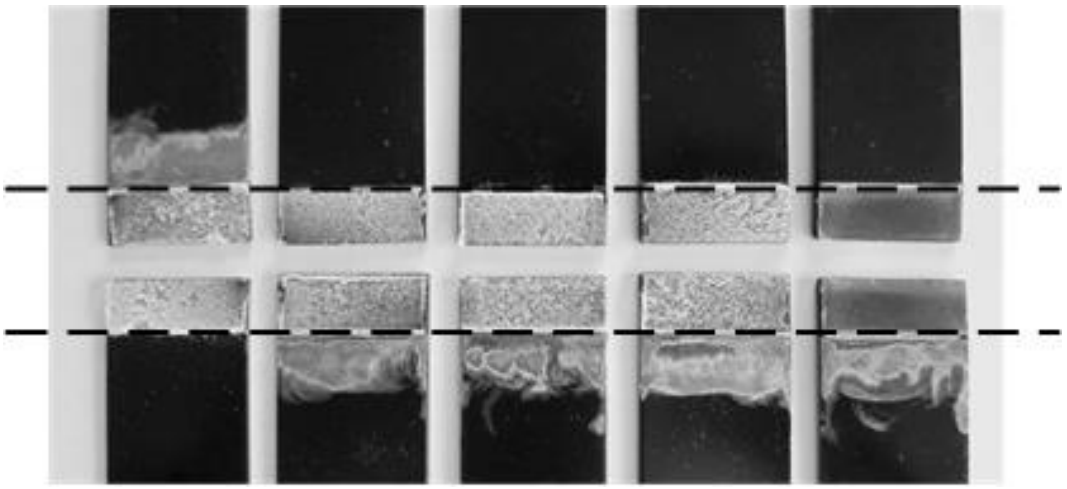

Figure B.9 - Cataphoresis specimens bonded with methacrylate.

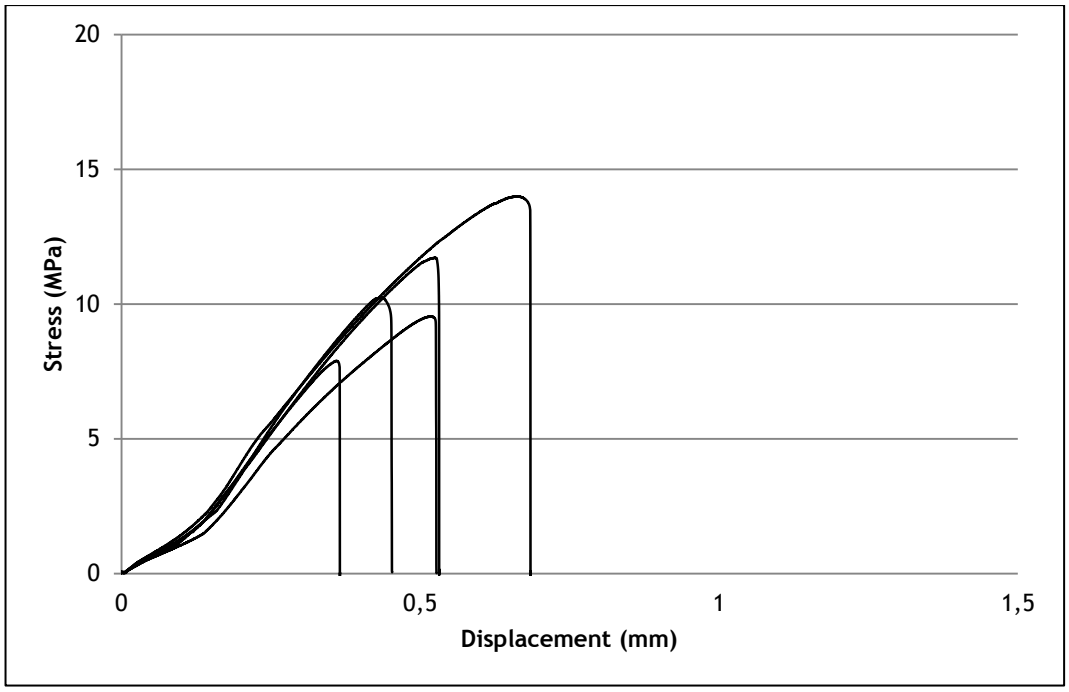

Figure B.10 - Results for aluminium bonded with epoxy.

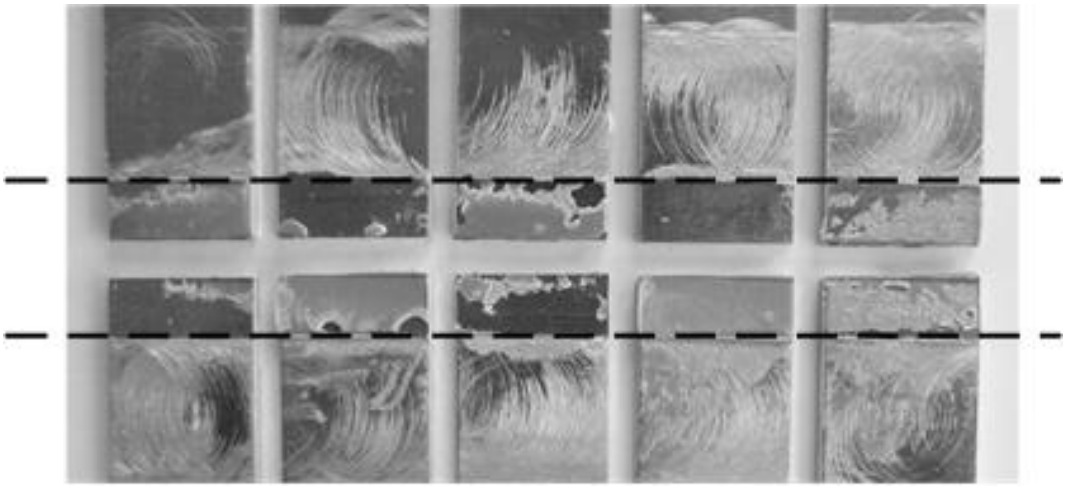

Figure B.11 - Aluminium specimens bonded with epoxy.

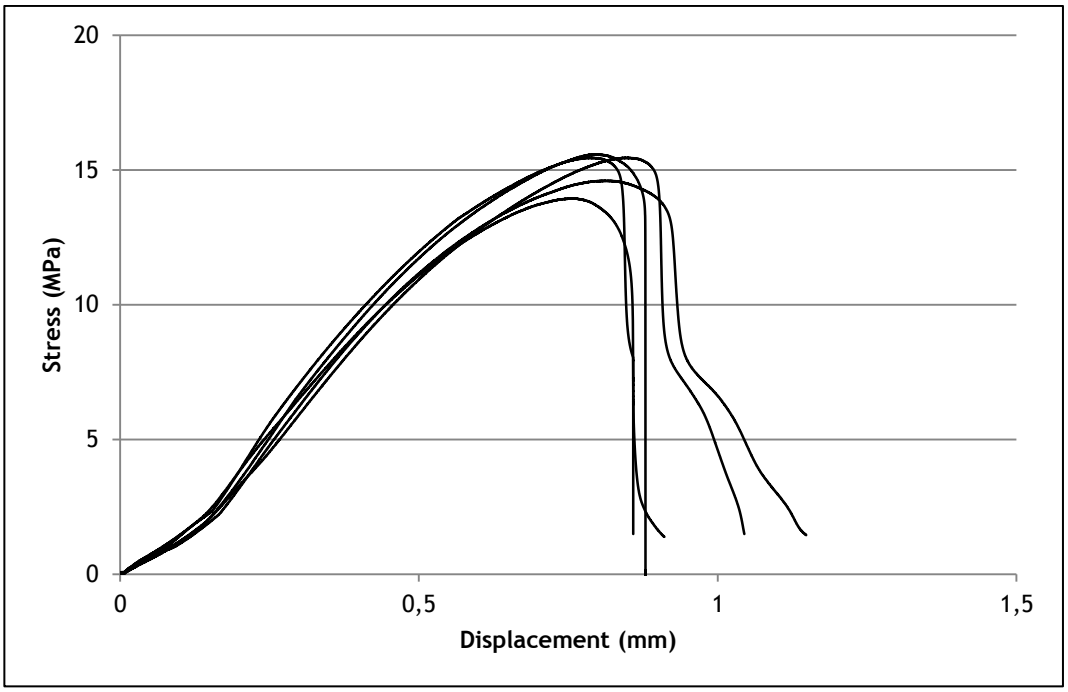

Figure B.12 - Results for aluminium bonded with methacrylate.

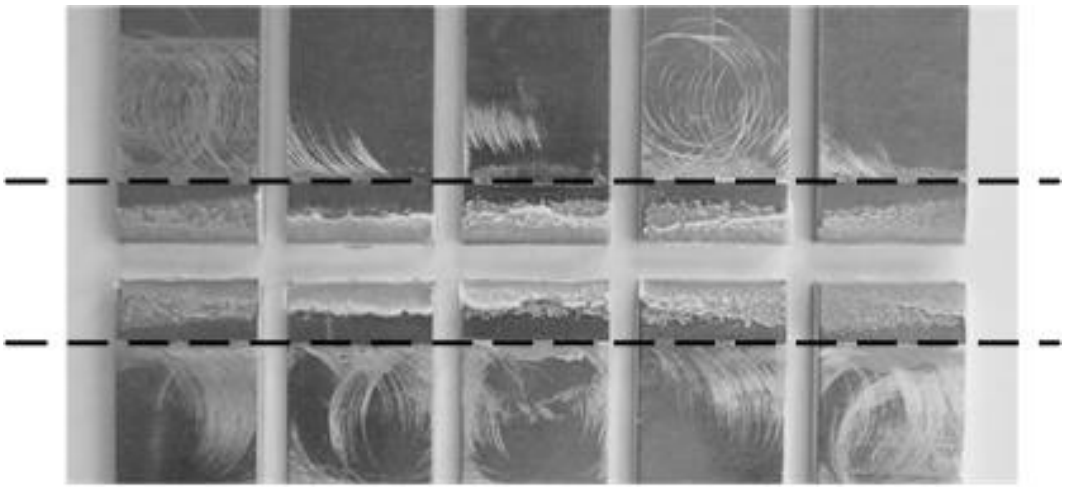

Figure B.13 - Aluminium specimens bonded with methacrylate.

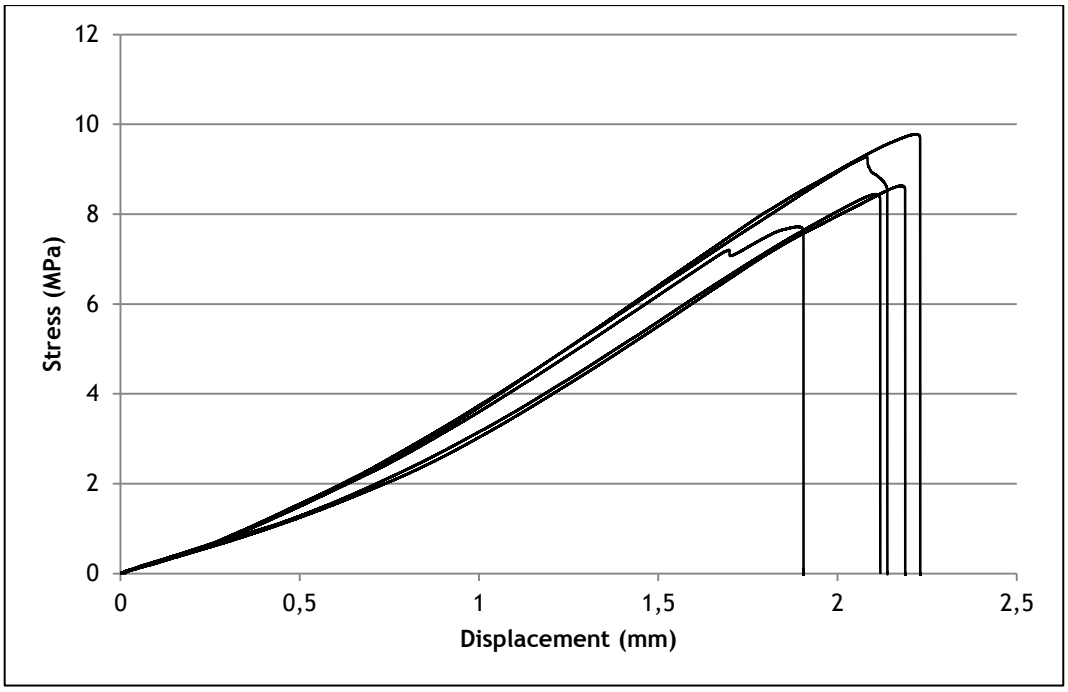

Figure B.14 - Results for PDCPD bonded with epoxy.

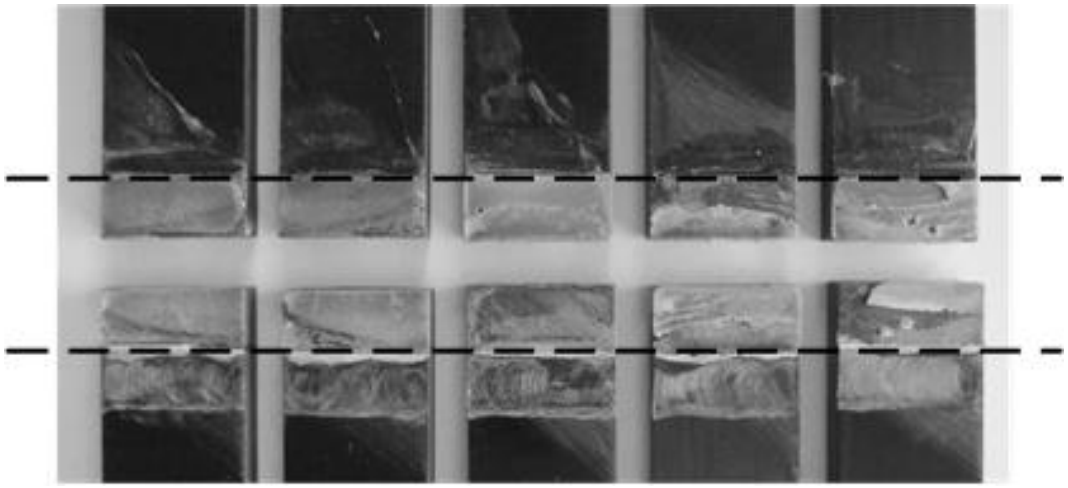

Figure B.15 - PDCPD specimens bonded with epoxy.

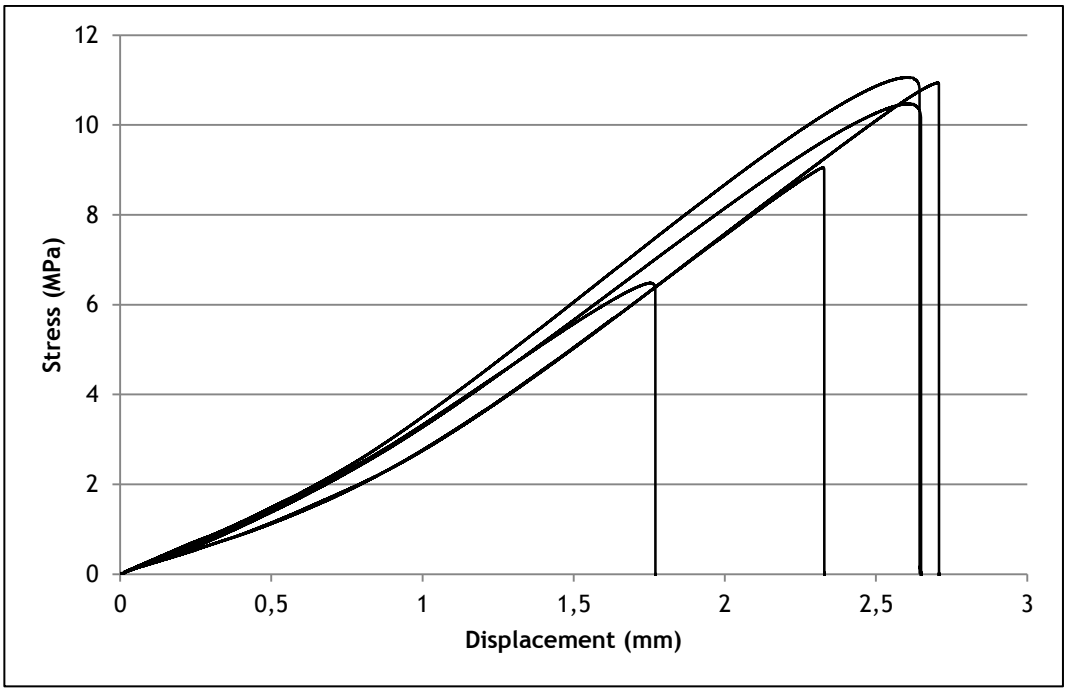

Figure B.16 - Results for PDCPD bonded with methacrylate.

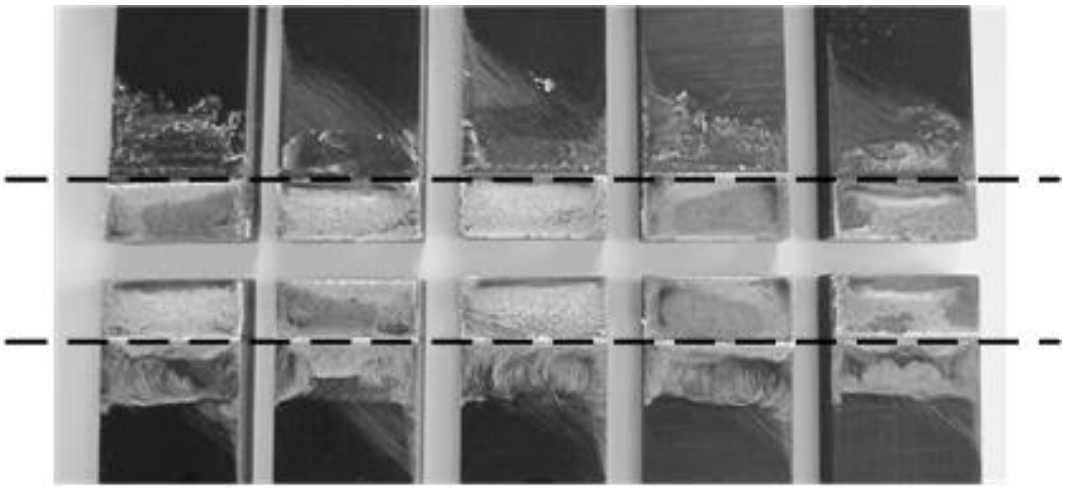

Figure B.17 - PDCPD specimens bonded with methacrylate.

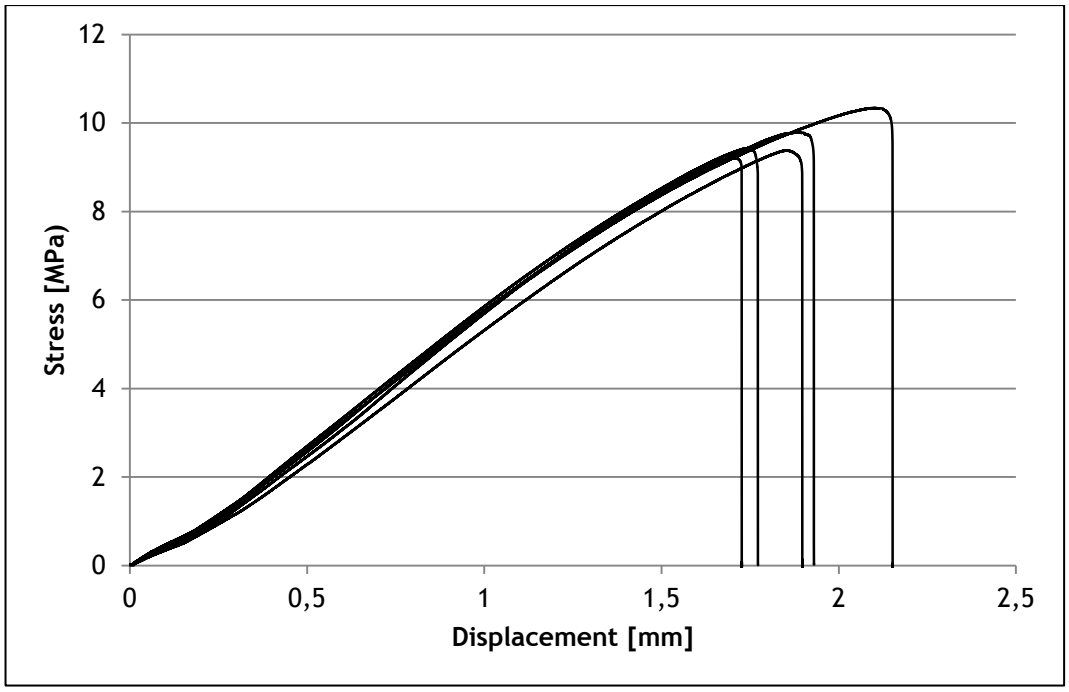

Figure B.18 - Results for PDCPD and aluminium bonded.

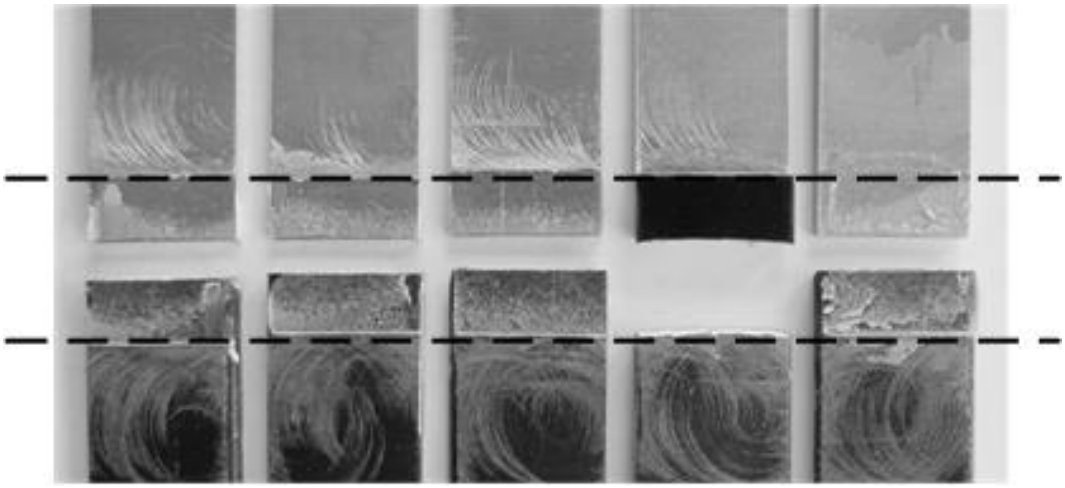

Figure B.19 - PDCPD and aluminium specimens bonded with methacrylate.

Section C– Test configurations

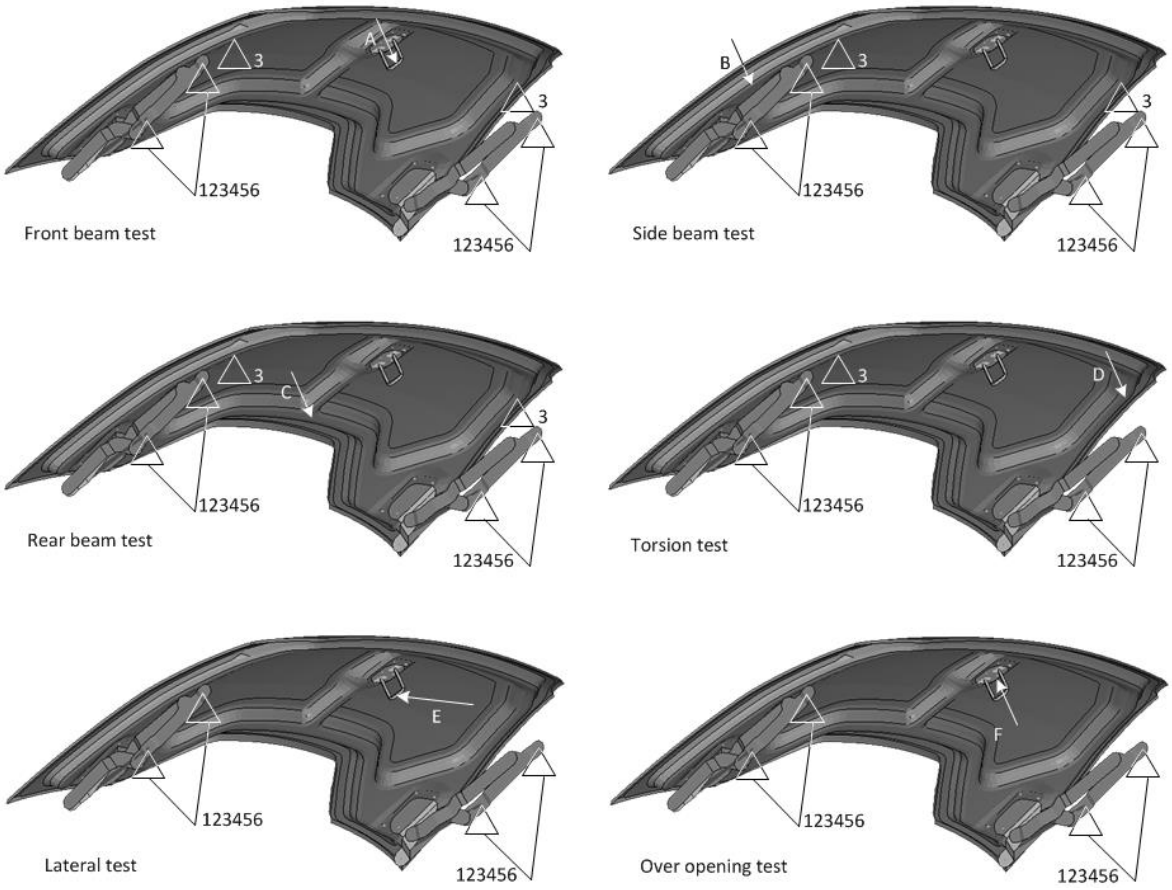

Figure C.20 – Detailed FEA testing configuration.

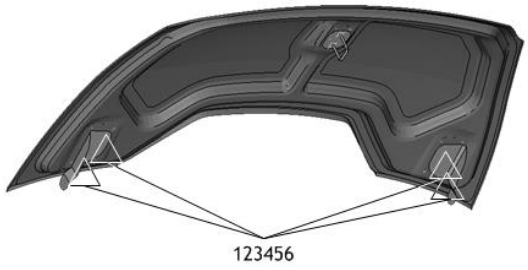

Figure C.21 – Detailed FEA testing configuration without hinges.

Section D - Frame testing visuals for configuration 1 (0.8mmx10mm)

	STRESS	DISPLACEMENT
Frame 1	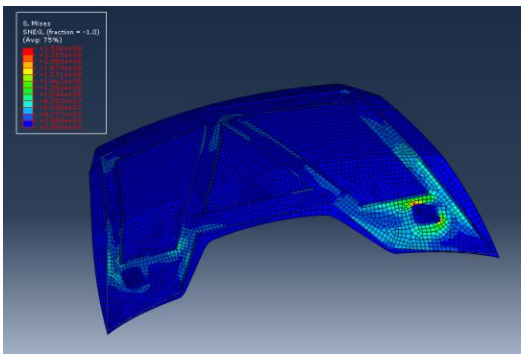	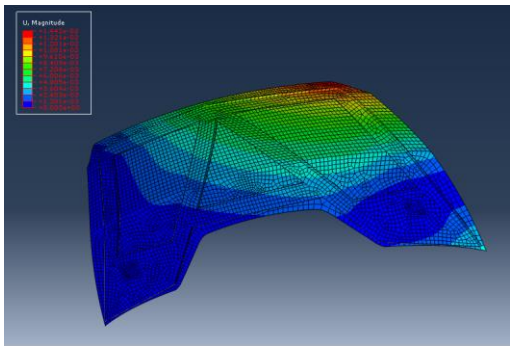
Frame 2	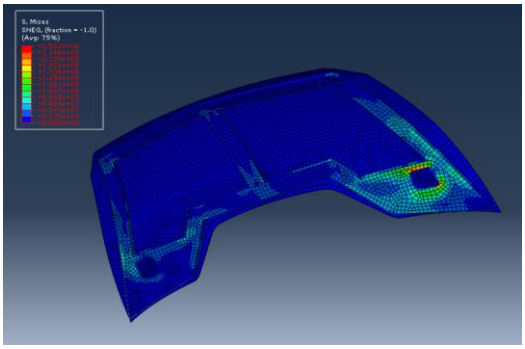	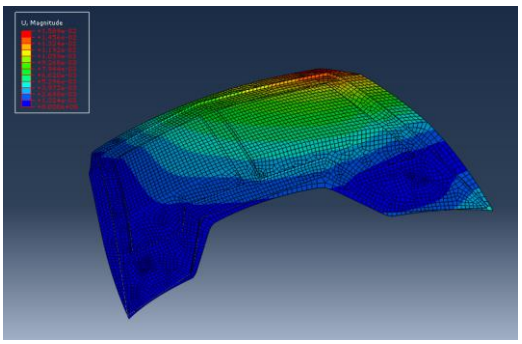
Frame 3	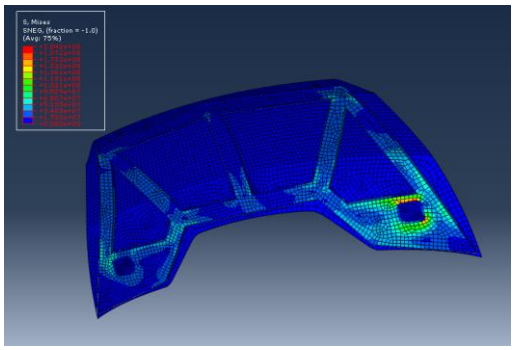	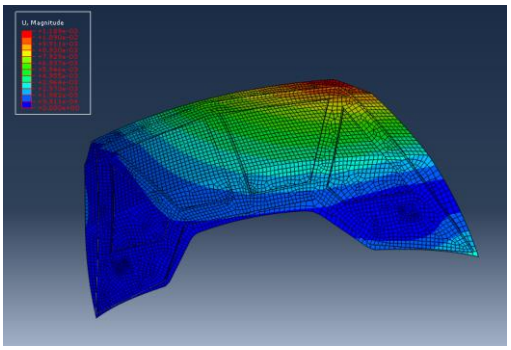

Section E – Bonnet drawing

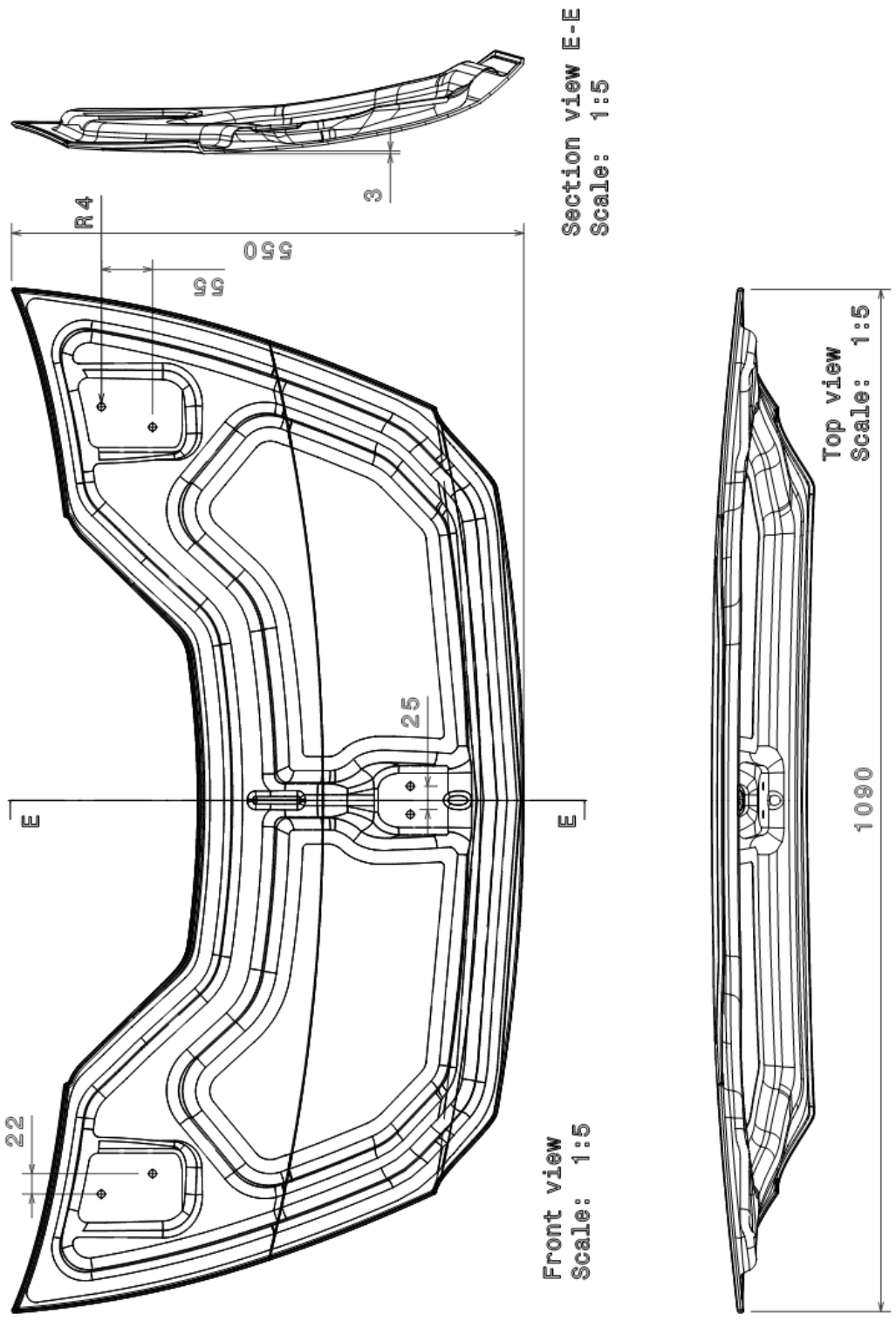

Figure E.22 -Bonnet drawing.

Section F - Stamping tool simulation results

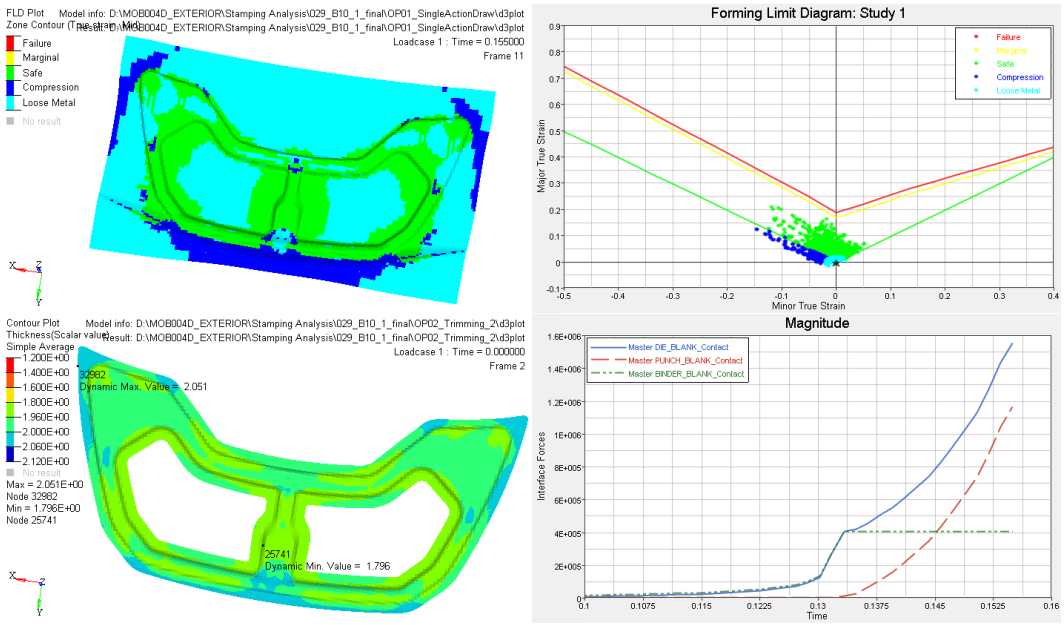

Figure F.23 - Stamping simulation results for T1 with 2mm thickness aluminium sheet.

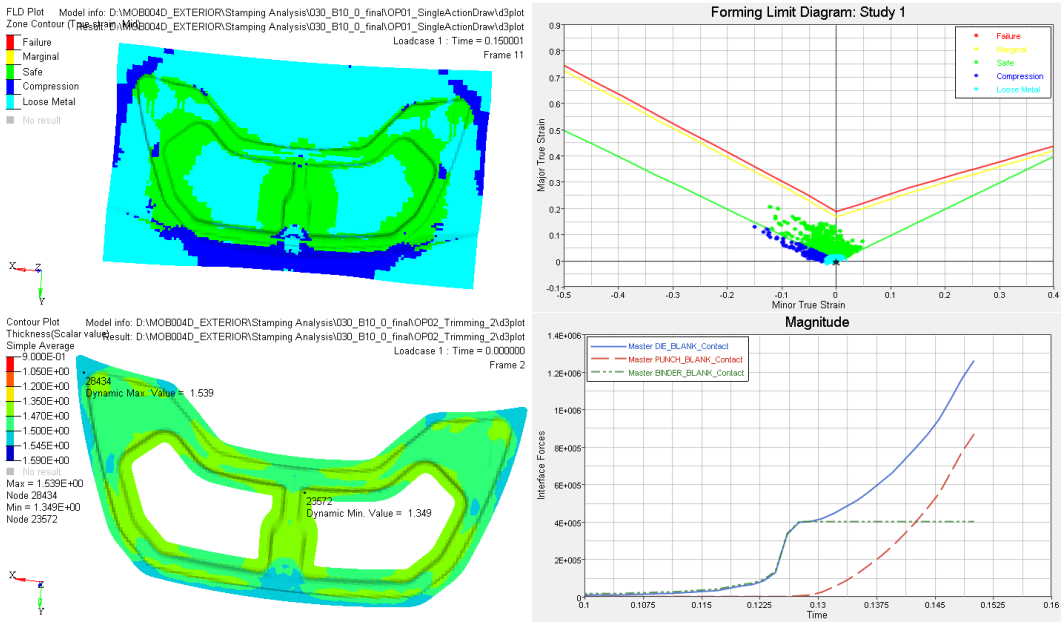

Figure F.24 - Stamping simulation results for T1 with 1.5mm thickness aluminium sheet.

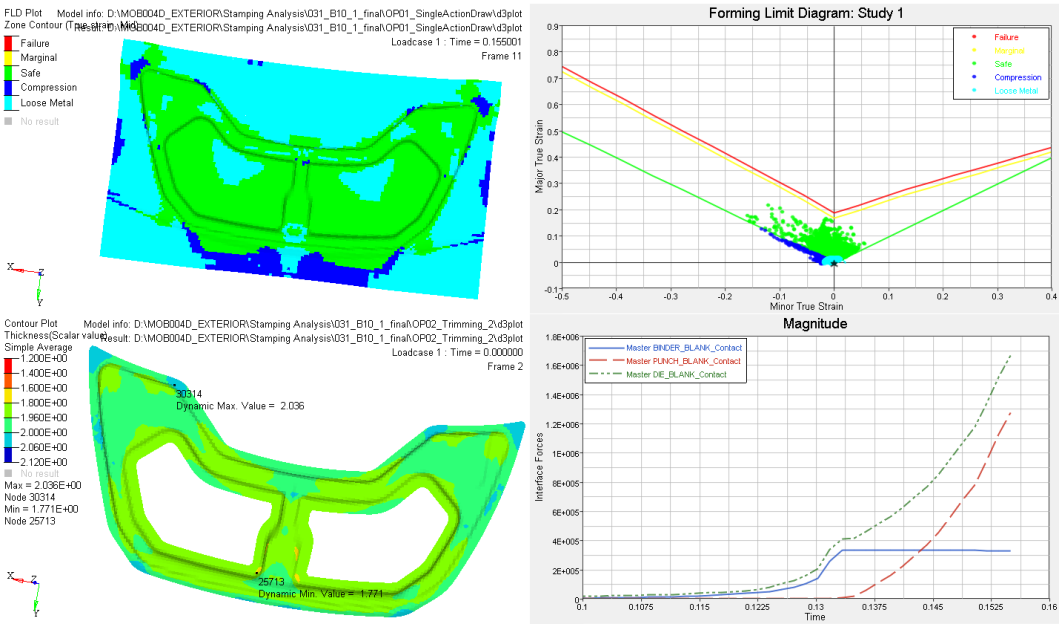

Figure F.25 - Stamping simulation results for T2 with 2mm thickness aluminium sheet.

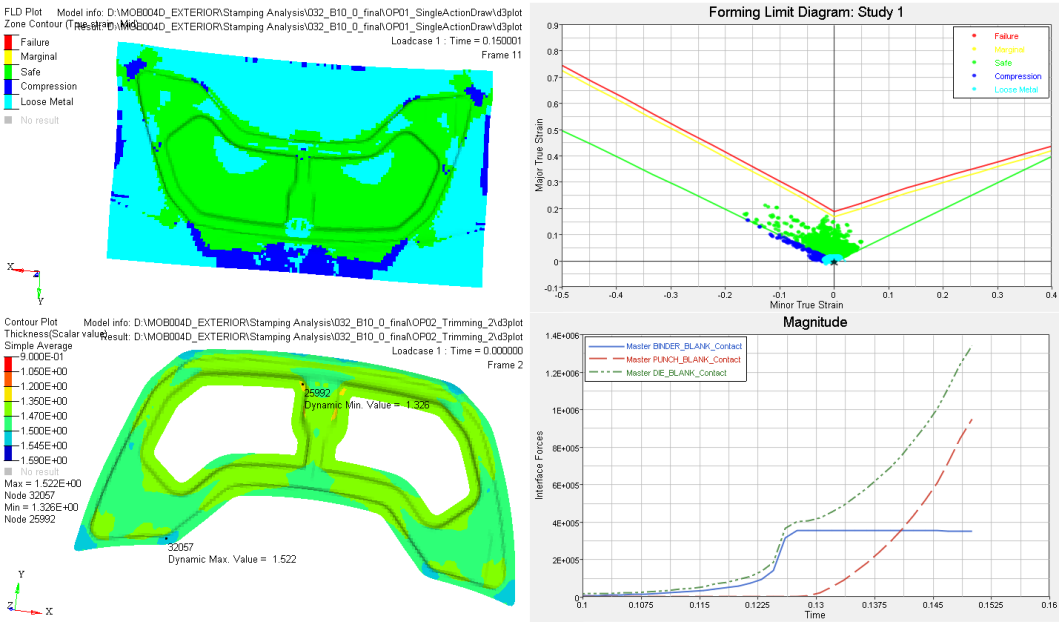

Figure F.26 - Stamping simulation results for T2 with 1.5mm thickness aluminium sheet.

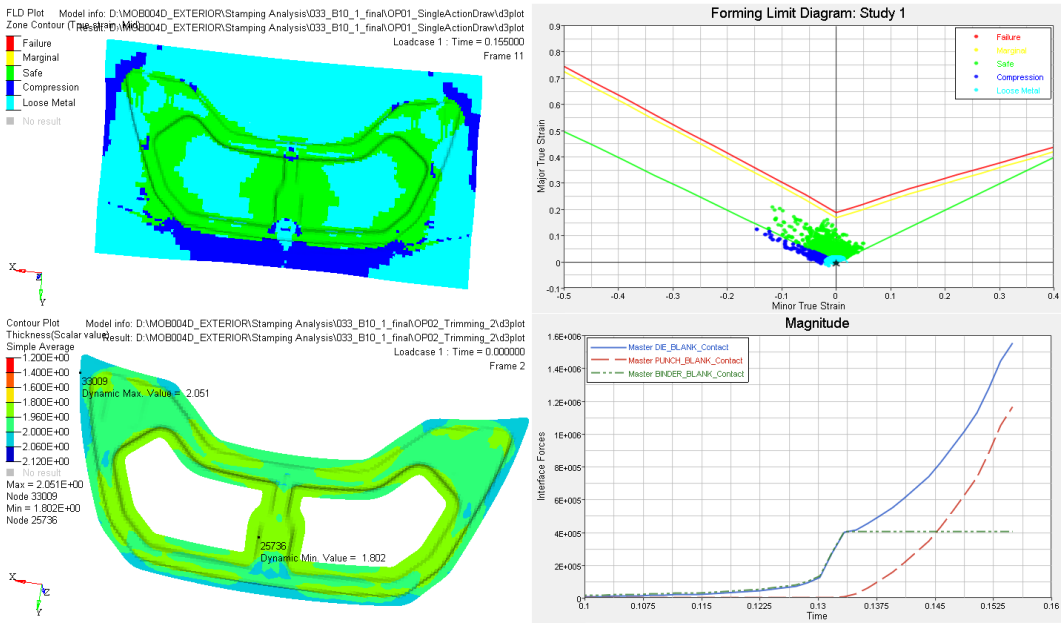

Figure F.27 - Stamping simulation results for T3 with 2mm thickness aluminium sheet.

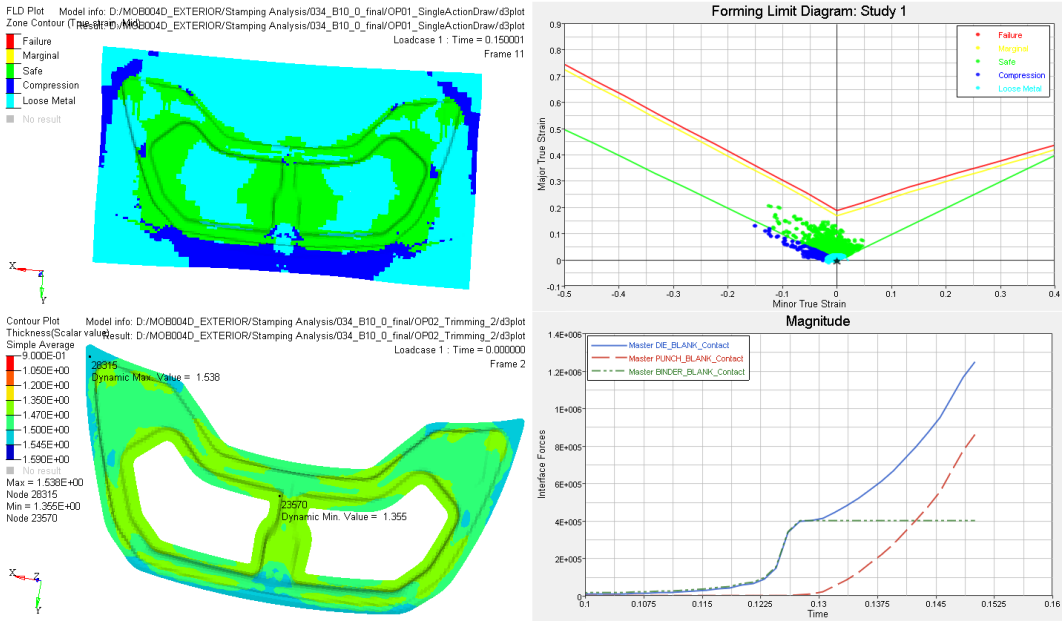

Figure F.28 - Stamping simulation results for T3 with 1.5mm thickness aluminium sheet.

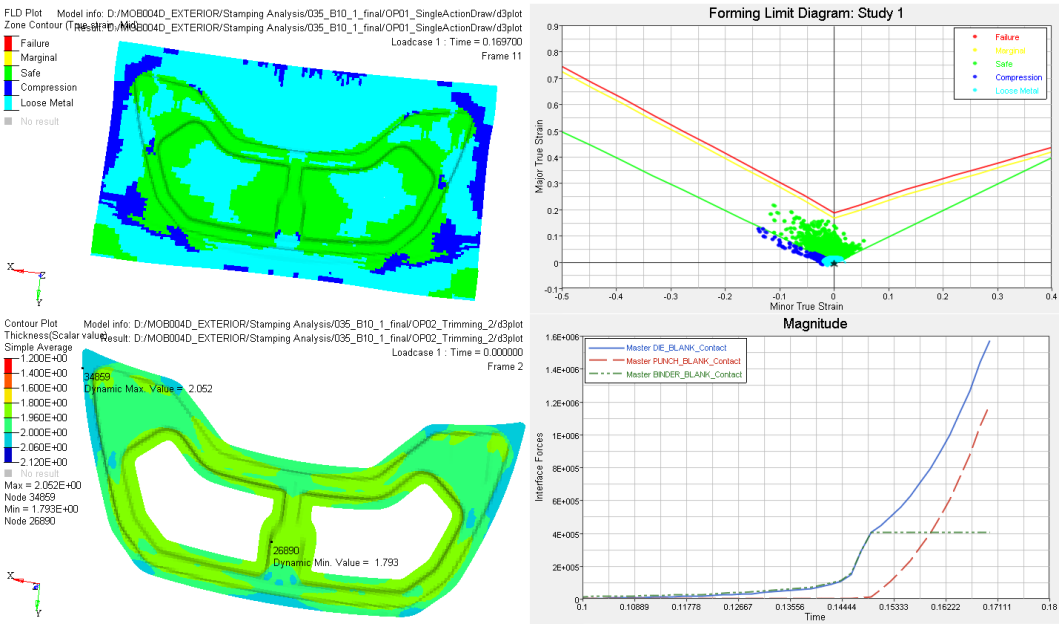

Figure F.29 - Stamping simulation results for T4 with 2mm thickness aluminium sheet.

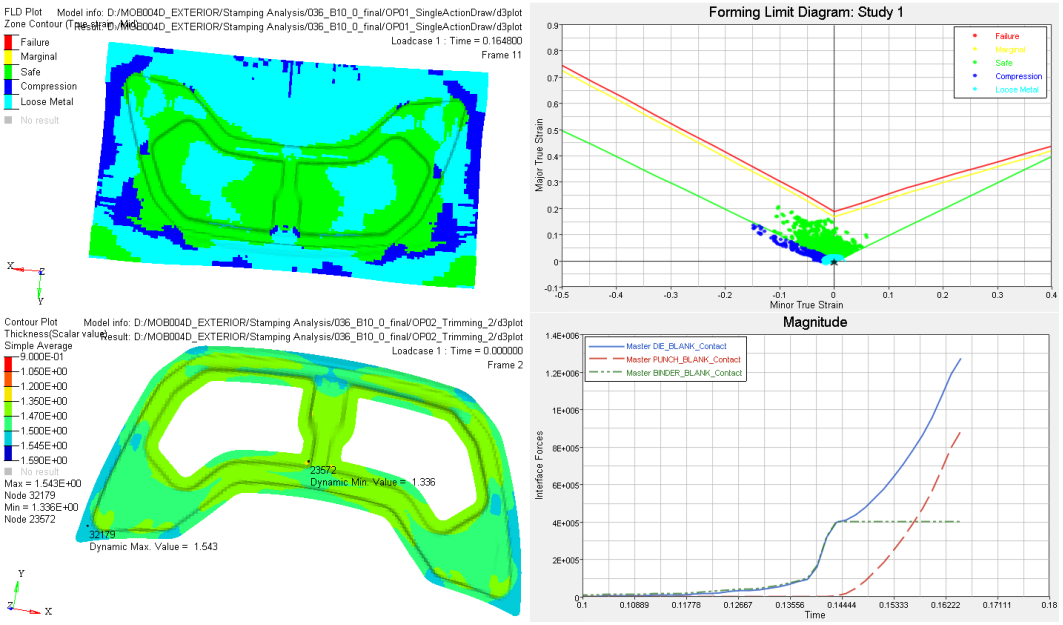

Figure F.30 - Stamping simulation results for T4 with 1.5mm thickness aluminium sheet.

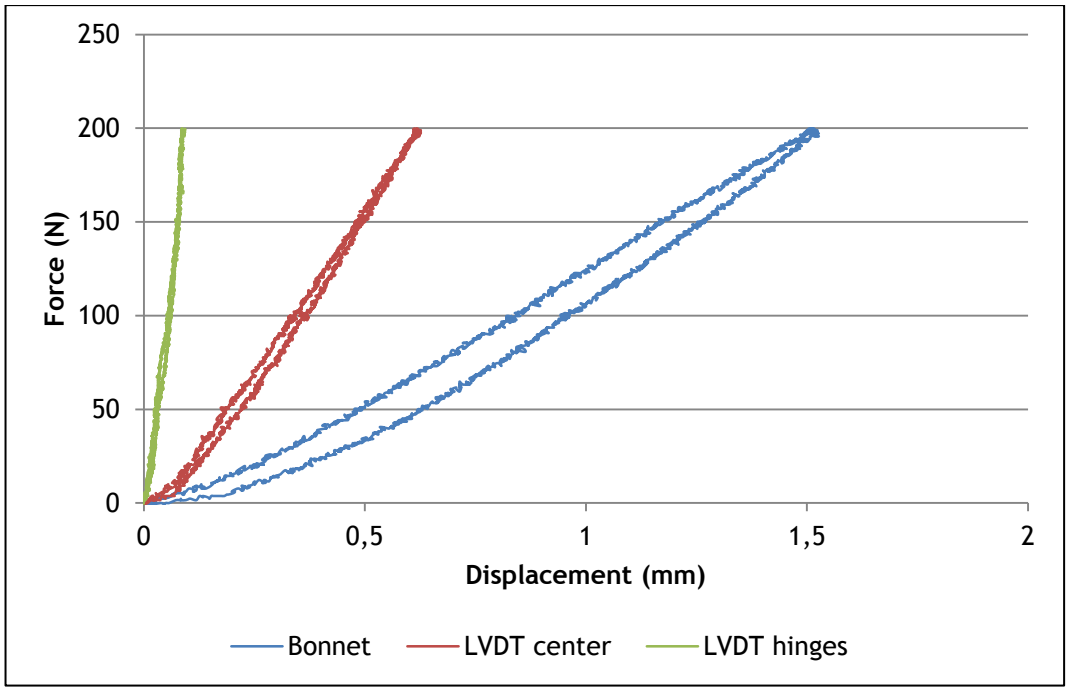

Figure G.31 - Bonnet displacement on front beam test.

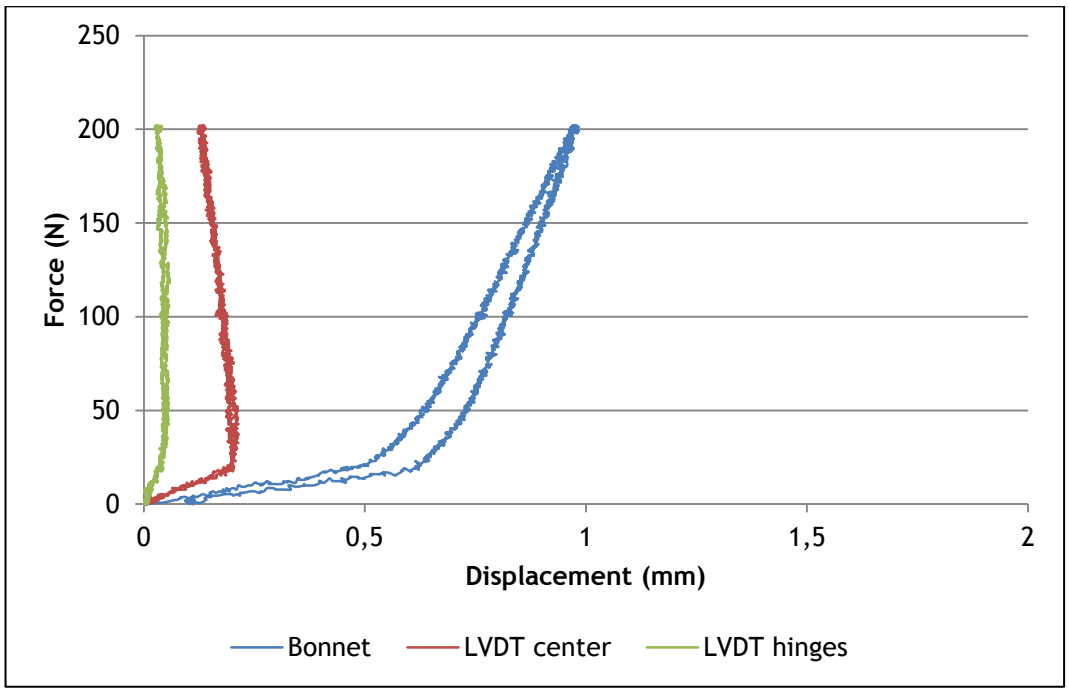

Figure G.32 - Bonnet displacement on side beam test.

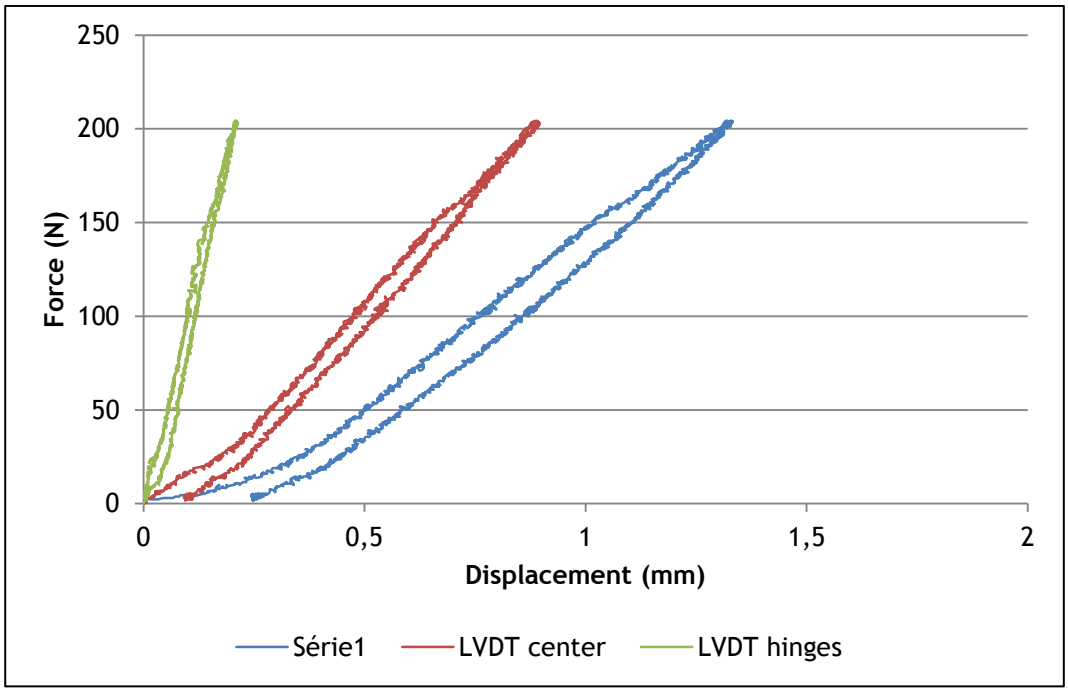

Figure G.33 - Bonnet displacement on rear beam test.

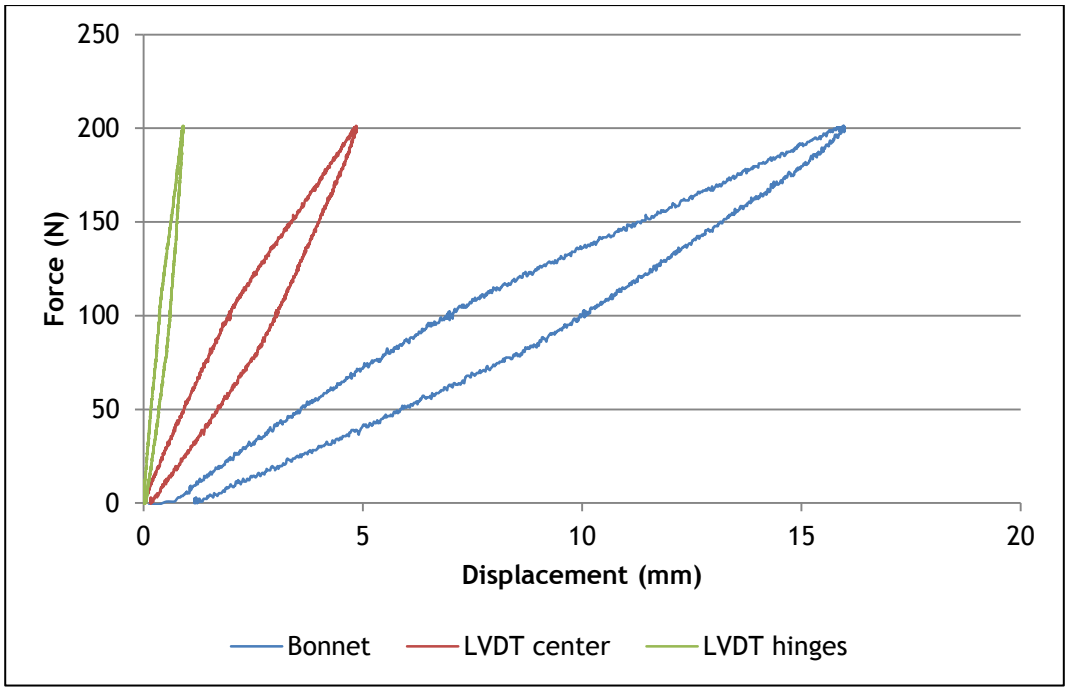

Figure G.34 - Bonnet displacement on torsion test.

Section H- Cost breakdown results

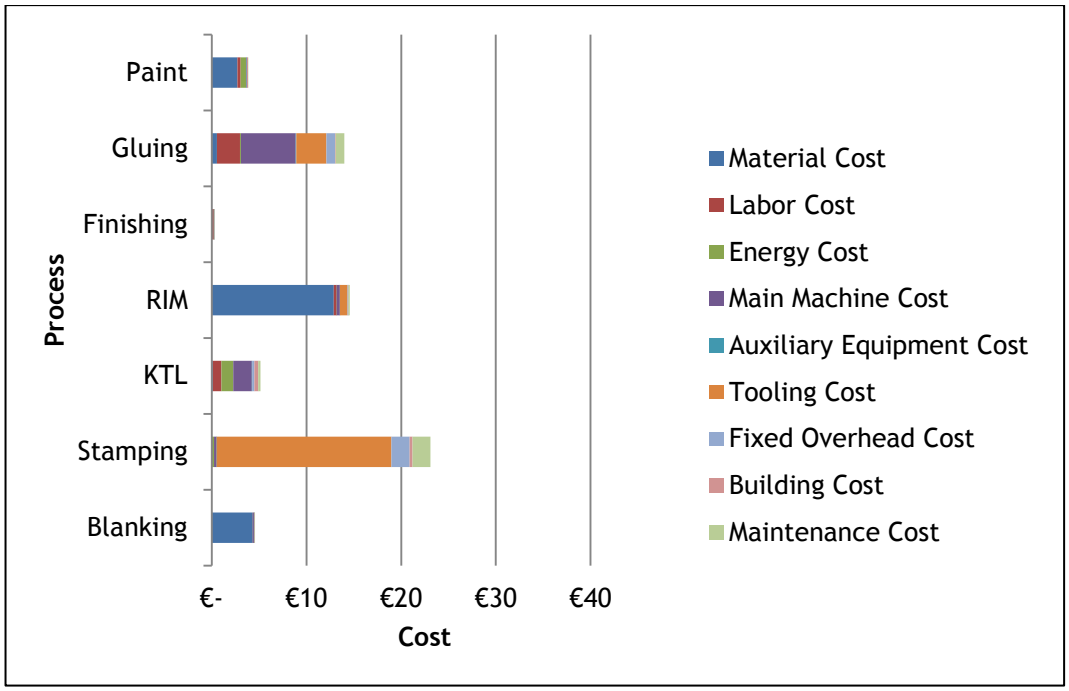

Figure H.35 - Bonnet1 cost breakdown.

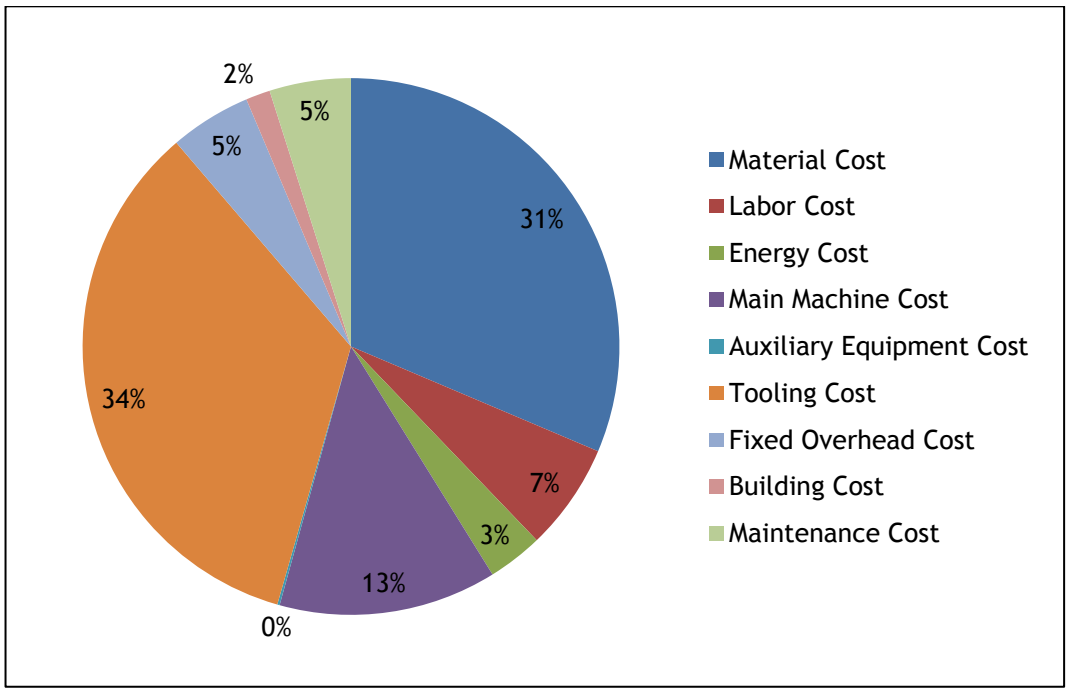

Figure H.36 - Cost percentage by element for Bonnet1.

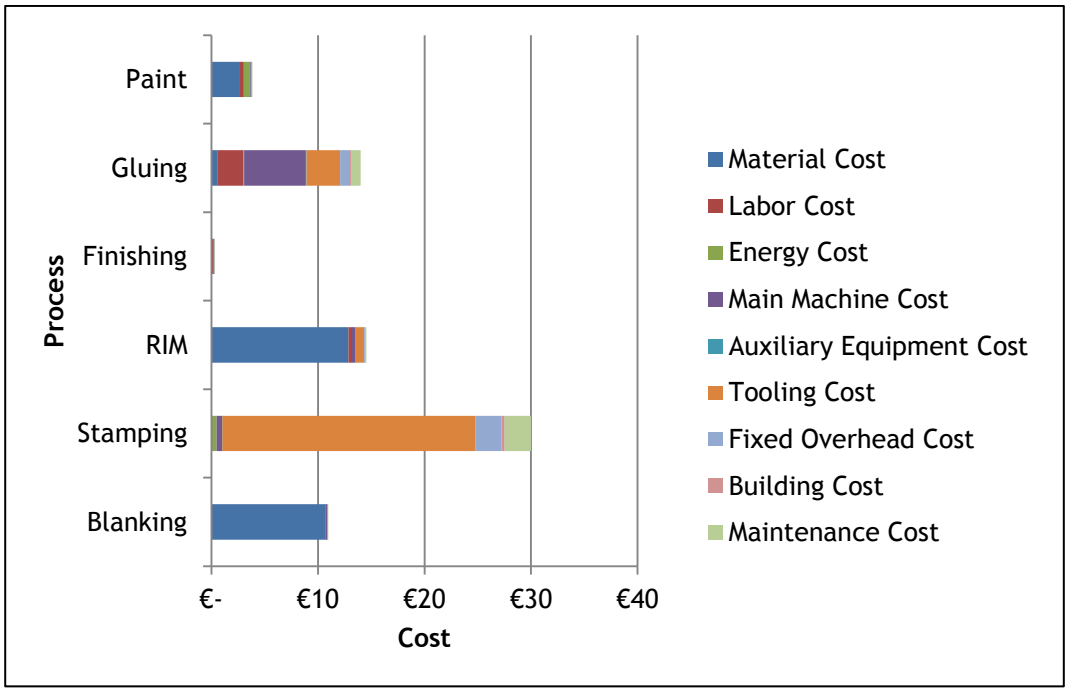

Figure H.37 - Bonnet2 cost breakdown.

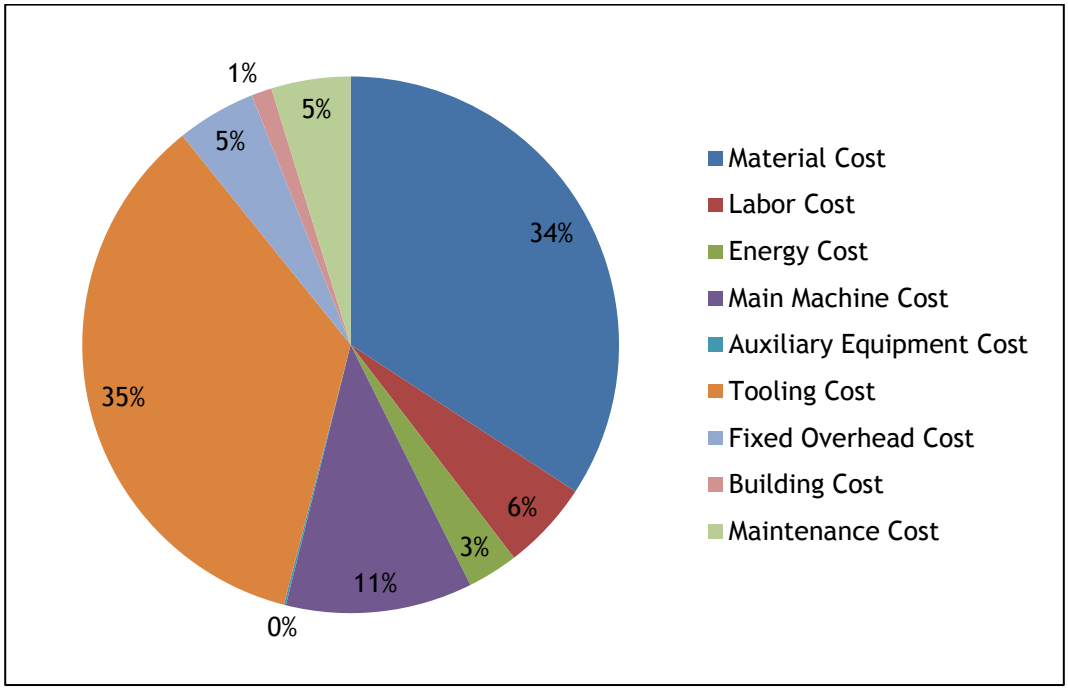

Figure H.38 - Cost percentage by element for Bonnet2.

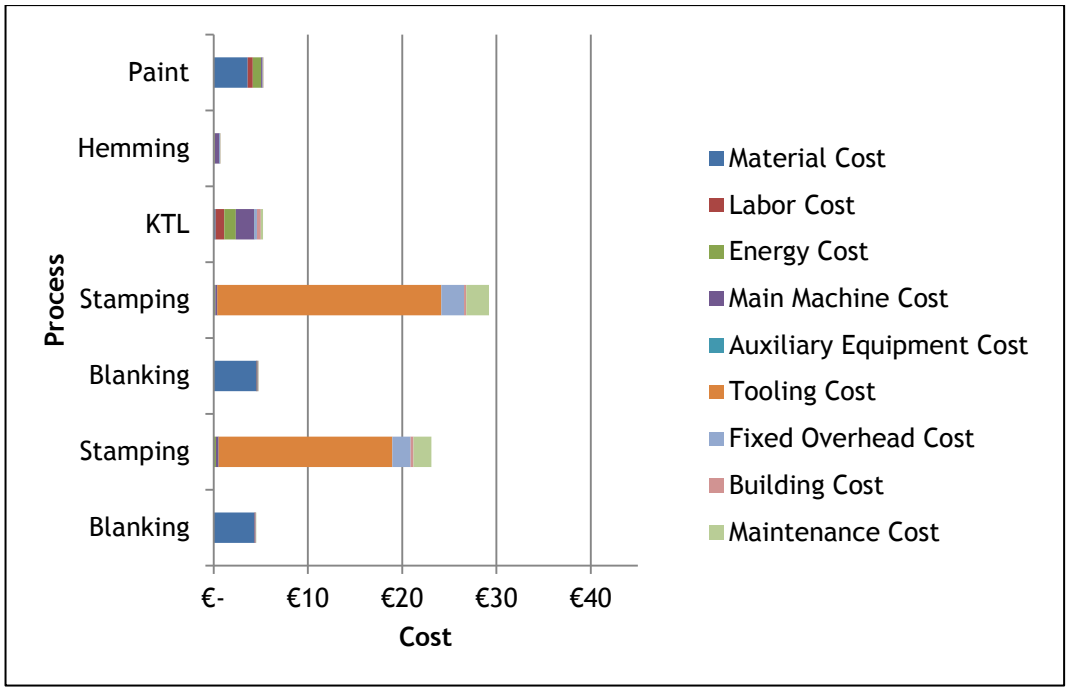

Figure H.39 - Bonnet3 cost breakdown.

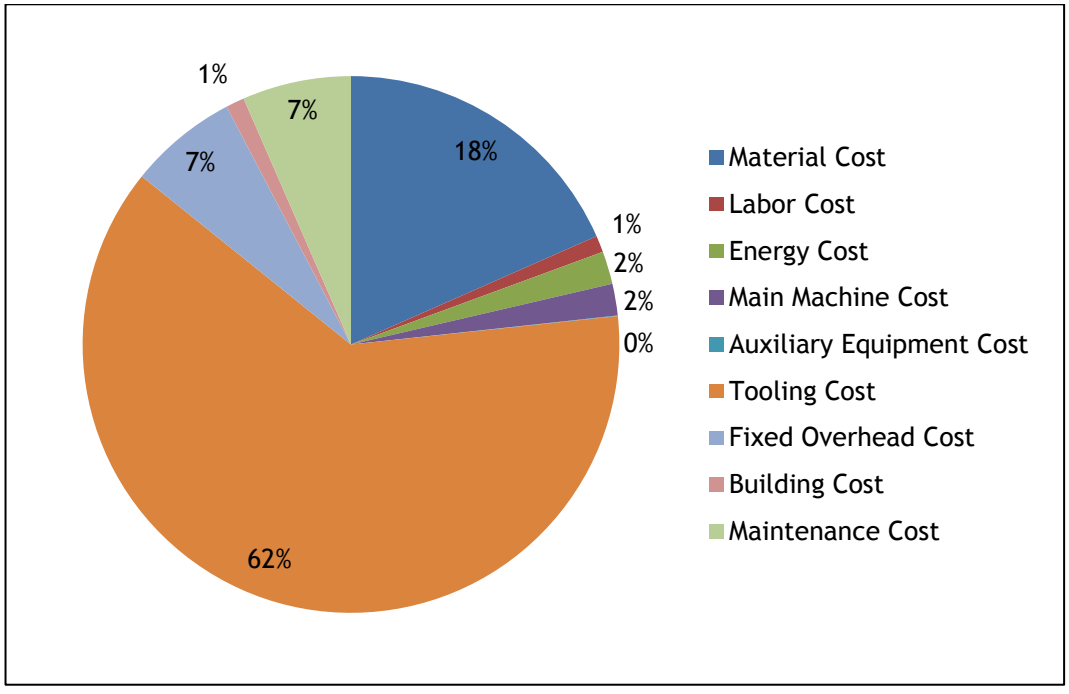

Figure H.40 - Cost percentage by element for Bonnet3.

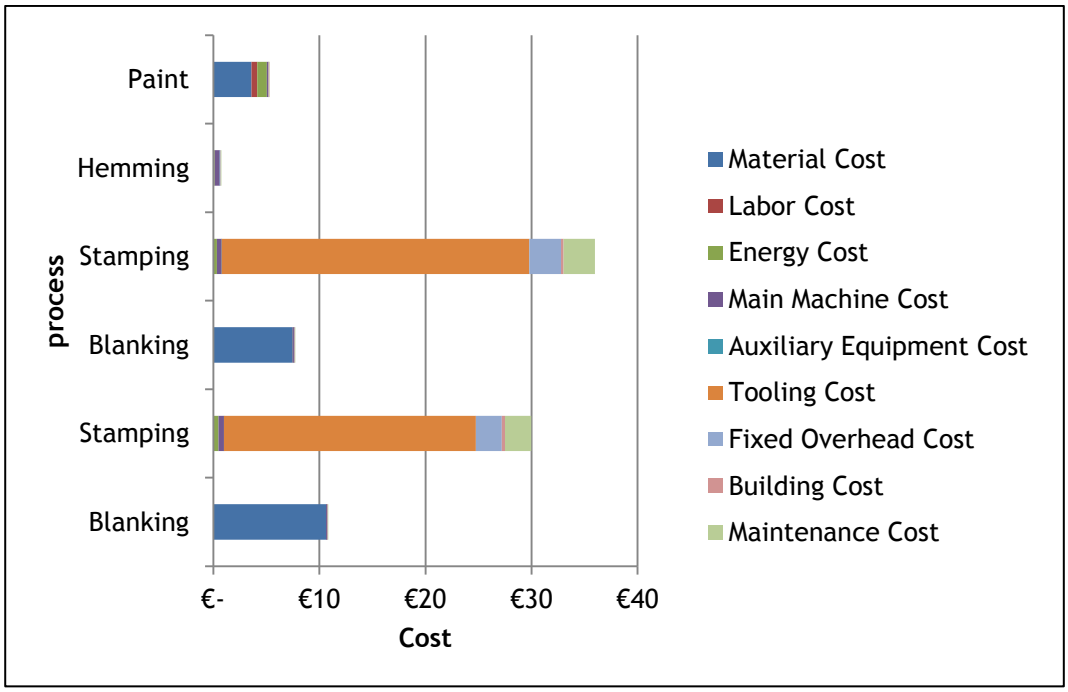

Figure H.41 - Bonnet4 cost breakdown.

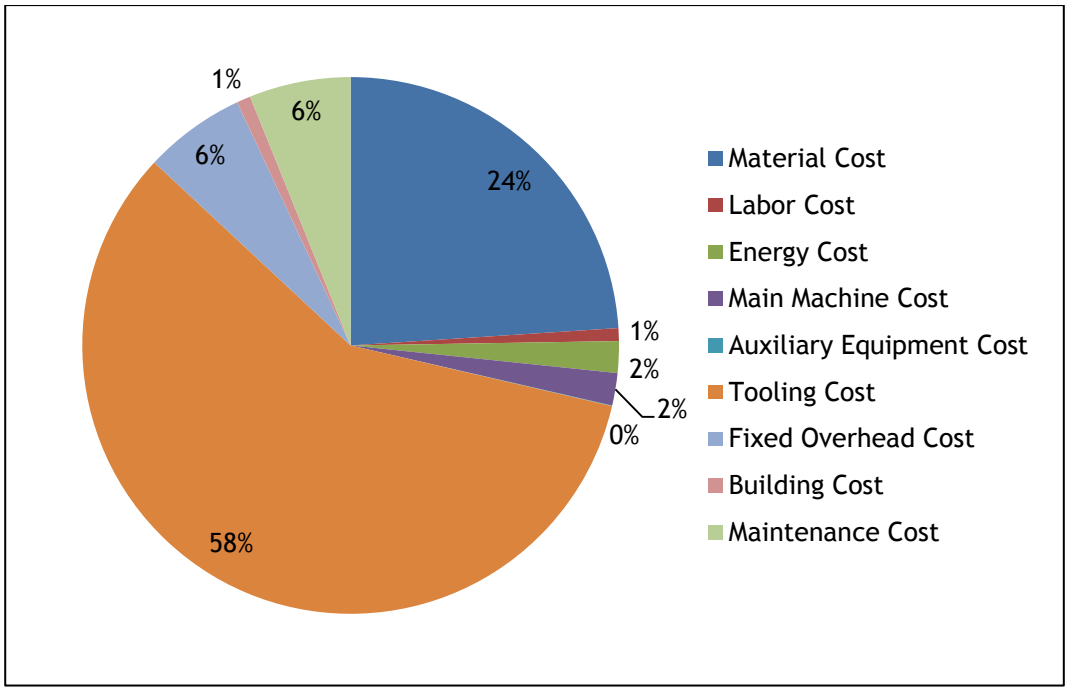

Figure H.42 - Cost percentage by element for Bonnet4.

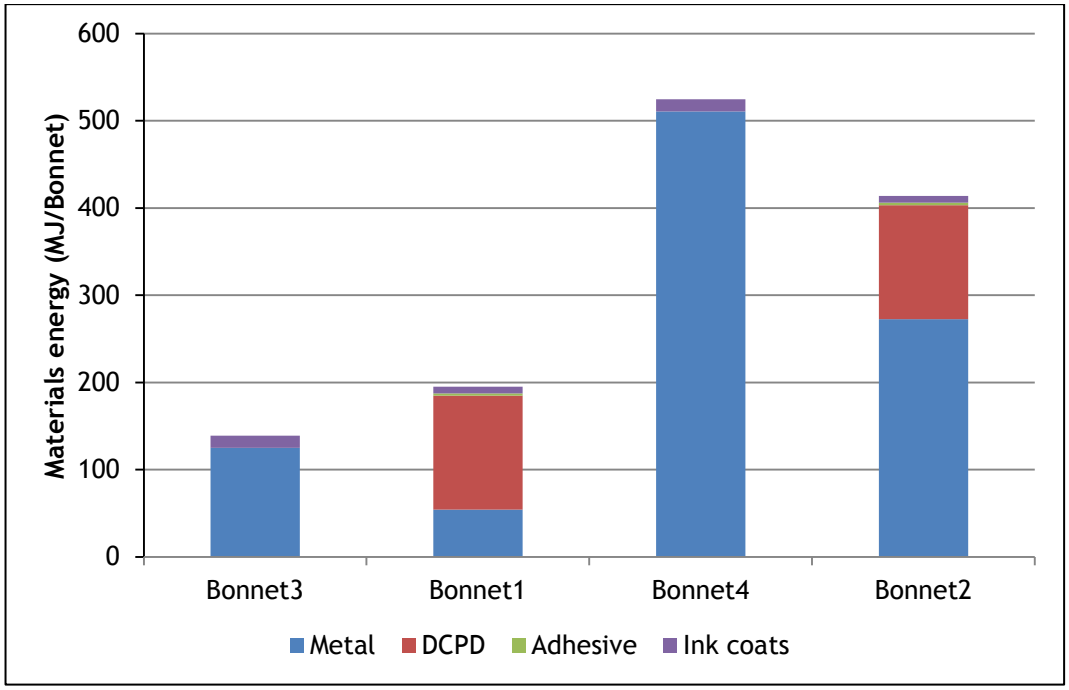

Figure I.43 - Total embodied energy of the required materials.

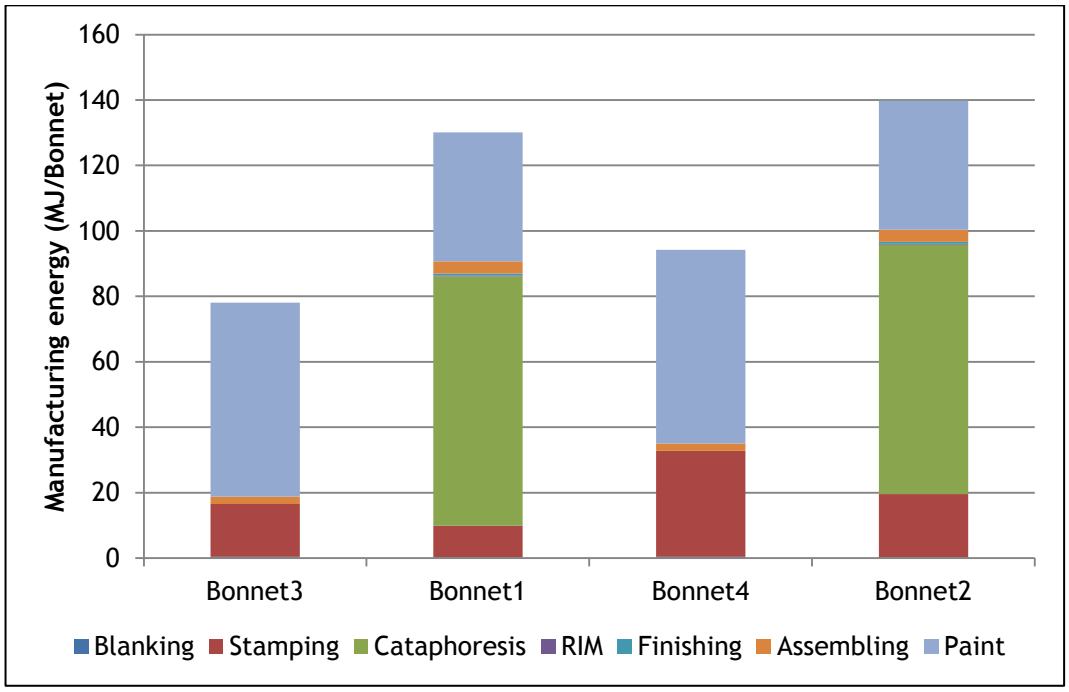

Figure I.44 - Total energy required for bonnet manufacturing.